SOME THEORETICAL CONSIDERATIONS RELATED TO THE EXPERIMENTAL TESTS OF A TEMPORAL BELL'S INEQUALITY

BY

MAO-CHUANG YEH

DISSERTATION

Submitted in partial fulfillment of the requirements
for the degree of Doctor of Philosophy in Physics
in the Graduate College of the
University of Illinois at Urbana-Champaign, 2016

Urbana, Illinois

Doctoral Committee:

Professor Vishveshwara Smitha, Chair
Professor Anthony J. Leggett, Director of Research
Professor Paul G. Kwiat
Professor Naomi Makins

Abstract

According to the quantum superposition principle, quantum mechanics at the macroscopic scale predicts that a macroscopic system can be in more than one distinct state at the same time. Such an extrapolation of quantum mechanics contradicts our everyday instinct, summarized by Leggett and Garg (LG) under the heading of macrorealism (MR) [1]. To resolve the conflict and to determine whether MR or quantum mechanics is the right description of macroscopic objects, in 1985, Leggett and Garg [1] proposed the temporal Bell's inequality (TBI). If a macorealist description is possible, the inequality is satisfied - quantum mechanics, on the other hand, predicts a violation. Thereafter, people were motivated to engineer macroscopic quantum systems and to test the TBI. In the TBI, one of the most critical postulates is that of the noninvasive measurability (NIM) : it is in principle possible to determine which state the system is in with an arbitrarily small effect on the subsequent system dynamics. To satisfy the NIM postulate in the TBI experiment, the implementation of the "ideal negative result" (INR) measurement was also proposed by LG [1]. In a two-state system, an INR measurement is designed to interact (in each run) with only one of two system states. Only runs where the measurement reported no outcome are kept.

Although in the last few years there have been tests of the TBI on microscopic systems with the use of INR measurements [4] and on macroscopic systems using weak measurement [5], no one has ever implemented INR measurements on macroscopic systems in TBI tests so far. In addition, the NIM postulate was simply assumed, and not verified by an ancillary test [9, 3].

With these considerations in mind, there are two main tasks in this thesis: the first one is to analyze the realization of an INR measurement on a macroscopic object. I propose an experiment based on coupling a flux-qubit to a dcSQUID, which mirrors the approach of Knee et al. [4], where the system of interest is coupled to another quantum system which acts as a measuring device. In order to accomplish the first task, we analyze the escape dynamics of a flux-qubit SQUID composite system in various limits and discuss the prospects of operating in a regime realizing a von Neumann ("projective")-like measurement onto the qubit flux basis. Later in the thesis, I discuss current feasibility of the proposed experiment based on the possible measurement error (the "venality" [4]) of our INR measurement.

The second task is to analyze experimental tests of measurement invasiveness. I propose a concrete protocol, ancillary to the main TBI experiment, which may narrow some loopholes in the test of MR [3]. I generalize the approach of Wilde and Mizel [3], using the behavior of the two-time correlator of a system as an indicator of measurement invasiveness. The measured invasivities can be used to give a improved lower bound for the TBI.

The author thanks Hayato Nakano for fruitful discussions of the experiments and of the numerical analysis of ref.[21] and for sending us the updated version of this reference, and Alec Maassen van den Brink for helpful discussions of theory. I am particularly grateful to Adrian Lupascu for a careful reading of the manuscript of Chapter 2 and many constructive comments. I also thank George Knee and Lance Cooper for helping writing the abstract and introduction. Most importantly, the author thanks his advisor Anthony J. Leggett very much for patiently discussing all the research topics and revising the thesis. This work was supported in part by the National Science Foundation through grants number [488437-244014-19110 NSFDMR 09-06921 and 496696-244022-191100 A07 NSF EIA 01-21568ITR], by the Department of Energy through grants [488732-220001-191100 A03] and by the Macarthur Professorship endowed by the John D.and Catherine T.Macarthur Foundation at the University of Illinois.

Table of Contents

Chapter 1

Introduction

Quantum mechanics is considered to be the most reliable theory in the world because of its incredible accuracy in experimental prediction. Despite its predictive accuracy, the principal assumptions of quantum mechanics remain puzzling. For example, people generally find puzzling the premise in quantum mechanics that a system can exist in a superposition of states – like $\Psi = a\Psi_1 + b\Psi_2$, where Ψ_1 and Ψ_2 are different states (or wavefunctions) of the system and a and b are probability amplitudes for those states – and that the system will collapse into a particular state Ψ_1 or Ψ_2 (with a probability $|a|^2$ or $|b|^2$, respectively) only after a measurement of the system is made. Even though these assumptions have been verified by experimental results, they are difficult to grasp because they do not follow our natural intuition. The concept of a system existing in a superposition of two distinct realities is difficult to reconcile with the so-called 'local realism' point of view–in which objects are assumed to be influenced by their local surroundings and to exist independent of whether or not they are observed. Local realism also cannot explain how the wavefunction of a system collapses, which is the so-called measurement problem that people have studied since the discovery of quantum mechanics.

To demonstrate the counterintuitive consequences of quantum mechanics compared to our everyday experiences with classical mechanics, the implications of quantum mechanics are often naively extrapolated to the macroscopic world in the so-called Schroedinger's cat paradox, in which Schroedinger's cat can be simultaneously dead and alive, i.e., described by the superposition state $\Psi = a\Psi_{alive} + b\Psi_{dead}$. Actually, the validity of extrapolating the consequences of quantum theory to the macroscopic world is still questionable. Experimental evidence, at least, is required to show that the macroscopic system exhibits macroscopic quantum coherence [18, 19], i.e., that the state describing the macroscopic system can indeed be described as a superposition exhibiting a temporal oscillation between macroscopically distinct states. But such experimental evidence is not sufficient: it has been speculated that macroscopic realism ("macrorealism")–in which a macroscopic object must be in a macroscopically distinct state at any given time–can give the same prediction. More rigorously, to disprove macrorealism and support the validity of quantum mechanics to macroscopic objects, an experimental violation of a Bell-type inequality must be demonstrated. To

achieve this goal, in 1985, Leggett and Garg[1] proposed a Temporal Bell's inequality (TBI) (also called the Leggett-Garg inequality(LGI)) constructed from the assumptions of macrorealism. Similar to the role of Bell's inequality with respect to quantum mechanics, we expect that experimental tests of TBI will show violation of this inequality if quantum mechanics applies to macroscopic objects.

In principle, the TBI is mainly based on the following postulates: (a) Macroscopic realism per se (MR) – a macroscopic object, which has two or more macroscopically distinct states available to it, must have a definite state at any particular time. (b) Noninvasive measurability (NIM) – it is possible, in principle, to determine which of the macroscopically distinct states the system is in with a measurement that has an arbitrarily small effect on the subsequent dynamics of the system. (c) Induction – there is no retro-causality, i.e., the system's dynamics is exclusively determined by its history and not by its future behavior.

Before addressing the TBI, let's first consider what is measured in the main TBI experiment. To simplify the testing of MR, the TBI experiment focuses on a system with only two macroscopically distinct [2] states, which correspond respectively to the measurement outcomes $Q = \pm 1$. We assume we have a distinct measurement outcome $Q_i = Q_i(t_i)$ only available at each of the following three times t_1, t_2, and t_3. In addition, there is only one system considered in each experimental run, and the system is prepared initially and measured only twice, at two of the three possible times provided by the time sequence t_1, t_2, and t_3 described above. After repeating the experiment to get the time ensemble of the system, we can obtain the two time correlators $\langle Q_i Q_j \rangle_{i,j}$ of the system. Here the pointed brackets represent the time ensemble average for the required quantity, and the subscripts i, j on the pointed brackets specify at which two times, t_i and t_j, the two measurements are performed. In total, there are only three possible two-time correlators given by the experiment, which are $\langle Q_1 Q_2 \rangle_{1,2}$, $\langle Q_1 Q_3 \rangle_{1,3}$, and $\langle Q_2 Q_3 \rangle_{2,3}$. According to these correlators, we can define the Leggett-Garg function[4] by

$$L\left(t_1, t_2, t_3\right) \equiv \langle Q_1 Q_2 \rangle_{1,2} + \langle Q_2 Q_3 \rangle_{2,3} + \langle Q_1 Q_3 \rangle_{1,3} + 1 \tag{1.1}$$

In general, because the correlators belong to different ensembles, the correlators can be independent, e.g., it is possible that all three correlators are equal to $-\frac{1}{2}$ so that the Leggett-Garg function is less than zero. But if we consider Eq.(1.1) restricted to the postulates (a), (b), and (c), where the measurement in experiment needs to be non-invasive according to postulate (b), Eq.(1.1) should have a classical bound. After imposing postulates (a), (b), and (c) and some additional analysis (the details of which will be given in the next section), the so-called TBI can be written:

$$L\left(t_1, t_2, t_3\right) \geq 0. \tag{1.2}$$

Therefore, a violation of Eq.(1.2) implies a failure of at least one of the postulates (a), (b), and (c) above. To rule out the MR postulate correctly, we need to make sure that the other two postulates are true. Because we still believe the legitimacy of induction, this implies that only the NIM postulate needs to be checked. In addition, to provide a noninvasive measurement (also called NIM here), an ideal negative result (INR) measurement was also suggested by Leggett and Garg [1]. An INR measurement is designed to interact with only one of two system states, and only those experimental runs on which no positive outcome is detected are kept to accomplish the (negative-outcome) measurement. As an example, suppose we can design a measuring apparatus which only interacts with the measured system in the "$Q = +$" state. Then, we can keep the system of non-triggered runs as the collection of negative outcomes in which the system is purported to be in the "Q=-" state. Similarly, we can collect the ensemble of the system in the "Q=+" state based on a measurement that interacts only with the system in a "$Q = -$" state. From these data set we can determine the complete two-time correlators.

But even if an INR measurement is set up, we still need an additional test to confirm its NIM characteristics [9], or at least to quantify the degree of measurement invasiveness to place a correct bound on TBI. This is one of the main topics in this thesis, and we will return to this soon.

After the TBI was proposed, people more actively investigated this macroscopic quantum phenomenon with the help of improved quantum techniques and the architecture of quantum computing. Around 1999, several experiments realized macroscopic quantum-persistent-current states in a superconducting ring of Josephson junctions, which is called the superconducting flux qubit [11, 17, 18]. In a flux qubit, two qubit states correspond to two different current states of superconductor, so that they have two distinct macroscopically induced fluxes. (We will give a more detailed review of flux qubit soon in the following sections.) Moreover, to demonstrate quantum mechanics on a macroscopic scale, quantum coherent control was performed on these macroscopic states [18], e.g. Rabi oscillations or Ramsey fringes are observed in flux qubits. There have been other experiments developed for studying quantum coherence in macroscopic systems, but the flux qubit is one of the best systems for studying macroscopic quantum coherence so far (with the difference of magnetic moment between the flux states being about 10^6 to 10^9 Bohr magnetons). Consequently, we consider the flux qubit to be the primary system for TBI experiments. Concerning the implementation of measurements on the flux qubit, we only focus on the single shot measurement by a dcSQUID (the superconducting quantum interference device with dc current, which will be reviewed at the end of this chapter) because it contains the most promise for realizing a projective measurement on the flux qubit. Please note that the dcSQUID contributed a lot in those pioneering experiments [17, 18, 11], though the measurements were not of a projective type at the time.

In the last few years, people attempted to realize the TBI test on a microscopic system with a projective type of measurement [4, 6, 7]. One of the most successful of these measurements was an experiment reported by Knee's group using an INR measurement [4, 8]. (Knee et al.'s INR measurement is based on a paired nuclear-electron system, in which the electron spin has different resonant frequencies corresponding to two different nuclear states. The negative measurement of the system's state is considered to be the outcome in which the electron ensemble is not excited after resonant pumping. We will introduce this experiment again in Section 2 of Chapter 3.) Although these experimental groups have made significant progress on testing the TBI, none of their attempts included the ancillary test needed to complete the TBI experiment [8]. In 1988, A.J. Leggett suggested using the ancillary test [9] to check the NIM postulate in order to avoid the possible loophole [3] that would rule out the MR postulate; however, no explicit protocol was given at that time. More recently, Wilde and Mizel [3] gave a concrete definition of measurement invasiveness (associated with the second measurement), called ϵ-adroitness. ϵ-adroitness is evaluated by summing all possible absolute values of the joint probability changes between the first and third measurements due to the presence of the second measurement. Although their ϵ-adroitness precisely describes measurement invasivity, it does not directly permit calculation of the correction to the TBI. By considering the application of the ancillary test to the TBI experiment, measurement invasivity must be quantified by the two-time correlators; only considering the ϵ-adroitness is not enough to construct this quantity. Therefore, providing an explicit and useful protocol of the ancillary test as applied to the TBI experiment is one of the most important topics in this thesis. On the other hand, because there is no TBI test on a macroscopic object so far, we are also going to propose an experimental scheme of performing INR measurement with a flux qubit-dcSQUID system. With previous experience testing the TBI on the microscopic scale and the current technology for achieving macroscopic quantum coherence, we are ready to test the TBI on a macroscopic object.

The main content of the thesis is decomposed into Chapters 2 and 3. In the rest of this chapter, we will introduce the derivation of the TBI along with some background information on the flux qubit and the dcSQUID. Chapter 2 focuses on the mechanism of the qubit state measurement by a dcSQUID, which is dominated by the escape behavior of a dcSQUID and is also related to the net flux induced by the flux qubit. Because the flux can be induced by the qubit in a superposition state, it is not a conventional escape problem. Furthermore, which measurement basis this qubit-SQUID composite system prefers is the most relevant problem we need to answer; the answer to this problem will be approached analytically in various limits in different sections of the thesis. In the discussion section, we will use the dcSQUID's escape properties to investigate other related questions: For example, how does the density matrix evolve before the current switching taking place? how does the entanglement between the qubit and the SQUID change during

the measurement? And how is the measurement related to the weak measurement based on the behavior of the current switching distribution? At the end of the chapter, we will analyze how to use this qubit-SQUID system to set up a flux-basis-preferred projective measurement in preparation for the INR measurement in the next chapter.

In Chapter 3, based on the escape analysis of Chapter 2, we generalize Knee et al.'s INR measurement setup to our qubit-SQUID composite system. On the other hand, we also examine how to quantify measurement invasiveness in the ancillary test and to make this test applicable to the TBI experiment, so that we can find a more accurate lower bound for the TBI. Moreover, we give a simple estimation of measurement invasivity based on the generalized "venality" of the INR measurement [4]. Here the term "venality" is introduced in Knee's experiment as the fraction of the ensemble for which the electron spin is incorrectly prepared, where the electron spin is coupled to the system to indicate the system's state. In this thesis, we generalize the definition of "venality" to refer to the fraction of any kind of ensemble that is mis-sampled. Accordingly, we can estimate the maximum tolerated venality of the INR measurement in the TBI experiment. At the conclusion of the chapter, we also investigate possible sources causing measurement venality.

The last chapter, Chapter 4, is a summary of the thesis.

1.1 The derivation of the Temporal Bell inequality

As mentioned previously, the TBI experiment measures the three two-time correlators $\langle Q(t_1)Q(t_2)\rangle_{1,2}$, $\langle Q(t_2)Q(t_3)\rangle_{2,3}$, and $\langle Q(t_1)Q(t_3)\rangle_{1,3}$. Because these correlators belong to different experimental setups or ensembles, which give different pairs of measurements, generally we don't expect that there will be a relationship among the correlators. But by applying the above three TBI postulates, a lower bound of the Leggett-Garg function can be obtained. This lower bound gives the TBI. In the following, we give a detailed derivation of the TBI.

First, because of the NIM postulate, in the experiment for $\langle Q(t_2)Q(t_3)\rangle_{2,3}$ the presence of the Q_1 measurement (before Q_2 and Q_3) have nothing to do with the outcomes of Q_2 and Q_3. Therefore, we have $\langle Q(t_2)Q(t_3)\rangle_{2,3} = \langle Q(t_2)Q(t_3)\rangle_{1,2,3}$. Here the subscripts $1, 2, 3$ on the pointed brackets represent the ensembles associated with three measurements at t_1, t_2, and t_3 respectively. Additionally, according to the induction postulate, in the experiment for $\langle Q(t_1)Q(t_2)\rangle_{1,2}$, the Q_3 measurement (made after measurements Q_1 and Q_2) cannot change the outcomes of Q_1 and Q_2. Consequently, we have $\langle Q(t_1)Q(t_2)\rangle_{1,2} = \langle Q(t_1)Q(t_2)\rangle_{1,2,3}$. Similarly, in the experiment for $\langle Q(t_1)Q(t_3)\rangle_{1,3}$, the Q_2 measurement (made between measurements Q_1 and

Q_3) cannot change the outcomes of Q_1 and Q_3 because of the induction and NIM postulates, respectively. Consequently, we have $\langle Q(t_1)Q(t_3)\rangle_{1,3} = \langle Q(t_1)Q(t_3)\rangle_{1,2,3}$. (Please note that in quantum mechanics the presence of the measurement in front or after a two-time correlator can not change the correlator itself, which automatically satisfies the NIM postulate; only the measurement staying between the two times of correlator can make a change of correlator in quantum mechanics. Therefore, the second measurement can be invasive in quatnum mechanics even it classically satisfies the NIM postulate, and then the correlator $\langle Q(t_1)Q(t_3)\rangle_{1,3}$ plays a more significant role than other two for testing the TBI.) In sum, with the help of the three TBI postulates, we make an extrapolation of the correlators in Eq.(1.1) to new ones belonging to the same ensemble of a sequence of three consecutive measurements at t_1, t_2, and t_3. Consequently, we can write the extrapolated result of Eq. (1.1) as follows:

$$L\left(t_1,t_2,t_3\right) = \langle Q_1Q_2\rangle_{1,2,3} + \langle Q_2Q_3\rangle_{1,2,3} + \langle Q_1Q_3\rangle_{1,2,3} + 1. \tag{1.3}$$

On the other hand, it's not hard to see that

$$\langle Q_1Q_2\rangle_{1,2,3} + \langle Q_2Q_3\rangle_{1,2,3} + \langle Q_1Q_3\rangle_{1,2,3} + 1 = \langle Q_1Q_2 + Q_2Q_3 + Q_1Q_3 + 1\rangle_{1,2,3} \geq 0 \tag{1.4}$$

Furthermore, we have $Q_1Q_2 + Q_2Q_3 + Q_1Q_3 + 1 \geq 0$ for the measurements Q_1, Q_2, and Q_3 appearing in the same experimental run because the value of the Q_i is always either 1 or -1. For example, for $Q_1 = Q_2 = 1$ and $Q_3 = -1$, we have $Q_1Q_2 + Q_2Q_3 + Q_1Q_3 + 1 = 0$ as the minimum value; we can not find the result lower than zero for any possible composition. Therefore, we can conclude that Eq.(1.3) is bounded from zero, which gives the conventional form of TBI as shown in Eq.(1.2).

Basically, the TBI gives the macro-realistic bound of the experimental result which can be violated in quantum mechanics. If we want to disprove the MR postulate: first, we need to find out the possible experimental parameter region where TBI can be violated (by quantum mechanics), and next we need to make an ancillary test to check the NIM postulate such that we can preclude the possible violation by measurement invasiveness. In the end, we can more confidently confirm the violation of TBI is due to the assumption of MR, which may support quantum mechanics at macroscopic scale. (Here we had excluded the possible failure of induction postulate.)

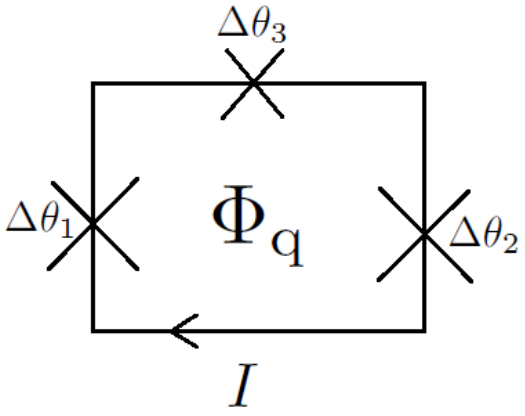

Figure 1.1: The flux qubit of three Josephson junctions.

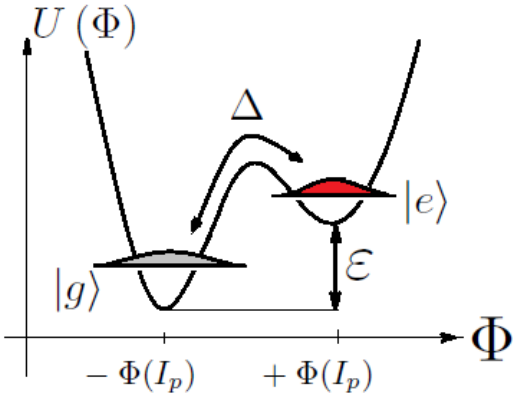

Figure 1.2: The double well potential as a function of the flux Φ penetrating through superconducting loop of the qubit.

1.2 The flux qubit

Before we investigate the measurement of the flux qubit, let's have a brief review of the flux qubit itself. Typically, the flux qubit is made of superconducting loop interrupted by Josephson junctions and there is an applied flux Φ_q penetrating the circuit, please see Fig. 1.1. It's well known that the flux qubit is claimed to have macroscopic quantum coherent property, where each flux state corresponds to a definite circuit current and then has macroscopic distinct flux. To simplify the demonstration, here we consider the single-junction model of flux qubit (and will provide the corresponding formulas for three-junction model later) . Although the three-junction structure is more popular for qubit engineering[13],[12], the choice of the qubit structure doesn't change our analysis of principle in the following.

Let's first construct the effective potential for the circuit in semi-classical limit. Because the superconducting circuit has loop inductance L, circuit current I, and the applied flux $\Phi_{\rm q}$, we can have its magnetic

energy $\frac{1}{2}LI^2 = \frac{(\Phi-\Phi_q)^2}{2L}$, which can be considered as part of the effective potential in the flux coordinate Φ, which is the total flux enclosed by the superconducting loop. To complete the required potential, we also need to consider another energy term from the Josephson junction. The Josephson junction inherits the properties of superconductor and has its super current I controlled by the phase difference $\Delta\theta$ across the junction, according to the formula

$$I = I_c \sin(\Delta\theta) \tag{1.5}$$

with I_c as the critical current of the junction. Accordingly, based on this current formula we can construct a potential term for Josephson junction

$$U(\Delta\theta) = -E_J \cos\Delta\theta \tag{1.6}$$

, where $E_J = \frac{I_c\Phi_0}{2\pi}$ is named as Josephson coupling energy. Please note that because of the $U(1)$ gauge symmetry of the superconducting wave function there is a relation between the phase difference $\Delta\theta$ of the junction and the flux Φ within the loop:

$$\Delta\theta = 2\pi\Phi/\Phi_0. \tag{1.7}$$

Here $\Phi_0 = \frac{h}{2e}$ is called the flux quantum. Based on above formulas, totally we can have the circuit effective potential as a function of Φ:

$$U_{effective} = \frac{(\Phi-\Phi_q)^2}{2L} - E_J \cos 2\pi\frac{\Phi}{\Phi_0} \tag{1.8}$$

With appropriately chosen parameters, we can see that the potential looks as a double well in some Φ region, where the minimum in two wells corresponding to two distinct flux values. As we will see, the states respectively localized around the two minima are the so-called flux basis $|L\rangle$ and $|R\rangle$; each state has a definite flux value closed to the minimum of the well. Please see Fig. 1.2.

Next, in order to complete the circuit Hamiltonian, we also need to consider the charge energy term from the Josephson junction. Because the Josephson junction has the structure of two superconductors separated by a very thin insulating barrier, it can act as a capacitance C and contributes a charge energy $E_c = \frac{Q^2}{2C}$. Here Q represents for the charge stored in the capacitance of the junction.

In the end, we have the total Hamiltonian

$$H = \frac{Q^2}{2C} + \frac{(\Phi-\Phi_q)^2}{2L} - E_J \cos 2\pi\frac{\Phi}{\Phi_0} \tag{1.9}$$

At first sight, we can see the first quadratic term looks like the kinetic energy, and guess that the charge Q acts as the momentum conjugating to Φ. More rigorously, we can derive the conjugation relation from the Faraday's law $\dot{\Phi}(t) = -v(t)$, where $v(t)$ is the voltage on the loop(or the voltage across the junction more precisely). Combining it with the formula of capacitance $Q = cv(t)$, we can have $Q = -C\dot{\Phi}$, then the first term can be rewritten as $\frac{C\dot{\Phi}^2}{2}$, which exactly corresponds to the kinetic term in the $L\left(\Phi, \dot{\Phi}\right)$ (because other terms only depend on Φ). Therefore, the momentum conjugate to Φ is given by

$$P = \partial L\left(\Phi, \dot{\Phi}\right)/\partial\dot{\Phi} = C\dot{\Phi} = -Q.$$

This conjugate relation may imply us the quantum mechanical commutation relation between Φ and Q, but more rigorous argument of why we can treat Φ as a quantum mechanical variable should reference Leggett's lecture[14]. In total, the net flux Φ and the capacitance charge Q are quantum mechanically conjugated :

$$[\Phi, Q] = -i\hbar. \tag{1.10}$$

Once we have the circuit Hamiltonian and quantization formula, we can have all spectrum of the system. Then the next step is to establish the two state behavior for the flux qubit. In general, people engineer the effective potential[11],[12],[13] of the phase (or the flux Φ) into the double-well shape under the appropriate parameter setting, where the minimum of the two wells correspond to the fluxes of two opposite circulating current $\pm I_p$. Besides, the ratio between the Josephson energy E_J and the charge energy E_c are also appropriately chosen such that the first two energy levels are well separated from other higher ones and eventually becomes two well defined energy states. Therefore, similar to the standard double well problem, the ground state $|g\rangle$ and the excited state $|e\rangle$ can be represented as superpositions of the states of the flux localized in the left and right wells, which are the flux states $|L\rangle$ and $|R\rangle$ and respectively correspond to the clockwise and counterclockwise circulating current states(of the current magnitude I_p). In sum, we finally have the effective Hamiltonian(see ref.[13]) to describe to flux qubit

$$H_q = \varepsilon\sigma_z - \Delta\sigma_x. \tag{1.11}$$

Here σ_z and σ_x are the Pauli matrices in the flux basis $|L\rangle$ and $|R\rangle$, Δ is the tunneling energy between two flux states, and the $\varepsilon \approx I_p\left(\Phi_q - \frac{\Phi_0}{2}\right)$ is the qubit bias energy [28].

In the three-junction model, we have similar arguments for the derivation of two state in Eq.(1.11). We have three junctions (with phase differences $\Delta\theta_1, \Delta\theta_2$, and $\Delta\theta_3$) respectively distributed on the supercon-

ducting loop as shown in Figure 1.1. Correspondingly, we can have the effective potential as

$$U_{effective} = \frac{(\Phi - \Phi_q)^2}{2L} - \sum_{i=1}^{3} E_J \cos \Delta\theta_i \tag{1.12}$$

under a new phase constraint

$$\sum_{i=1}^{3} \Delta\theta_i = 2\pi\Phi/\Phi_0. \tag{1.13}$$

Similarly, we can find out the minimum of its effective potential and the quantization formulas for the total Hamiltonian

$$H = \sum_{i=1}^{3} \frac{Q_i^2}{2C} + \frac{(\Phi - \Phi_q)^2}{2L} - \sum_{i=1}^{3} E_J \cos \Delta\theta_i \tag{1.14}$$

According to Eq. (1.13), $\Delta\theta$s only have two independent degree of freedoms, and therefore the double well of a qubit correspond to two local minima in 2-dimensional $\Delta\theta$s' space. Correspondingly, based on the Faraday's law, we have equation of Qs

$$\sum_{i=1}^{3} Q_i = c\dot{\Phi} = c\sum_{i=1}^{3} \Delta\dot{\theta}_i \tag{1.15}$$

and therefore only two Q variables are independent; there should be two independent quantization formulas in this system. If the ratio between the Josephson energy E_J and the charge energy E_c are also appropriately chosen, we can make the first two energy levels of the Eq.(1.14) well separated from other higher ones (in the chosen double well). Eventually, we effectively construct a two state system in the three-junction qubit.

1.3 The dcSQUID

Basically, we use dcSQUID to measure the induced flux from the qubit as a method to detect the qubit state. Therefore, the flux qubit is usually fabricated together with the dcSQUID by sharing common area (with flux) such that they can inductively couple to each other(see Fig(1.3)), where the inner loop with three junctions is the flux qubit and outer loop is the dcSQUID.

The dcSQUID usually consists of a superconducting loop symmetrically (with respect to the incoming and outgoing current I) interrupted by two identical Josephson junctions (of the same critical current I_{c0}) on the left and the right branches, please see the Fig.(1.4). As we know that the super current of each junction is a function of phase difference across the junction, therefore the two branch currents I_1 and I_2 in dcSQUID are respectively described by $I_1 = I_{c0} \sin \Delta\theta_1$ and $I_2 = I_{c0} \sin \Delta\theta_2$. Here $\Delta\theta_1$ and $\Delta\theta_2$ are the

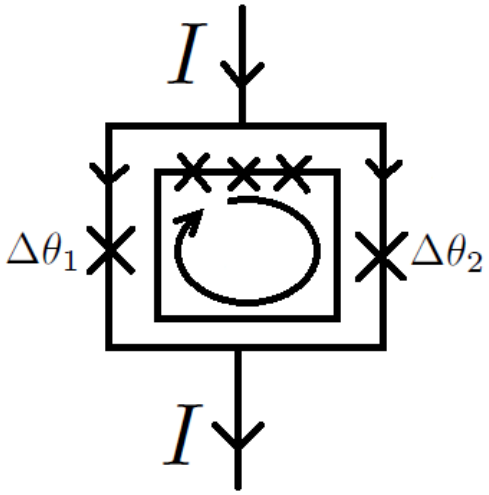

Figure 1.3: colorred Usually the flux qubit is fabricated together with the dcSQUID by sharing common area such that they can inductively couple to each other; the inner loop with three junctions is the flux qubit and outer loop is the dcSQUID. For the SEM picture of "persistent-current qubit" sample with dcSQUID, please see the ref.[12].

phase difference of two junctions. Furthermore, if we represent two branch currents as the sum (difference) of the total current I and circulating current J, then we can rearrange them and have new equations

$$\begin{cases} I = 2I_{c0}\cos\left(\pi f_{SQ}\right)\sin\left(x\right) \\ J = I_{c0}\sin\left(\pi f_{SQ}\right)\cos\left(x\right) \end{cases} \tag{1.16}$$

, where $f_{SQ} \equiv \frac{\Phi_{SQ}}{\Phi_0} = \left(\Delta\theta_1 - \Delta\theta_2 + 2n\pi\right)/(2\pi)$ with Φ_{SQ} being the flux enclosed by the SQUID loop and $x = \frac{\Delta\theta_1+\Delta\theta_2}{2}$ the average phase of two junctions. According to the first equation in Eq.(1.16), we can consider the dcSQUID as a Josephson junction with flux dependent critical current $I_c(f_{SQ}) = 2I_{c0}\cos(\pi f_{SQ})$. Because the dcSQUID inductively couples to the flux qubit, the flux will depend on the qubit state and then we can measurement the qubit state by investigating the critical current. Furthermore, to study the flux-dependent dynamics of dcSQUID, it will be helpful to analyze its Hamiltonian with the effective potential of the phase variable x. Here the SQUID effective potential is

$$U_0\left(x, f_{SQ}\right) = -2E_{J0}\cos\left[\pi f_{SQ}\right]\cos\left[x\right] - \frac{\Phi_0 I}{2\pi}x \tag{1.17}$$

, and it's first derivative with respect to x exactly gives the current equation of I in Eq.(1.16). The shape of this potential looks like a washboard (see Fig.(1.5)) and we can treat the dcSQUID dynamics in

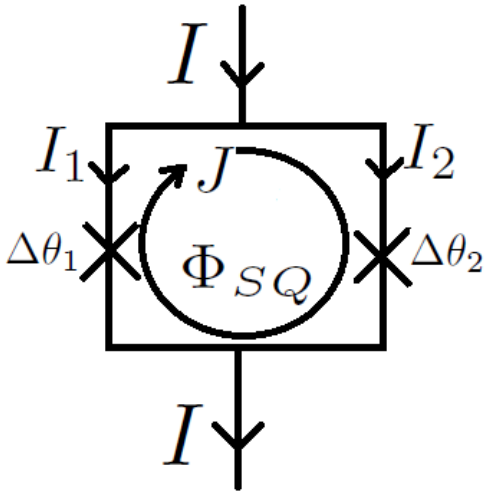

Figure 1.4: the dcSQUID

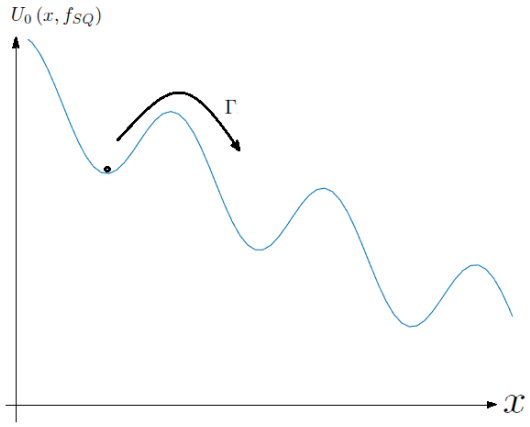

Figure 1.5: The effective potential of the phase variable x of dcSQUID.

analogy with the problem of a particle in this washboard potential. Based on the formula given in Eq.(1.17), we can tell that each well of the washboard potential becomes shallower as the current increases, and then the "phase particle" has more probability to escape. Basically this phase particle has two ways to escape the well, one is via the quantum tunneling, the other is activated by thermal fluctuation. Both of them are stochastic process and characterized by the escape rate Γ. In this thesis we only focus on its quantum tunneling and will mention the WKB formula of it in the next chapter. Please note that once the phase particle escapes the minimum of the well, it will have velocity $\frac{dx}{dt}$, and the junction will have corresponding voltage drop $V = \frac{\Phi_0}{2\pi}\frac{dx}{dt}$; the dcSQUID is no more in the superconducting state, rather it is in what is called the voltage state. Consequently we can measure the voltage of dcSQUID to detect a switching (or an escape) event and repeat the measurement to get the switching probability which is directly related to the escape rate. Because the SQUID potential and its escape rate are flux dependent, the switching probability also

depends on the flux Φ_{SQ}. Therefore, the in principle scheme of using the dcSQUID to measure the flux is based on analyzing the change of the switching probability at a given bias current near the critical one, so called DC-switching readout.

Chapter 2

Measuring the state of a flux qubit via the escape statistics of a dcSQUID

2.1 Introduction to measurement of "macroscopic" flux qubit with dcSQUID

As mentioned in the last chapter, the flux qubit is developed due to the demands on both exploring the quantum mechanical limit up to macroscopic level [1] and the architecture of the quantum computer [10]. Therefore we expect the flux qubit can stay coherently between two macroscopic distinct flux states. It is famous for its breakthrough on testing the macroscopic extrapolation of quantum prediction with the pioneering experiments [11, 17, 18] in both statics and dynamics (the first successful experiment of displaying the quantum coherent oscillation is by Chiorescu et al. in 2003 [18]). After these experiments, there are also many extensive studies of flux qubit on various aspects, which are mostly related to the decoherence problem or other interesting topics of quantum mechanics in the engineering of quantum computer, lasting more than a dozen of years (see Ref. [10] as an example).

Basically, the most intuitive way to measure the qubit state is to detect its total magnetic flux enclosed by its superconducting loop. As we can see in the last chapter, the total flux is contributed by both the applied flux on the qubit and its own compensation flux due to the super current. As claimed, the most important property of flux qubit related to macroscopic quantum mechanics is that the total flux of the qubit can be considered as a quantum mechanical variable[14], which is similar to the position of particle in quantum physics. Therefore, if the qubit is in superposition of two qubit eigenstates of distinct flux values, the total flux can have quantum mechanical indeterminacy between two macroscopically distinct values. Because so far the dcSQUID [15] is still one of the most popular and promising ways to measure the flux qubit, in this chapter we mainly focus on the topic of the dcSQUID inductively coupling to flux qubit as a qubit measurement; we investigate how its escape rate behavior changes with qubit state such that we can correctly read out the information about qubit state.

Because the escape rate of dcSQUID is a function of both bias current(on dcSQUID) and detected flux,

people usually record the dcSQUID switching current, which is the current recorded when the dcSQUID switches to the voltage mode, to measure the flux. However, the switching current itself always reflects the stochastic property of the escape process and has a distribution width. Even if there is no classical(Arrhenius-Kramers) thermal activation at $T = 0$ [17], the distribution width is still contributed by quantum tunneling; the histogram of measured switching current always distributes with a nonzero width before the dcSQUID couples to the flux qubit. Moreover, such a stochastic width seems to dominate the qubit's effect on the switching current behavior [17]; the current distributions corresponding to two qubit states of distinct fluxes almost look the same to each other such that we need to repeat the experiment tens of thousands of times to measure the change of average current instead of reading out the qubit state. Any single run in the repeated measurements is not enough to tell any information from the qubit. This kind of measurement strategy seems very different from the conventional von Neumann measurement. Instead, it's closer to the weak measurement scheme of Albert et al. [16] (though we don't consider the post-selection here).

Besides, another interesting question motivating us is what the measurement basis of this qubit-SQUID coupled system is. Because the way of qubit coupling to dcSQUID is based on their mutual inductance, that will make the qubit-dcSQUID interaction term proportional to σ_z (see Eq.(3.2) in the flux basis representation). Therefore, according to the conventional understanding of the projective measurement, we would expect the qubit state after the measurement to collapse to a flux eigenstate. However, the further experimental result seems to tell us a different story. Since the NTT group has a great improvement on reducing the width of current distribution and then improving the resolution of the experiment, they observed that if we vary a control parameter (i.e. the external applied flux on qubit) so as to change the form of the ground state (see Fig.1.2), the center of the current distribution (for the ground state) varies smoothly from the lower value to the higher one (see Fig. 2.1), where these two limit values should correspond to the two flux states [24]. But this result seems contradictory to our prediction of the current distribution for the flux-basis-preferred measurement (see Fig. 2.2). Because if the projective measurement prefers flux basis, the qubit state should collapse into one of the flux states such that there is only two distinct current distributions (centering at two limit values) respectively corresponding to the two flux states; no current distribution shifting continuously within two limits values (due to the ground state change) should be observable in the flux-basis-preferred measurement. Therefore we guess that the qubit measurement by dcSQUID prefers energy basis instead of flux basis in some parameter regime. We want to investigate analytically what the measurement basis of this composite system is, which is directly related to the escape behavior of the system.

Actually, people put more attention to the analytical study of qubit intrinsic dynamics instead of its

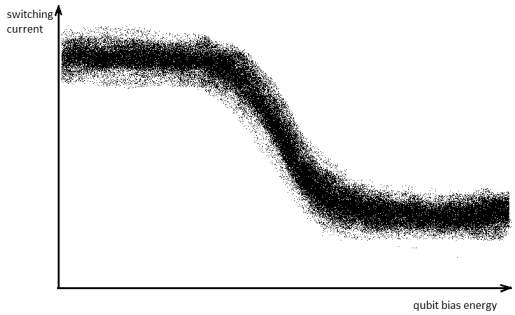

Figure 2.1: The switching current distribution of qubit ground state under energy-basis-preferred projective measurement at various qubit bias energy, where each point in the plot represents a switching event at certain qubit bias energy (X-axis) and switching current (Y-axis). See ref.[24] for the detailed experimental results.

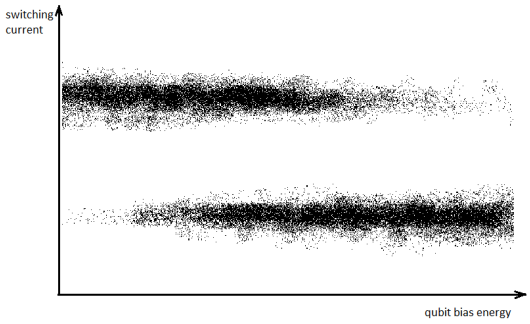

Figure 2.2: The switching current distribution of qubit ground state under flux-basis-preferred projective measurement at various qubit bias energy, where each point in the plot represents a switching event at certain qubit bias energy (X-axis) and switching current (Y-axis). See ref.[24] for the detailed experimental results.

readout physics; there have not been many related papers [20, 21, 22] considering this topic, and most of them were numerical. Especially, the NTT group [21, 22] has investigated the topic in both the presence and the absence of the decoherence. They gave the conclusion that the von-Neumann-like measurement only happens in strong coupling limit, in which the coupling energy is comparable to (or not negligible with) the transition energy between the lowest two states of the dcSQUID, with sufficient decoherence. As we will see in the following analysis of this chapter, to realize a von-Neumann-like measurement of flux basis, the presence of decoherence is not the necessary condition.

The purpose of this chapter is to give an analytical treatment to investigate the escape physics of dcSQUID inductively coupled to the flux qubit in the weak couping limit. We will approach the problem by starting with the static experiments, which probe the dependence of the switching current behavior on the applied flux on the qubit [17, 24, 25]. Next, we will generalize our theory by considering the dynamic experiments (especially for "large escape rate" limit where the escape rate is faster than the qubit tunnelling rate) which shows the switching probability oscillation due to the coherent manipulation of qubit state [18]. Among

these investigations, we keep asking how does the current distribution depend on the applied flux on qubit, and what kind of basis does this current switching measurement prefer in various parameter regimes? In addition, to realize a macroscopic projective measurement for testing the temporal Bell inequalities (TBI) [1], we also try to find out the possible ways to perform the flux-basis-preferred projective measurement with our coupled qubit-SQUID composite system in different parameter regimes.

In the next section, we will set up the background information and estimate the related experimental parameters (especially for static experiment); it's helpful to know what the relevant energy scales of our experiment are before analyzing the problem, e.g. the energies listed in increasing order: the escape energy $\Gamma\hbar$ of the dcSQUID, the qubit tunneling energy Δ, the qubit bias energy ε, and the plasma frequency (or excited energy $\omega\hbar$) of dcSQUID. Also, we need to know that the current ramping rate (the increasing rate of dcSQUID bias current) would vary a lot depending on the type of experiments; the typical current ramping rate in static experiment is around 10^3Hz, which can be smaller than any scale above, but in the dynamic experiment it can be larger than the qubit tunneling energy and even be comparable with the plasma frequency of dcSQUID. In Section 3, because the escape dynamics has the smallest energy scale in the static experiment (especially in small escape rate limit where the escape rate is much smaller than the qubit tunneling rate), we drop the cubic term of SQUID potential first and then keep the 'harmonic-like' Hamiltonian such that we find the appropriate eigenbasis of the composite system (i.e. the preferred basis of the measurement) before considering the escape dynamics; that's why we called it 'harmonic' approximation. In the last step, we need to restore the cubic term back to the Hamiltonian after the harmonic approximation for analyzing the escape dynamics of composite system. In the end of the section, we justify our harmonic approximation by comparing the behavior of the theoretical result with the data from the NTT and Delft experiments. Section 4 is the study of escape physics in the dynamic experiments especially for the large escape rate limit where the escape rate is much larger than the qubit tunneling rate. In Section 5, we propose a truncated model, where the dcSQUID spectrum is truncated and only its ground state is kept, to simplify the problem and attempt to use it to approach the results in two different limits described in previous sections. Both analytical and numerical treatment are provided and show a great consistency. Section 6 gives the overall discussion, in which we integrate the answers to the measurement basis problem discussed in the previous sections, analyze how qubit density matrix evolves before SQUID switching to voltage mode, clarify the quantum Zeno and anti-Zeno effect of negative measurement operated by our qubit-SQUID system, investigates how entanglement changes during the measurement, and study the scenario and properties of our measurement in the weak measurement limit etc. Section 7 is the preparation for the next chapter, on testing TBI, in which we investigate the possible ways to perform the flux-basis-preferred projective

measurement with our qubit-SQUID coupled system under different parameter controls. In the end, we will give a brief summary of this chapter. Throughout we work at zero temperature; possible thermal-activation corrections to the zero-temperature WKB tunnelling exponents are estimated at the end of Section 2 and shown to be small for existing experiments. In Appendix B, we confirm the results of Section 3 by an explicit calculation of the energy levels of the coupled system. Appendix C analyzes how the maximum point of current distribution changes with the current ramping rate. In Appendix H, a pictorial way is given to see how entanglement between qubit and dcSQUID changes during the measurement. Appendix I gives the numerical and analytical study of non-adiabatic transition between states due to the rapid current ramping.

In the rest of this section, we will give a brief review of some experimental protocols in the static and dynamic experiments:

In the static measurement of qubit with dcSQUID, people usually ramp up the bias current slowly, e.g. at around 10^3Hz to critical current, record the current when the SQUID switching takes place, and finally give a histogram like switching current distribution as the switching probability distribution after repeated measurements. People can detect the qubit state via analyzing this current distribution, e.g. the measured shift of average switching current can be used to determine the qubit state.

In the dynamic (Rabi oscillations or Ramsey fringe) experiments [18], the ramping rate of bias current I_b is faster than in the static measurement, and I_b usually reaches a definite value at which the averaged switching probability is maintained at 50%. The bias current I_b usually consists of a short pulse followed by a trailing plateau, where the height of short pulse is just equal to the required value for 50% switching probability and the height of the trailing plateau is about 70% of short pulse [26]. The purpose of the trailing plateau is to avoid missing the voltage signal due to the re-trapping of SQUID phase.

In a Rabi experiment, the qubit is initialized to the ground state and then manipulated coherently between the ground state and excited state by applying microwaves of a frequency equal to the energy difference of the qubit states. To obtain the switching probability, we repeat the switching-event detection of applying the current bias pulse right after the microwave operation on qubit. The switching probability is observed to oscillate as a function of the microwave operation time and the oscillation frequency (called the Rabi frequency Ω_r) is proportional to the microwave amplitude, which is the Rabi oscillation phenomenon.

In Ramsey experiment, the qubit's state is initialized and then manipulated coherently by applying two microwave ($\frac{\pi}{2}$) pulses (of a microwave frequency ω equal to the energy difference of the qubit states), where the duration τ of each $\frac{\pi}{2}$ pulse satisfies the equation $\Omega_r\tau = \frac{\pi}{2}$ with Ω_r as the Rabi frequency. By changing the interval t between two $\frac{\pi}{2}$ pulses, we can observe the temporal behavior of Ramsey interference based on the measured switching probability right after the second pulse, where the Ramsey fringe period is $\frac{1}{\delta F}$ for

the microwave frequency detuned from resonance by δF. The function of the first $\frac{\pi}{2}$ pulse is to generate a $\frac{\pi}{2}$ rotation with respect to y-axis in the Bloch sphere (for the ground state being aligned with z-axis) from the ground state and then creates an equal superposition of the qubit energy states. Right after the first pulse, the state starts to precess (relative to z-axis) at a rate ω. If the microwave frequency is detuned from the resonance by δF, it will result in a rotation of state (relative to z-axis) at a rate δF in the rotating frame of the applied microwave; after an interval t, the state will rotate by an angle $t\delta F$ in the rotating frame. Therefore, the components of two states after the second $\frac{\pi}{2}$ pulse (relative to y-axis of rotating frame) will depend on the angle $t\delta F$. That is why we can see the Ramsey interference in time at frequency δF by observed the switching probability.

2.2 The basic analysis of qubit-SQUID coupled system

Let's first introduce our starting model. It is believed that we can give a simplified description of the flux qubit as a two-level system with the two flux states $\{|R\rangle, |L\rangle\}$ and a tunnelling energy Δ between them. The qubit effective Hamiltonian can be represented by the Pauli spin matrices $\sigma_{z,x}$, that is

$$H_q = \varepsilon\sigma_z - \Delta\sigma_x \tag{2.1}$$

with 2ε being the energy difference between two flux states. The relation between ε and the flux Φ_q applied to the qubit is [18, 21]

$$\varepsilon \equiv \varepsilon(f_q) \approx I_p\Phi_0\left(f_q - \frac{1}{2}\right), \tag{2.2}$$

where I_p is the maximum qubit persistent current [28] and we have defined $f_q \equiv \Phi_q/\Phi_0$ and $f_{SQ} \equiv \Phi_{SQ}/\Phi_0$ for flux parameters of the qubit and dcSQUID respectively, where Φ_q and Φ_{SQ} are the corresponding applied fluxes and $\Phi_0 = h/2e$ is the flux quantum.

On the other hand, we can consider the dcSQUID as a system of one degree of freedom x which is the average of the phases of the two junctions [31]. As we have mentioned, the SQUID potential changes with the applied flux Φ_{SQ} and bias current $I_b(t)$, and each qubit state induces a different flux on the SQUID. The total flux on the SQUID will be $\Phi_{SQ} \pm \Phi_M$ depending on which of the qubit states is realized, where $2\Phi_{\mathrm{M}}$ is the net flux difference on the SQUID induced by the qubit states. Denoting by E_{J0} the Josephson energy of a single junction, we can construct our SQUID phase potential, including the effect of the induced

flux from the qubit, as follows:

$$U_0\left(x, f_{SQ}+g\sigma_z\right) = -2E_{J0}\cos\left[\pi f_{SQ}+\pi g\sigma_z\right]\cos\left[x\right] - \left(\frac{\hbar}{2e}\right) I_b\left(t\right) x \tag{2.3}$$

, where we define the dimensionless coupling(or flux) parameter g as $\frac{\Phi_{\mathrm{M}}}{\Phi_0}$. Expanding in terms of the small parameter g, we can rewrite the potential as

$$U_0\left(x, f_{SQ}+g\sigma_z\right) \approx U_0\left(x, f_{SQ}\right) + \varepsilon_{\mathrm{int}}\left(x\right)\sigma_z \tag{2.4}$$

with the coupling energy $\varepsilon_{\mathrm{int}}\left(x\right)$ defined by the formula

$$\varepsilon_{\mathrm{int}}\left(x\right) = 2\pi g E_{J0}\sin\left[\pi f_{SQ}\right]\cos\left[x\right]. \tag{2.5}$$

In the above approximation we have assumed $g \ll 1$, which is additional to the weak coupling assumption that the coupling energy is much smaller than the ground state energy of the dcSQUID.

Considering the potential of Eq.(2.4) together with the SQUID kinetic energy and the qubit Hamiltonian, the total Hamiltonian of the coupled system is

$$H = H_q + H_{SQ} + H_{coupling} \tag{2.6}$$

, where we have

$$H_{\mathrm{SQ}} = \frac{-\hbar^2}{2m}\partial_x^2 - 2E_{J0}\cos\left[\pi f_{SQ}\right]\cos\left[x\right] - \left(\frac{\hbar}{2e}\right) I_b x \tag{2.7}$$

$$H_{\mathrm{coupling}} = \varepsilon_{\mathrm{int}}\left(x\right)\sigma_z. \tag{2.8}$$

Here the effective mass $m \equiv 2C_0\left(\frac{\hbar}{2e}\right)^2$, and C_0 is the capacitance of one junction of the SQUID.

Before applying the WKB decay analysis to our coupled system, we need to make a further approximation to the potential. With a Taylor expansion around the minimum of the well $x = x_0$, where

$$\sin\left[x_0\right] = \frac{\left(\frac{\hbar}{2e}\right) I_b\left(t\right)}{2E_{J0}\cos\left[\pi f_{SQ}\right]} \tag{2.9}$$

, we can approximate the washboard potential $U_0(x, f_{SQ})$ as

$$v(R) = \frac{1}{2}kR^2 - \frac{1}{2}\frac{k}{R_c}R^3. \tag{2.10}$$

Here we have $R = x - x_0$ and

$$k = 2E_{J0}\cos[\pi f_{SQ}]\cos[x_0]. \tag{2.11}$$

The classical turning point is defined by

$$R = R_c = 3\cot[x_0] \tag{2.12}$$

[29]; that is $v(R) > 0$ for $0 < R < R_c$. Besides, we can also approximate the form of $\varepsilon_{\text{int}}(x)$ around x_0, that is

$$\varepsilon_{int}(R) = \pi g \tan[\pi f_{SQ}]\left(k - 3\frac{k}{R_c}R - \frac{k}{2}R^2 + \frac{1}{2}\frac{k}{R_c}R^3\right). \tag{2.13}$$

Finally, we obtain our approximate Hamiltonian

$$H_{approx} = \frac{-\hbar^2}{2m}\partial_R^2 + v(R) + \varepsilon(R)\sigma_z - \Delta\sigma_x \tag{2.14}$$

with the qubit total bias energy $\varepsilon(R) \equiv \varepsilon + \varepsilon_{int}(R)$. The analysis below is based on this approximate Hamiltonian. The first two terms should determine the standard decay physics of SQUID single shot measurement. And near the minimum of the well, the effect of the cubic term of the potential $v(R)$ is relatively small in comparison with the square term, and therefore we can consider our potential as a simple harmonic one with oscillation frequency $\omega = \sqrt{\frac{k}{m}}$, where the corresponding simple harmonic energy levels are $|\mathrm{n}'\rangle$.

In static experiments [17, 24, 25], the bias current I_b usually increases over a time interval long compared to the inverse of the tunnelling rate, so that we can consider the dcSQUID potential changes adiabatically; on each run, as the bias current I_b across the dcSQUID is increased towards its critical value, the value of I_b at which a non-zero voltage drop develops (the switching current I_{SW}) is recorded, and it is the distribution of I_{SW} averaged over many runs which constitutes the raw data of the experiment. In one experiment of this type [17] the Delft group determined the average value of I_{SW} as a function of the flux applied to the qubit,

which determines the ground-state energy and wave function of the latter. In a second such experiment, the NTT group[25] found a pattern of two peaks in the distribution of I_{SW} which cross as a function of the applied flux(the so-called χ-structure, the fig(4a) of Ref. [25]), and interpreted these as corresponding to the switching behaviour for the ground state and excited state of the qubit.

For the experimental setup of NTT group [21], we have the parameters:

πg	~ 0.003
f_{SQ}	0.4
Δ	$1\text{GHz} = 6.6 \times 10^{-25} J$
I_{c0}	$\sim 200nA$
$m \equiv 2C_0 \left(\frac{\Phi_0}{2\pi}\right)^2$	$7.4 \times 10^{-44} Js^2$
$E_{J0} = \frac{\Phi_0 I_{C0}}{2\pi}$	$100GHz = 6.6 \times 10^{-23} J$
$k = 2E_{J0} \cos[\pi f_{SQ}] \cos[x_0]$	$4.1 \times 10^{-23} \cos[x_0]\, J$
$\omega\hbar = \sqrt{\frac{k}{m}}\hbar$	$2.5 \times 10^{-24} \sqrt{\cos[x_0]} J$

The corresponding parameters for the Delft experiment [17] are:

πg	~ 0.005
f_{SQ}	0.76
Δ	$0.33GHz = 2.2 \times 10^{-25} J$
I_{c0}	$\sim 110nA$
$m \equiv 2C_0 \left(\frac{\Phi_0}{2\pi}\right)^2$	$1.3 \times 10^{-46} Js^2$
$E_{J0} = \frac{\Phi_0 I_{C0}}{2\pi}$	$3.6 \times 10^{-23} J$
$k = 2E_{J0} \cos[\pi f_{SQ}] \cos[x_0]$	$5.3 \times 10^{-23} \cos[x_0]\, J$
$\omega\hbar = \sqrt{\frac{k}{m}}\hbar$	$6.7 \times 10^{-23} \sqrt{\cos[x_0]} J$

Before analysing the physics of our system, we can briefly estimate the expectation value of the coupling energy based on the ground state wave function of the harmonic well, which is $\langle 0' | \varepsilon_{int}(R) | 0' \rangle \sim 10^{-25} J$. It is of the same order of magnitude as the qubit tunnelling energy, but much smaller than the zero point energy of the dcSQUID:

$$\begin{array}{c} \omega\hbar \\ \left(10^{-24} J \sim 10^{-23} J\right) \end{array} \gg \begin{array}{c} \Delta \\ \left(\sim 10^{-25} J\right) \end{array} \cong \begin{array}{c} \langle 0' | \varepsilon_{\text{int}}(R) | 0' \rangle \\ \left(\sim 10^{-25} J\right). \end{array}$$

In comparison with these energy scales, the estimated dcSQUID escape rate in static experiments($\Gamma\hbar \sim 10^{-26} J$ for the bias current I_b around the value which gives the maximum switching probability of dc-SQUID(based on Eq.2.29)) has the smallest energy among them. Here we estimated $\Gamma\hbar$ by the formula

$$\Gamma = \omega 60^{1/2} \left(\frac{B}{2\pi\hbar}\right)^{1/2} \exp -[(B/\hbar)\left(1 + \frac{0.87}{Q}\right)]. \tag{2.15}$$

, where B $=\frac{8}{15}m\omega R_c^2$ is the decay bounce action and $Q=\omega R_s C_0$ is the damping factor with net resistance R_s [30]. As a result, we can ignore the escape effect in some steps by considering its relatively small energy scale, which can help us to simplify the analysis of qubit-SQUID system in the next section. We note in passing that the thermally activated escape rate $\Gamma_T\hbar$ [27] is of order $10^{-55}J$, which is negligibly small. Thus, it is adequate to consider only zero-temperature WKB tunnelling in our analysis.

2.3 The Harmonic approximation for decay dynamics of qubit-SQUID system in static experiments

Because the decay dynamics has the smallest energy scale in static experiment, the behaviour of the harmonic kernel is believed to dominate most of the properties of the wave function of the coupled system. It will simplify the analysis if we can ignore the decay process for a moment. What we want to do is to try to approximately diagonalize the system in the ground state (at least within the harmonic region of potential) before we really take the decay physics into account.

Therefore, the first step is to to drop the cubic terms of the potential:

$$v\left(R\right) \rightarrow v^H\left(R\right)=\frac{1}{2}kR^2 \tag{2.16}$$

$$\varepsilon\left(R\right) \rightarrow \varepsilon^H\left(R\right)=\varepsilon+\pi g\tan\left[\pi f_{SQ}\right]\left(k-3\frac{k}{R_c}R-\frac{k}{2}R^2\right) \tag{2.17}$$

Then we can get a new simple-harmonic-approximate Hamiltonian, namely

$$H^H = \frac{-\hbar^2}{2m}\partial_R^2+v^H\left(R\right)+\varepsilon^H\left(R\right)\sigma_z-\Delta\sigma_x. \tag{2.18}$$

This Hamiltonian will be helpful for us to determine the system's behaviour within the harmonic region of the potential.

According to our previous analysis of the energy scales, the ground state expectation value of the last two terms in H^H is much smaller than the ground state energy of the harmonic well. Therefore, we may treat these two terms by a perturbation analysis. On the other hand, we have assumed that the system always starts from the lowest simple harmonic state of the well, in order to follow the traditional WKB decay analysis.

Once we rewrite our Hamiltonian in harmonic form H^H, the next step is to change our representation into the new spin basis that is determined by diagonalization of the ground state expectation value of

perturbation term $\langle 0'|\,\varepsilon(R)\,\sigma_z - \Delta\sigma_x\,|0'\rangle$, where $|0'\rangle$, as we defined in last section, is the simple harmonic ground state at minimum of the SQUID potential. The relations between new and old Pauli matrix are $\tau_z = \cos\chi\sigma_z + \sin\chi\sigma_x$ and $\tau_x = -\sin\chi\sigma_z + \cos\chi\sigma_x$, where the angle is defined by

$$\sin\chi = \frac{-\Delta}{\sqrt{\varepsilon_{00}^{H2} + \Delta^2}},\ \cos\chi = \frac{\varepsilon_{00}^{H}}{\sqrt{\varepsilon_{00}^{H2} + \Delta^2}} \tag{2.19}$$

with the definition $\varepsilon_{00}^{H} \equiv \langle 0'|\,\varepsilon^{H}(R)\,|0'\rangle$.

After rewriting our Hamiltonian in the new spin basis, we can rearrange it in the following form:

$$H^H = \frac{-\hbar^2}{2m}\partial_R^2 + v^H(R) + \left(\varepsilon^H(R)\cos\chi - \Delta\sin\chi\right)\tau_z - \left(\varepsilon^H(R)\sin\chi + \Delta\cos\chi\right)\tau_x \tag{2.20}$$

In this new representation, the Hamiltonian can be divided into two parts; one is the off diagonal part $V^H = -\left(\varepsilon^H(R)\sin\chi + \Delta\cos\chi\right)\tau_x$, and the rest is the diagonal part H_d^H. The diagonal part describes the physics of two independent harmonic channels with different spring constants; their eigenstates are denoted as $\left|n'_-\right\rangle$ and $\left|n'_+\right\rangle$. The off diagonal part now can be considered as new perturbation term instead, and its perturbative correction to the eigenenergy of two harmonic channels can be evaluated with $2\delta\omega\hbar$ being the energy difference between two states $\left|0'_-\right\rangle$ and $\left|0'_+\right\rangle$, where the dominate term is $\frac{\left|\left\langle 0'_+\right|V^H\left|0'_-\right\rangle\right|^2}{[2\delta\omega\hbar]} \cong (\omega\hbar)\,\frac{g^5}{1024}\tan^5[\pi f_{SQ}]\cos\chi\sin^2 2\chi \sim 10^{-34}J$, see appendix A. Therefore, this perturbation correction to the eigenenergy is much smaller than the decay energy scale of the SQUID near the maximum of switching probability, so that we will neglect this off diagonal term in the following discussion.

The last step is to restore the cubic terms in the SQUID potential and the coupling energy, that is to replace $v^H(R)$ and $\varepsilon^H(R)$ by $v(R)$ and $\varepsilon(R)$ respectively in the diagonal part of H^H. Finally, we have the kernel Hamiltonian which describe the dominant physics of the system:

$$\begin{aligned} H_d &= \frac{-\hbar^2}{2m}\partial_R^2 + v(R) + \left(\varepsilon(R)\cos\chi - \Delta\sin\chi\right)\tau_z \\ &= \begin{pmatrix} H_+ & 0 \\ 0 & H_- \end{pmatrix} \end{aligned} \tag{2.21}$$

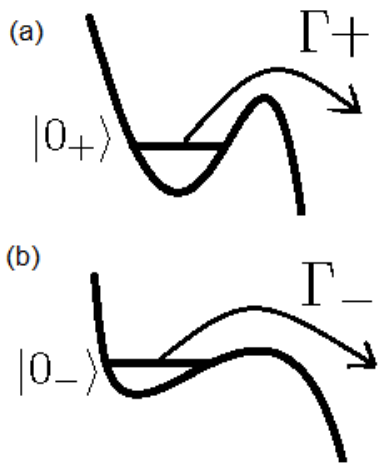

Figure 2.3: The two possible escape ways corresponding to two qubit states $|+\rangle$ and $|-\rangle$ are shown in (a) and (b) where two SQUID potentials have different ground states($|0_+\rangle$ and $|0_-\rangle$) and independent escape rates ($\Gamma+$ and Γ_-).

, here we have $H_\pm = \frac{-\hbar^2}{2m}\partial_R^2 + k_0^\pm + \frac{1}{2}\overline{k}_\pm R^2 - \frac{1}{2}\frac{\overline{k}_\pm}{\overline{R}_{c\pm}}R^3$ and parameters given by:

$$\begin{aligned}
\overline{k}_\pm &\equiv k\left(1 \pm \pi g \cos\chi \tan\left[\pi f_{SQ}\right]\left(1 + \left(\tfrac{3}{R_c}\right)^2\right)\right) \\
\overline{R}_{c\pm} &\equiv R_c\left(1 \pm \left(\tfrac{3}{R_c}\right)^2 \pi g \cos\chi \tan\left[\pi f_{SQ}\right]\right) \\
k_0^\pm &= \mp\left(\sqrt{\varepsilon_{00}^{H2} + \Delta^2} + \tfrac{\pi g}{4}\omega\hbar \tan\left[\pi f_{SQ}\right]\cos\chi\right).
\end{aligned} \tag{2.22}$$

Based on Eq.(2.21), we can clearly see that H_+ and H_- describe two independent decay channels (for spin+ and spin $-$) respectively. Therefore, we simplify the escape dynamics of qubit-dcSQUID composite system by the two-channel decay dynamics where each channel has its own ground state and the corresponding conventional escape rate (as shown in Fig. 2.3); the composite system can be in superposition of these ground states.

The corresponding oscillation frequency and bounce actions are

$$\omega_\pm = \sqrt{\frac{\overline{k}_\pm}{m}} \simeq \omega \pm \delta\omega. \tag{2.23}$$

$$B_\pm = B \cdot \left(\frac{\omega_\pm \overline{R}_{c\pm}^2}{\omega R_c^2}\right) \tag{2.24}$$

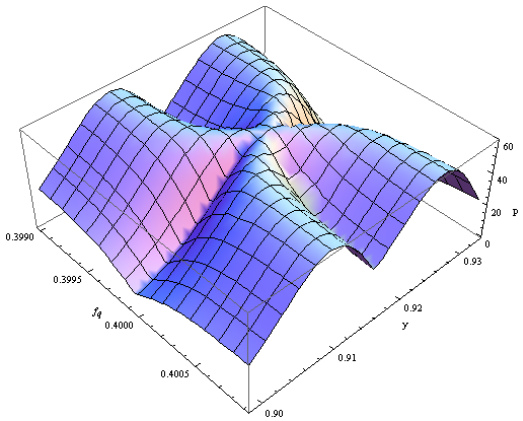

Figure 2.4: The calculated switching current probability corresponding to the ground state and excited state in the NTT group's set-up. Here the X-axis and Y-axis represent the applied flux f_q and current parameter $y \equiv I_b/2I_{C0}\cos\pi f$ respectively. We can see two clear ridges crossing one another, where each ridge structure corresponds to escape-probability behaviour for flux qubit being in either the ground state or excited state; this χ-cross structure was shown in NTT's experiments(i.e. Fig.4(a) of [25]) with ground and excited states being in thermal distribution.

Here we have

$$\delta\omega \simeq \frac{\pi g}{2}\omega\cos\chi\tan\left[\pi f_{SQ}\right]\left(1+\left(\frac{3}{R_c}\right)^2\right) \tag{2.25}$$

.

With the use of Eq.(2.15),(2.23), and(2.24), we can easily derive the decay rate of two spin channels:

$$\begin{aligned}\Gamma_\pm &= \omega_\pm 60^{1/2}\left(\frac{B_\pm}{2\pi\hbar}\right)^{1/2}\exp-\left[\left(B_\pm/\hbar\right)\left(1+\frac{0.87}{Q_\pm}\right)\right] \\ &= \Gamma\left(\frac{\omega_\pm}{\omega}\right)\left(\frac{B_\pm}{B}\right)^{1/2}\exp-\left[\frac{B}{\hbar}\left(\left(\frac{\omega_\pm\overline{R}_{c\pm}^2}{\omega R_c^2}-1\right)+\frac{0.87}{Q}\left(\frac{\overline{R}_{c\pm}^2}{R_c^2}-1\right)\right)\right]\end{aligned} \tag{2.26}$$

With the further approximation of keeping only the first order of $\delta\omega$ and δR_c for $\omega_\pm, B_\pm$, and $\overline{R}_{c\pm}$, we have

$$\Gamma_\pm \simeq \Gamma\left(1\pm\frac{3}{2}\frac{\delta\omega}{\omega}\pm\frac{\delta R_c}{R_c}\right)\exp\mp\frac{B}{\hbar}\left(\frac{\delta\omega}{\omega}+2\left(1+\frac{0.87}{Q}\right)\frac{\delta R_c}{R_c}\right). \tag{2.27}$$

Here

$$\delta R_c \equiv \pm\left(\overline{R}_c^{\pm}-R_c\right)=\frac{9\pi g}{R_c}\cos\chi\tan\left[\pi f_{SQ}\right] \tag{2.28}$$

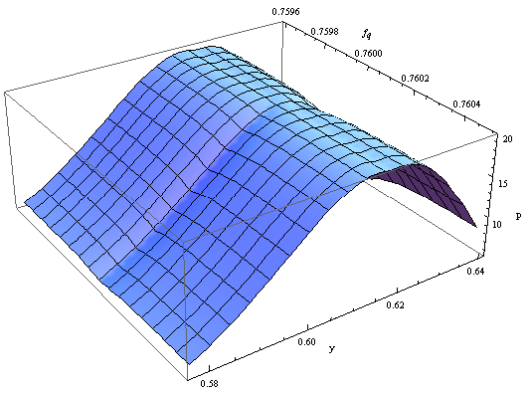

Figure 2.5: The switching current probability in the experiment of the Delft group calculated from our formula. Here we can't clearly see the flux dependence of the ground and excited states.

.

Together with the assumption that the state of the coupled system evolves adiabatically with the change of bias current, we can use the formula

$$P_{\pm}(y) = \frac{\Gamma_{\pm}(y)}{dy/dt} \exp\left[-\frac{1}{dy/dt}\int_0^y \Gamma_{\pm}(y')\,dy'\right] \tag{2.29}$$

to determine the switching current probabilities for the ground and excited states of the flux qubit. Here $y(t) \equiv \frac{I_b(t)}{2I_{C0}\cos\pi f_{SQ}}$ is the current parameter, and $I_{C0} = \frac{2e}{\hbar}E_{J0}$ is the critical current of each junction on the dcSQUID. We will assume that in static experiments of the type conducted in Refs [25] and [17] the ramping rate lies in the range $\sim 10^3 - 10^5 Hz$. The calculated results for the experiments of the NTT [25] and Delft groups [17] are shown in the Fig.2.4 and 2.5 respectively. In the limit where $\frac{B}{\hbar}\left(\frac{\delta\omega}{\omega}\right), \frac{B}{\hbar}\left(1+\frac{0.87}{Q}\right)\left(\frac{\delta R_c}{R_c}\right) \ll 1$, (thr condition satisfied in most experiments), we have the further approximate formula for the decay rate difference

$$\frac{|\Gamma_+ - \Gamma_-|}{\Gamma} \simeq 2\left(\frac{B}{\hbar}-\frac{3}{2}\right)\frac{\delta\omega}{\omega} + 2\left(\frac{2B}{\hbar}\left(1+\frac{0.87}{Q}\right)-1\right)\frac{\delta R_c}{R_c}. \tag{2.30}$$

From this equation, roughly we can see that there are two ways to make the decay rate difference larger(to the point that the switching distributions of the two qubit energy states are distinguishable from one another); one is to have the coupling g large so as to give large ratios $\frac{\delta\omega}{\omega}$ and $\frac{\delta R_c}{R_c}$, which corresponds to pushing the two current distributions apart, and the other one is to make a larger bounce action $\frac{B}{\hbar}$ (or reduce the factor Q. But in order to simplify the analysis, we put the discussion of Q factor into footnote [42]), which increases the resolution of the measurement by reducing the width of the switching current distribution. According to the above analysis, if we want the ground state flux-dependent switching current distribution to be easily

distinguishable from the excited one, as shown by the crossing feature in FIG.2.4, a large capacity C_0 and Josephson coupling energy E_{J0} is needed to increase B (since $\frac{B}{\hbar} \propto \sqrt{C_0 E_{J0} \cos \pi f_{SQ}}$.) That's why the NTT experiment, with its large values of C_0 and E_{J0}, can show two distinct current distributions for qubit's eigen states.

From Eqns.(20), (23), and(2.30), we know that the escape rate difference is also proportional to $\cos \chi = \frac{\varepsilon_{00}^H}{\sqrt{\varepsilon_{00}^{H2}+\Delta^2}}$. The explicit formula for ε_{00}^H is

$$\begin{aligned} \varepsilon_{00}^H &= \varepsilon + \langle 0' | \varepsilon_{int}(R) | 0' \rangle \\ &= I_p \Phi_0 \left(f_q - \frac{1}{2} \right) + \pi g k \tan [\pi f_{SQ}] \left(1 - \frac{\omega \hbar}{4k} \right). \end{aligned} \tag{2.31}$$

If we consider ε_{00}^H as the total qubit bias energy for the qubit-SQUID coupled system, then here we can see that the expectation value of coupling energy $\langle 0' | \varepsilon_{int}(R) | 0' \rangle$ also contributes to it. In other words this coupling energy effectively induce a phase(or flux) deviation on qubit, which can change with the bias current and is non-zero even if there is no bias current. The estimated flux deviation on qubit(for the Delft group) is $\delta f_q = \frac{\pi g k}{I_p \Phi_0} \tan [\pi f_{SQ}] \left(\frac{\omega \hbar}{4k} - 1 \right) = 0.00049$. Although this phase deviation is much smaller than what is due to the appearance of SQUID circulating current right after switching on bias current($\delta f_q = 0.005$) [18], we still need to consider the corresponding coupling energy in the effective qubit bias energy ε_{00}^H because $\cos \chi$ is directly determined by the ratio between ε_{00}^H and the qubit tunnelling energy Δ.

Another physics aspect behind our harmonic-approximation analysis can be understood as follows. It is well known that a convenient approach to evaluate quantum decay is to utilize the current-density-type formula

$$\Gamma = J(R) \Big/ \int_{-\infty}^{R} dR' \left| \psi(R') \right|^2 \tag{2.32}$$

Here we have $J(R) = (\hbar/m) \, \mathrm{Im} \psi_{out}^* \frac{\partial \psi_{out}}{\partial R}$ being the outgoing probability current near the turning point R_c and $\int_{-\infty}^{R} dR' \left| \psi(R') \right|^2$ as the normalization factor [30].

Because the harmonic wave function around the minimum of the potential dominates the outgoing wave function ψ_{out} near R_c in the quasi-classical approximation, the quantum decay is totally controlled by the wave function within the harmonic region. Therefore, once we find an appropriate basis to effectively diagonalize the harmonic part of the Hamiltonian into two escape channels(where the minimized tunnelling energy between the channels is negligible compared to escape energy), we may consider the escape dynamics separately in the two channels. A more comprehensive way to evaluate the energy levels of the composite

system in a perturbation approximation is given in the appendix B, which also gives a improvement of our harmonic approximation near the critical current.

In this section we have discussed the escape dynamics in the small escape rate limit and realize that the coupled system prefer to escape as energy state or the escape rates are different by energy states instead of flux states, which help us to give the main conclusion that our measurement of qubit can behave as an energy-basis projective measurement in the small escape rate limit. Under this circumstance, the possible way to make it as flux-basis measurement is to let the energy basis approach the flux basis by setting $\cos\chi \to 1$. Otherwise, for flux-basis measurement, we need to consider another limit where the escape rate is much larger than the qubit tunnelling energy($\Gamma\hbar \gg \Delta$), which will be discussed in the next section.

Before we end the section, it may worth to keep in mind that the current of maximum point of switching probability always increase with the current ramping rate; please see appendix C for the detailed analysis. This property of switching probability will be helpful in the following analysis.

2.4 Large escape rate limit and the dynamic experiments

In the dynamic experiments the current ramping time can be less than $5ns$, which means that the required escape rate should be much larger than $0.2GHz$ [32]. Consequently the escape energy of SQUID can be comparable to or larger than the qubit tunnelling energy and our harmonic approximation in previous section would not work correctly. It's inevitable to consider the large escape rate limit in the dynamic experiment.

As we will see in the following analysis, in the large escape rate limit of the dcSQUID ($\Gamma\hbar \gg \Delta$), the measurement of qubit can behave as a projective measurement onto flux basis instead of energy eigenbasis, which is different from our previous analytical result of the harmonic approximation for small escape rate($\Gamma\hbar \ll \Delta$).

Let's simplify the problem by considering the time evolution operator $e^{-iHt/\hbar}$ for the coupled system with Hamiltonian $H = H_0 - \Delta\sigma_x$ given by Eq.(2.6), in which the H_0 is the diagonal part of H in spin representation and the corresponding eigenstates are $|n_L, L\rangle$, $|n_R, R\rangle$, i.e., $H_0 |n_L, L\rangle = E_{n_L} |n_L, L\rangle$ and $H_0 |n_R, R\rangle = E_{n_R} |n_R, R\rangle$. Here R and L represent the qubit flux states; $|n_L\rangle$ and $|n_R\rangle$ are the corresponding SQUID wave functions. In principle, we allow the eigenenergies E_{n_L} and E_{n_R} to contain small imaginary part as escape energy $\Gamma_{n_L}(\ll |E_{n_L}|)$ and $\Gamma_{n_R}(\ll |E_{n_R}|)$ respectively. Next, we will take the qubit tunnelling term $\Delta\sigma_x$ as perturbation for the large escape limit ($\Gamma_{n_R}, \Gamma_{n_L} \gg \Delta$). Besides, we also assume the SQUID always starts with its two lowest energy levels $|0_L, L\rangle$) and $|0_R, R\rangle$, and the state $|0_\sigma, \sigma\rangle$ ($\sigma \in \{R, L\}$) evolves to itself respectively if there is no presence of tunnelling between two qubit flux states during the time evolution . According to above arguments, the approximated matrix elements of the time evolution

operator can be derived.

$$\langle 0_{\sigma'}, \sigma' |\, e^{-iHT/\hbar} \,|0_{\sigma}, \sigma\rangle = \langle 0_{\sigma'}, \sigma' |\, e^{-i(H_0 - \Delta\sigma_x)T/\hbar} \,|0_{\sigma}, \sigma\rangle$$

$$= \begin{pmatrix} e^{-iE_{0L}T/\hbar}(1+D_L) & e^{-i\frac{(E_{0L}+E_{0R})T}{2\hbar}} \frac{\Delta 2i\langle 0_L \,|0_R\rangle}{(E_{0R}-E_{0L})} \sin\left(\frac{(E_{0R}-E_{0L})T}{2\hbar}\right) \\ e^{-i\frac{(E_{0L}+E_{0R})T}{2\hbar}} \frac{\Delta 2i\langle 0_R \,|0_L\rangle}{(E_{0L}-E_{0R})} \sin\left(\frac{(E_{0L}-E_{0R})T}{2\hbar}\right) & e^{-iE_{0R}T/\hbar}(1+D_R) \end{pmatrix} \tag{2.33}$$

Here we have $\sigma', \sigma \in \{R, L\}$ and take D_σ as the higher order Δ expansion of the diagonal term (with $\sigma'' \neq \sigma$).

$$D_\sigma = |\langle 0_\sigma \,|0_{\sigma''}\rangle|^2 \left(\frac{i\Delta}{\hbar}\right)^2 \frac{\hbar}{i\left(E_{0\sigma''} - E_{0\sigma}\right)} \left(T - \frac{\hbar\left(e^{-i\left(E_{0\sigma''}-E_{0\sigma}\right)T/\hbar} - 1\right)}{-i\left(E_{0\sigma''} - E_{0\sigma}\right)}\right) + O\left(\Delta^4\right) \tag{2.34}$$

Please see appendix D for the detail derivation of these formulas.

Based on the matrix form of the time evolution operator, the existence of the off diagonal matrix element simply implies the qubit flux basis is not the eigenbasis of the coupled system and we expect the escape rate for eigenbasis of coupled system should stay between Γ_{0R} and Γ_{0L} according to the time dependence of the off diagonal element, i.e. $2ie^{-i(E_{0L}+E_{0R})T/2\hbar}\sin\left(\left(E_{0L}-E_{0R}\right)T/2\hbar\right) = e^{-iE_{0L}T/\hbar} - e^{-iE_{0R}T/\hbar}$, though we can not give an appropriate analytical formula for eigenbasis of coupled system. Besides, because the off diagonal element of the time evolution operator is proportional to $\frac{\Delta}{\left(E_{0\sigma'}-E_{0\sigma}\right)}$, if we make $|E_{0\sigma'} - E_{0\sigma}| \gg \Delta$ then we can properly eliminate the off diagonal elements such that the states $|0_R, R\rangle$ and $|0_L, L\rangle$ can decay independently and respectively with the rates Γ_{0R} and Γ_{0L}, and we can claim our escape process works as an flux-state projective measurement[33]. Basically, there are two extreme cases of making $|E_{0\sigma'} - E_{0\sigma}| \gg \Delta$. The first one is to enlarge the real part of $E_{0\sigma'} - E_{0\sigma}$ and it's equivalent to increasing the effective bias energy of qubit, which can be realize by strong qubit-SQUID coupling and the large deviation of applied flux on qubit. Similar to the argument in the last section, the energy basis of qubit behaves as the flux basis in the limit of large qubit bias energy and hence the our measurement can become a flux-basis measurement. The second case for performing a flux-basis measurement is to have $\mathrm{Im}\left(E_{0\sigma'} - E_{0\sigma}\right)$(or $|\Gamma_{0\sigma'} - \Gamma_{0\sigma}|\,\hbar$) much larger than Δ, and it can be realized by strong qubit-SQUID coupling strength and large escape rate reached by fast bias current ramp. In principle, especially in dynamic experiments, the escape rate difference between two qubit flux states can reach at least 1GHz [32], therefore the flux-basis projective measurement can exist for qubit tunnelling energy below 0.1GHz. Usually the real part and imaginary part of $E_{0\sigma'} - E_{0\sigma}$ can not

be zero simultaneously. Therefore the condition of

$$\frac{\Delta}{|E_{0\sigma'} - E_{0\sigma}|} \ll 1 \tag{2.35}$$

is a more general one for realizing the flux-basis projective measurement with our coupled system.

On the other hand, if we consider our formula of time evolution operator in the limit of very small coupling (where the coupling energy between qubit and dcSQUID is much smaller than qubit tunneling energy Δ and SQUID ground state energy $\frac{\omega\hbar}{2}$) and the limit of very small escape rate ($\Gamma\hbar \to 0$ faster than other energy scales in the experiment), where the very small coupling guarantee $|\langle n_\sigma, \sigma \, | n'_{\sigma'}, \sigma' \rangle| = 0$ for $n \neq n'$ and the very small escape rate guarantee $\langle n_\sigma, \sigma | \, e^{-iH_0 T/\hbar} \, | n'_\sigma, \sigma \rangle = 0$ for $n \neq n'$, we can restore the orthogonal and completeness properties of eigenstates and extrapolate the time evolution operator to a simpler form:

$$\begin{aligned} &\langle 0_{\sigma'}, \sigma' | \, e^{-i(H_0 - \Delta\sigma_x)T/\hbar} \, | 0_\sigma, \sigma \rangle \to e^{-i\left(\frac{(E_{0L}+E_{0R})}{2} + \frac{(E_{0L}-E_{0R})}{2}\sigma_z - \Delta\sigma_x\right)T/\hbar} \\ &= e^{-i\left(\frac{(E_{0L}+E_{0R})}{2} + \frac{\left(E'_{0+}-E'_{0-}\right)}{2}\tau'_z\right)T/\hbar} \end{aligned} \tag{2.36}$$

Here we have diagonalized and rewrote it in terms of new Pauli matrices τ'_z in the last equality. Besides, E'_{0+} and E'_{0-} are the eigenenergies of coupled system after diagonalization and both of them have very small imaginary part $\Gamma'_{0+}\hbar$ and $\Gamma'_{0-}\hbar$ in the zero escape limit, which are similar to $\Gamma_{0L}\hbar$ and $\Gamma_{0R}\hbar$ of E_{0L} and E_{0R}. It's not hard to derive

$$E'_{0+} + E'_{0-} = E_{0L} + E_{0R} \tag{2.37}$$

and

$$\frac{\Gamma'_{0+} - \Gamma'_{0-}}{\Gamma_{0L} - \Gamma_{0R}} = \frac{\mathbf{Im}\left(E'_{0+} - E'_{0-}\right)}{\mathbf{Im}\left(E_{0L} - E_{0R}\right)} = \frac{\varepsilon'}{\sqrt{\varepsilon'^2 + \Delta^2}}. \tag{2.38}$$

Here we define

$$\varepsilon' \equiv \mathbf{Re}\frac{(E_{0L} - E_{0R})}{2} \tag{2.39}$$

and consider it as the effective bias energy of the qubit, which is similar to the place of Eq.(2.31) in Harmonic approximation. According to Eq.(2.38), the escape rate difference between two energy states of coupled

system should be smaller than the escape rate difference for two qubit flux states, and their ratio is equal to $\frac{\varepsilon'}{\sqrt{\varepsilon'^2+\Delta^2}}$, which is totally consistent with our previous result of harmonic approximation (or Eq.(2.30)). This give us another evidence that the system tends to escape as energy state in the small escape rate limit($\Gamma \ll \Delta/\hbar$).

2.5 The truncated model

Actually, there is a simpler way to deal with escape physics of qubit-SQUID coupled system which may make the connection between the physics in both small escape limit and large escape limit. Similar to the last section, let's consider the Hamiltonian in Eq.(2.6) as $H = H_0 + \Delta\sigma_x$, in which the $H_0 = H_0(I_b)$ is the diagonal part of H in spin representation and the corresponding eigenstates are $|n_L, L\rangle$, $|n_R, R\rangle$, i.e. $H_0|n_L, L\rangle = E_{n_L}|n_L, L\rangle$ and $H_0|n_R, R\rangle = E_{n_R}|n_R, R\rangle$. Here R and L represent the qubit flux states; $|n_L\rangle = |n_L(I_b)\rangle$ and $|n_R\rangle = |n_R(I_b)\rangle$ are the corresponding SQUID wave functions and change with bias current. In principle, we allow the eigenenergies $E_{n_L} = E_{n_L}(I_b)$ and $E_{n_R} = E_{n_R}(I_b)$ to contain small imaginary part as escape energy $\hbar\Gamma_{n_L}(\ll |E_{n_L}|)$ and $\hbar\Gamma_{n_R}(\ll |E_{n_R}|)$ respectively, where $\hbar\Gamma_{n_{L,R}}$ also change with bias current I_b. Next, we will truncate the spectrum of the H_0 by considering only ground states $|0_L, L\rangle$ and $|0_R, R\rangle$, then any wave function $|\chi\rangle$ of coupled system can be decomposed into these two basis, that's $|\chi\rangle = a(t)|0_L, L\rangle + b(t)|0_R, R\rangle$. On the other hand, if we turn off the qubit tunnelling Δ in Eq.(2.22) we can derive corresponding parameters for L state and R state, i.e.

$$\begin{aligned}
k_{L,R} &\equiv k\left(1 \pm \pi g \tan[\pi f_{SQ}]\left(1 + \left(\tfrac{3}{R_c}\right)^2\right)\right) \\
R_{c_{L,R}} &\equiv R_c\left(1 \pm \left(\tfrac{3}{R_c}\right)^2 \pi g \tan[\pi f_{SQ}]\right) \\
k_0^{L,R} &= \mp\left(\varepsilon_{00}^H + \tfrac{\pi g}{4}\omega\hbar \tan[\pi f_{SQ}]\right). \\
&= \mp\left(\pi g k \tan[\pi f_{SQ}]\left(1 - \tfrac{\omega\hbar}{4k}\right) + \tfrac{\pi g}{4}\omega\hbar \tan[\pi f_{SQ}] + \varepsilon\right). \\
&= \mp\left(\pi g k \tan[\pi f_{SQ}] + \varepsilon\right).
\end{aligned} \tag{2.40}$$

Based on these parameters, we can rewrite H_0 with this energy-truncated spin representation, which gives

$$\begin{pmatrix} E_{0L} & 0 \\ 0 & E_{0R} \end{pmatrix} = \begin{pmatrix} k_0^L + \frac{\omega_{0L}}{2}\hbar - \frac{i\hbar\Gamma_{0L}}{2} & 0 \\ 0 & k_0^R + \frac{\omega_{0R}}{2}\hbar - \frac{i\hbar\Gamma_{0R}}{2} \end{pmatrix}. \tag{2.41}$$

Here $k_0^{L,R} = k_0^{L,R}(I_b)$ represents for the energy shift of potential minimum, which is contributed by the qubit original bias energy ε and the constant term of the qubit-SQUID coupling formula in Eq.(2.13).

Besides, the qubit-SQUID coupling also changes the shape of the potential; therefore it gives $k_{L,R} = k_{L,R}(I_b)$ and $R_{c_{L,R}} = R_{c_{L,R}}(I_b)$ such that the plasma frequencies $\omega_{0L}(I_b)$ and $\omega_{0R}(I_b)$ also change with R and L flux states. All these parameters are bias current dependent. In sum, the qubit-SQUID coupling can change the energy levels in two ways. The first one is to shift the minimum of the potential well, which gives the same change on each energy level. The second one is to change the shape of the potential, that changes each energy level differently.

Besides, as we know the minimum of the potential for the two flux channels can also be adjusted by ε(given in Eq.(2.1)). Accordingly we can engineer the ground state energies of two channels to be identical by controlling ε though the two channel's escape rates may not be the same. Because the identical ground state energy already implies zero effective bias energy in our truncated model, i.e. $\delta\varepsilon \equiv (k_{0L} - k_{0R}) + \hbar(\omega_{0L} - \omega_{0R})/2 = 0$, we can construct a truncated model with zero effective bias but different escape rates for two channels at any I_b, which will be useful in our following numerical analysis.

After taking Eq.(2.41) and the corresponding off diagonal term $\begin{pmatrix} 0 & -\Delta\langle 0_L|\, 0_R\rangle \\ -\Delta\langle 0_R|\, 0_L\rangle & 0 \end{pmatrix}$ into account, we finally have the simplified Schrdinger equation of the coupled system:

$$\begin{pmatrix} E_{0L} & -\Delta\langle 0_L|\, 0_R\rangle \\ -\Delta\langle 0_R|\, 0_L\rangle & E_{0R} \end{pmatrix} \begin{pmatrix} a_1 \\ a_2 \end{pmatrix} = i\hbar \frac{d}{dt} \begin{pmatrix} a_1 \\ a_2 \end{pmatrix} \tag{2.42}$$

If the current ramping rate is not too fast we can solve it as standard eigenvalue problem in which we always can find the transfer matrix U to have

$$U \begin{pmatrix} E_{0L} & -\Delta\langle 0_L \mid 0_R\rangle \\ -\Delta\langle 0_R \mid 0_L\rangle & E_{0R} \end{pmatrix} U^{-1} = \begin{pmatrix} E_+ & 0 \\ 0 & E_- \end{pmatrix} \tag{2.43}$$

, which gives

$$\begin{pmatrix} E_+ & 0 \\ 0 & E_- \end{pmatrix} U \begin{pmatrix} a_1 \\ a_2 \end{pmatrix} = \frac{d}{dt} U \begin{pmatrix} a_1 \\ a_2 \end{pmatrix}$$

and

$$E_\pm = \frac{1}{2}(E_{0L} + E_{0R}) \pm \frac{1}{2}\sqrt{(E_{0L} - E_{0R})^2 + (2\Delta\,|\langle 0_L \mid 0_R\rangle|)^2}$$

As we has mentioned, the current ramping rate is relative slow then we don't need to consider the time derivative of U. Here U is the general transfer matrix which is complex and not unitary but it has inverse operator U^{-1}

$$\mathrm{Im}\left(E_+ - E_-\right) = -\frac{1}{\sqrt{2}}\left(\sqrt{\left(\delta\varepsilon^2 - \hbar^2\delta\Gamma^2 + 4|\langle 0_L \mid 0_R\rangle|^2\Delta^2\right)^2 + \left(2\hbar\delta\varepsilon\delta\Gamma\right)^2}\right.$$
$$\left. - \left(\delta\varepsilon^2 - \hbar^2\delta\Gamma^2 + 4|\langle 0_L \mid 0_R\rangle|^2\Delta^2\right)\right)^{1/2} \tag{2.44}$$

$$\mathrm{Re}\left(E_+ - E_-\right) = \frac{1}{\sqrt{2}}\left(\sqrt{\left(\delta\varepsilon^2 - \hbar^2\delta\Gamma^2 + 4|\langle 0_L \mid 0_R\rangle|^2\Delta^2\right)^2 + \left(2\hbar\delta\varepsilon\delta\Gamma\right)^2}\right.$$
$$\left. + \left(\delta\varepsilon^2 - \hbar^2\delta\Gamma^2 + 4|\langle 0_L \mid 0_R\rangle|^2\Delta^2\right)\right)^{1/2} \tag{2.45}$$

Here we have $\delta\varepsilon \equiv \left(k_{0L} - k_{0R}\right) + \hbar\left(\omega_{0L} - \omega_{0R}\right)/2$ and $\delta\Gamma = \Gamma_{0L} - \Gamma_{0R}$. In particular, in the small escape limit we can derive

$$\mathrm{Im}\left(E_+ - E_-\right) = \frac{-\delta\varepsilon/2}{\sqrt{(\delta\varepsilon/2)^2 + \Delta'^2}}\delta\Gamma = -\cos\chi\delta\Gamma \tag{2.46}$$

with $\Delta' = \Delta\left|\langle 0_L \mid 0_R\rangle\right|$. This result is very consistent with our Harmonic approximation for the small escape limit(see Eq.(2.30)). And it can be understood as follows. Suppose we can approximately diagonalize the truncated Hamiltonian $\begin{pmatrix} E_{0L} & -\Delta\langle 0_L \mid 0_R\rangle \\ -\Delta\langle 0_R \mid 0_L\rangle & E_{0R} \end{pmatrix}$ only based on the it real components because the escape energy is relative small comparing to others. After rotating the truncated Hamiltonian, we only keep the diagonal part and take its imaginary part as the new escape rate of the energy states.

On the other hand, in the large escape limit we can also derive the similar result as shown in the last section. In large escape limit, two analysis both assume the truncated spectrum and it's reasonable to take qubit tunnelling Δ as perturbation, that's why them give consistent result.

If the current ramping rate is comparable to other time scales, then we need should consider its original truncated formula Eq.(2.42) or try to find an appropriate U to diagonalize

$$\left(U^{-1}\dot{U} + \begin{pmatrix} E_{0L} & -\Delta\langle 0_L \mid 0_R\rangle \\ -\Delta\langle 0_R \mid 0_L\rangle & E_{0R} \end{pmatrix}\right)$$

To sovle this dynamics problem, it's really hard to give the analytical solution, only possible way is to deal with it by numerical method.

2.5.1 The numerical analysis of truncated model[1]

Basically, in order to show the required phenomenon we are interested in, we need to have a narrower switching current distribution(compared with the distribution shift due to the qubit-SQUID coupling) such that any shift or separation of distribution can be easily seen in our numerical diagrams, e.g. Fig.2.6. Hence, as an illustration, in our numerical analysis we choose most of the parameters the same as the setup in the NTT static experiments except different current ramping rate, qubit tunnelling energy, and qubit bias energy setting for different specific experiments.

The Large escape limit with qubit starting in flux state

In order to show the required flux-basis-preferred phenomenon in the large escape rate limit, at least we may need to have switching current distributions corresponding to two qubit flux states to be distinct or separated enough in the numerical result of our truncated model. At same time, a large current ramping rate $\frac{dy}{dt}$ is also required to make sure that most switching events take place in the large escape rate limit.

Most importantly, if we want to justify that our phenomenon is indeed contributed by large escape rate difference, i.e. $(\Gamma_{0L} - \Gamma_{0R})\,\hbar \gg \Delta$, we need to show how does the distribution of the flux state change due to the increase of current ramping rate(or escape rate difference). Hence, we naively wish the two distributions to be identical in the small escape rate limit (e.g. for $\frac{dy}{dt} = 10^4$Hz) in order to easily see the change of the distribution in two limits.

Therefore our first task is to construct two identical distributions for different flux states before we increase the current ramping rate to reach the large escape rate limit. According to our previous analysis of harmonic approximation, because the switching measurement in the small escape rate limit prefers energy basis, if the switching distributions corresponding to two qubit energy states are the same in the small escape rate limit, that's similar to the situation at the crossing point of two distributions of energy states in the Fig.2.4, then we expect the switching distributions of flux states will be the same automatically.

Hence, to achieve above situation and improve it by steps, we will start with the simplest condition $\varepsilon = 0$ for bias energy to discuss its disadvantage, and then know how to replace it by another condition later; we are going to deduce the logic why we choose our special condition in the end, where the effective bias energy is asked to be zero for all I_b. Finally, we isolate the real contribution of the large escape rate difference to the flux-basis-preferred phenomenon.

Let's first start with the numerical analysis of truncated model in Eq.(2.42) with the simplest setup of zero applied bias on qubit ($\varepsilon = 0$), $\Delta = 10^8$Hz, $\frac{dy}{dt} = 10^7$Hz, and rest of parameters being the same as NTT's

[1]This subsection may be skipped at a first reading

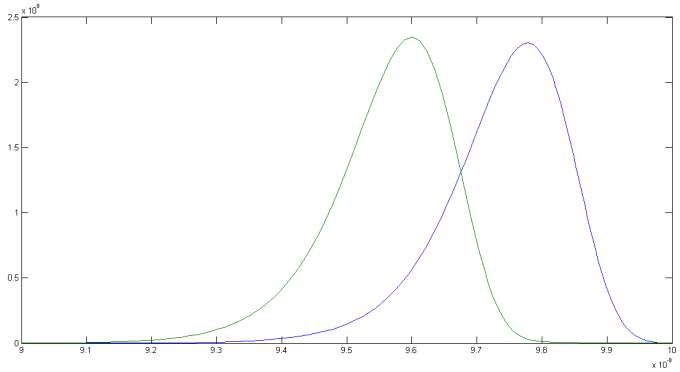

Figure 2.6: According to Eq.(2.42), the numerical result of current switching probability for qubit starting in a flux eigenstate, which is based on the NTT group's set-up except $\Delta = 10^8$Hz, $\frac{dy}{dt} = 10^7$Hz, and $\frac{E_{0L}-E_{0R}}{2} \neq 0$ (even if we set $\varepsilon = 0$) for all I_b. Here the X-axis and Y-axis correspond to the current ramping time t (sec) and switching amplitude $P\left(\sec^{-1}\right)$ respectively. The two color lines distinctly illustrate current switching distributions of different initial flux states $|L\rangle$ and $|R\rangle$. Here we have almost the ultimate separation for two distributions of flux states because the effective bias energy($\frac{E_{0L}-E_{0R}}{2} \approx 10^9$Hz) is much larger than $\Delta = 10^8$Hz and the energy state here is already close to the flux state. That's why this is the most clear diagram among three.

static experiments. The result is shown in Fig.2.6 in which two color lines represent the two distributions of qubit starting from different flux states $|L\rangle$ and $|R\rangle$. The distributions look separated enough such that we can claim they are distinct distributions. Actually, they almost reach their maximum separation according to our experimental setup. But we can not claim this is the required phenomenon caused by large escape rate difference because the effective bias energy $\frac{E_{0L}-E_{0R}}{2}$ is not zero (even if we start with $\varepsilon = 0$) and the energy states are already close to the flux states of different switching distributions no matter how current ramping rate changes; as shown in the Fig.2.4, the crossing point of two distributions of energy states has been shifted from $\varepsilon = 0$ by the nonzero effective bias energy. Hence we need to consider next possible condition of $\frac{E_{0L}-E_{0R}}{2}$(or ε) such that the effective bias energy can approach zero and then the switching distribution of two energy states will be the same in the small escape rate limit.

Let's consider another choice of the ε such that the effective bias energy $\frac{E_{0L}-E_{0R}}{2}$ is zero at the maximum of switching probability. The result is shown in Fig.2.7, where we only change the condition of effective bias energy and keep other setup the same as in Fig.2.6. As we expected, the distributions look less distinct than what we have in Fig.2.6 due to the reduction of the effective bias energy(especially around the maximum switching point) by our new choice of the ε. But this condition is still not enough for us to exclude the possibility of the effective bias energy because the effective bias energy does not vanish at the current other than the maximum switching point. Moreover the effective bias energy at the peak of distribution will start to be nonzero after we increase the current ramping rate. That's just because the change of the current ramping rate can shift the switching current distribution but the effective bias energy itself is still the same

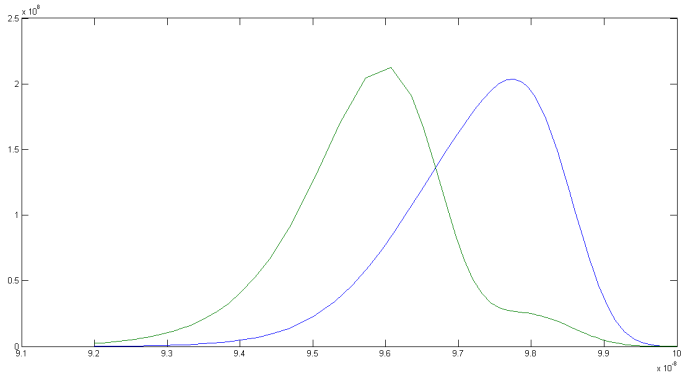

Figure 2.7: According to Eq.(2.42), the numerical result of current switching probability for qubit starting with its flux states, which is based on the NTT group's set-up except $\Delta = 10^8$Hz, $\frac{dy}{dt} = 10^7$Hz, and $\frac{E_{0L}-E_{0R}}{2} = 0$ specified at the maximum switching probability. Here the X-axis and Y-axis correspond to the current ramping time t (sec) and switching amplitude $P\left(\sec^{-1}\right)$ respectively. The two color lines respectively represent the current switching distributions of qubit starting with different flux states $|L\rangle$ and $|R\rangle$. Here we have less clear separation of two distributions than in Fig.2.6 because the effective bias energy $\frac{E_{0L}-E_{0R}}{2}$ is reduced around the maximum point of switching probability.

function of the bias current. Therefore, even if we can appropriately choose ε such that the distributions of the flux states are identical in the small escape rate limit, we still can not deny the contribution of the non-vanishing effective bias energy to the separation of two distributions in the large escape rate limit. In sum, our choices of ε so far can not reduce the effective bias energy efficiently to satisfy our requirement.

According to above analysis, in order to eliminate the contribution of effective bias energy to the flux-basis-preferred phenomenon, let's consider an extreme case where we allow ε changes with I_b to cancel the effect from qubit-SQUID coupling energy and then give $\frac{E_{0L}-E_{0R}}{2} = 0$ for all I_b, as shown in Fig.2.8. Maybe this is neither the necessary condition nor the realistic situation to make two identical switching distributions of energy states in the small escape rate limit, but it's the most straightforward way to eliminate the effective bias energy ideally for any bias current such that we can exclude all the possible contribution from the effective bias energy even if the distribution itself can change with current ramping rate. Based on this special condition, the corresponding energy states with zero effective bias energy are always $\frac{1}{\sqrt{2}}|L\rangle \pm \frac{1}{\sqrt{2}}|R\rangle$ for any I_b, which implies that the energy states should have the same escape rates and then have identical switching distributions because they all have the same weight of $|L\rangle$ and $|R\rangle$ no matter how current ramping rate changes. Therefore, the distributions for the two flux states should be the same as for the energy states in the small escape rate limit, and we can extrapolate this result of identical switching distributions of flux states to the large escape rate limit if the switching measurement still prefer energy basis. As shown in the Fig.2.8, the two distributions, which are expected to be exactly overlapped, have some significant separation though the separation itself is not as large as previous cases in Fig.2.7 and Fig.2.6. Because we

have excluded the contribution from effective bias energy we can claim this separation is due to the increase of escape rate difference. Moreover the $|\Gamma_{0L} - \Gamma_{0R}|\hbar$ bases on our setup has not reach the large escape rate limit, that's $|\Gamma_{0L} - \Gamma_{0R}|\hbar \gg \Delta$, hence we can improve the separation in Fig.2.7 to give the required flux-basis-preferred phenomenon by either increasing the current ramping rate to $\frac{dy}{dt} = 10^8$ or lowering the qubit tunnelling energy to $\Delta = 10^7$Hz, which will give the same result as Fig.2.6. Finally, we have shown the required flux-basis-preferred phenomenon in the large escape rate limit based on our numerical analysis of our truncated model, and we also justify this phenomenon is indeed caused by increasing the escape rate to the large escape rate limit.

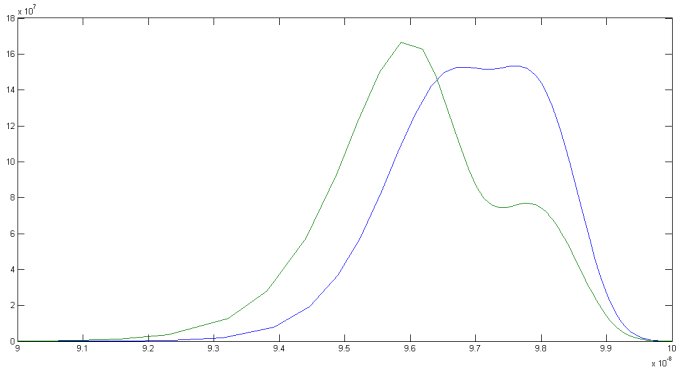

Figure 2.8: According to Eq.(2.42), the numerical result of current switching probability for qubit starting with its flux states, which is based on the NTT group's set-up except $\Delta = 10^8$Hz, $\frac{dy}{dt} = 10^7$Hz, and $\frac{E_{0L}-E_{0R}}{2} = 0$ for all I_b. Here the X-axis and Y-axis correspond to the current ramping time t (sec) and switching amplitude $P\left(\sec^{-1}\right)$. The two color lines represent the two current switching distributions of qubit starting with flux states $|L\rangle$ and $|R\rangle$. If the measurement prefer energy basis then we expect the switching distribution should be independent of the qubit's initial state because the corresponding energy states at zero effective bias energy are $\frac{1}{\sqrt{2}}|L\rangle \pm \frac{1}{\sqrt{2}}|R\rangle$ and therefore the corresponding escape rates for two energy basis are exactly the same. But the result shows that two distributions are different and more separated with the increase of the current ramping rate. Therefore we can conclude that the current switching prefers flux basis if the current ramping rate is fast enough such that we can reach the large escape rate limit before most of the switching events take place. Please note that the setup in Fig.(2.8) has not reach the required large escape rate limit. Hence it's similar to the situation where energy state is close to but not exactly equal to the flux state. That's why each distribution of the flux state may have two peaks at different bias current.

The Large escape limit with qubit starting in energy state

Furthermore, if the qubit starts in a given energy state, i.e. $\frac{1}{\sqrt{2}}|L\rangle \pm \frac{1}{\sqrt{2}}|R\rangle$, it requires a higher current ramping rate to achieve the required distribution of two peaks for the flux-basis-preferred phenomenon. In Fig.(2.9), we lower Δ to 10^7Hz instead of increasing the ramping rate, and we only consider effective bias energy under the same condition as in Fig.(2.7) because the diagrams of three possible conditions of effective bias energy are almost the same. The two lines in Fig.(2.9) seems to indicate that the dcSQUID prefers

to escape as the flux state of lower switching current (the distribution peak looks higher at lower critical current). But, actually it's just the addition of two switching probabilities of flux states with equal weights. Therefore, according to the two distributions of the flux states in Fig.(2.6), we can see why the first peak of lower switching current has higher amplitude in Fig.(2.9).

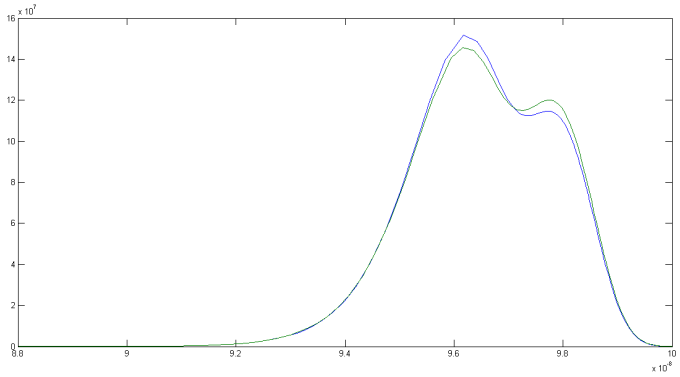

Figure 2.9: The numerical switching current probability based on Eq.(2.42) of the same parameters and condition of effective bias energy as given in Fig.(2.7) except with different initial state and lower qubit tunneling energy $\Delta = 10^7$Hz, where the two color lines illustrate the current-switching distributions for qubit starting with different energy states $\frac{1}{\sqrt{2}}|L\rangle \pm \frac{1}{\sqrt{2}}|R\rangle$. Here the X-axis and Y-axis correspond to the current ramping time $t\,(\text{sec})$ and switching amplitude $P\left(\text{sec}^{-1}\right)$ respectively. The two distributions looks almost the same and they will be exactly overlapped if we replace the condition of bias energy by $\frac{E_{0L}-E_{0R}}{2} = 0$ for all I_b. Besides, if we use the same qubit tunnelling energy as in Fig.(2.7), i.e. $\Delta = 10^8$Hz, we can not give same clear diagram. In brief, the higher current ramping rate is required if we want to see flux-basis-preferred phenomenon clearly for qubit starting with its energy state.

The small escape limit with qubit starting in energy state

On the other hand, based on the same formula but in the small escape rate limit, if the qubit starts in an energy eigenstate our numerical result for slower current ramping rate as in the NTT static experiments is consistent with our harmonic approximation, i.e. the peak of current distribution of energy state shifts with the effective qubit bias energy from one critical current of flux state to the other. To simplify the analysis, let's first consider the condition of the effective bias energy being zero during the current ramping, then the qubit starting with its energy eigenstate $\frac{1}{\sqrt{2}}|L\rangle \pm \frac{1}{\sqrt{2}}|R\rangle$ will be stationary in the same energy state in the numerical analysis of truncated model. Then, we expect both distributions of two energy states will be the same as the numerical result given in Fig.(2.10), that is consistent with the result of Harmonic Approximation; the escape rates of two energy channels are exactly the same.

But there is still some intrinsic difference between the representations of our truncated model and the harmonic approximation, and it would be more clear if we compare the numerical diagrams of truncated model in Fig.(2.11) and Fig.(2.10) where the initial conditions are different but the parameters are based on

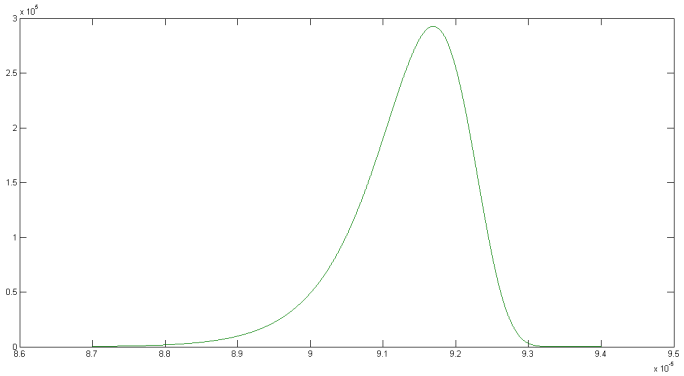

Figure 2.10: The numerical result of current switching probability according to Eq.(2.42) for qubit starting with either energy state and the parameters based on the NTT static experiments including $\Delta = 10^9$Hz, $\frac{dy}{dt} = 10^4$, and specified effective bias energy $\frac{E_{0L}-E_{0R}}{2} = 0$ during the current ramping. Here the X-axis and Y-axis correspond to the current ramping time $t\,(\text{sec})$ and switching amplitude $P\left(\text{sec}^{-1}\right)$ respectively. Because we have controlled the effective bias energy to be zero during current ramping, the qubit is stationary in the same energy state. Therefore, the two switching distribution of different energy states are simply described by the green line in the diagram, which is simpler than Fig.(2.11).

the NTT static experiments except fixed zero effective bias energy.

On the other hand, if we don't keep the effective bias energy as a constant zero during the current ramping but just make it zero only at the maximum switching probability instead, it will give the numerical result as Fig.(2.11), which looks more complicated than Fig.(2.10) and the blue area implies the small oscillation between states. Because the oscillation frequency is much faster than the current ramping rate that's why such a dense oscillating line looks like a blue area. But it is still consistent with the harmonic approximation because the peaks corresponding to two energy states appear approximately at same time(or I_b).

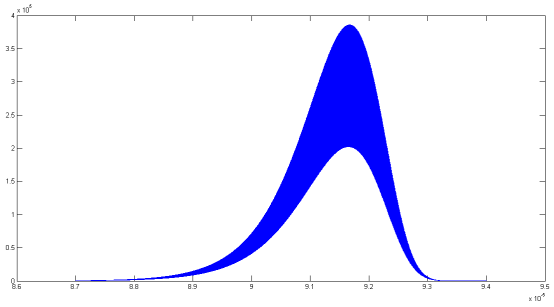

Figure 2.11: The numerical result for the current switching probability according to Eq.(2.42), for the same condition as in Fig.(2.10) except keeping $\frac{E_{0L}-E_{0R}}{2} = 0$ only at I_b of maximum switching probability. Here we only show the result for qubit starting with $\frac{1}{\sqrt{2}}|L\rangle + \frac{1}{\sqrt{2}}|R\rangle$, and the X-axis and Y-axis correspond to the current ramping time $t\,(\text{sec})$ and switching amplitude $P\left(\text{sec}^{-1}\right)$ respectively. Though the result looks more complicate than Fig.(2.10), the peak of each switching distribution of energy state implies approximately the same critical current of the SQUID, which is still consistent with the harmonic approximation.

The small escape limit with qubit starting in flux state

If the qubit starts with either flux state it must oscillate between one and the other flux states at a frequency equal to $\Delta = 1\text{GHz}$ because the flux state is not the energy eigenstate based on the zero effective bias energy. Actually, our truncated model in Eq.(2.42) already chose the flux basis as the preferred basis of the representation because Γ_{0L} and Γ_{0R} are given by flux states. Therefore we use the formula(the more correct one is in Appendix E)

$$P = \Gamma_{0L} |a_1|^2 + \Gamma_{0R} |a_2|^2 \tag{2.47}$$

to evaluate the switching probability and expect there must be the oscillation of switching probability between the maximum and the minimum due to the tunnelling between two flux states, which is shown in the Fig.2.12. On the other hand, in the Harmonic approximation, the distribution in Fig.2.10 is trivial and independent of initial state because both eigenstates in (energy-state-preferred) harmonic approximation have the same escape rate at zero effective bias energy. Hence, the numerical result in Fig.2.12 is a typical way to see the difference between the truncated model and harmonic approximation. But, experimentally we always get the result as Fig.(2.10) because what we measure actually is the average switching probability due to the fast oscillation even if the truth is described by Fig.(2.12). It looks like that both descriptions works well in small escape limit (due to the poor time resolution for observing the oscillation behavior within the scale of ramping time).

On the other hand, as we increase the effective bias energy continuously in the small escape rate limit we will see the distribution changing gradually from one peak to two peaks, where the two peaks move more apart as the increase of the effective bias energy. In the Fig.(2.13), we can see two separated peaks of distribution for given initial state $\frac{1}{\sqrt{2}} |L\rangle + \frac{1}{\sqrt{2}} |R\rangle$, this behaviour is consistent with the Harmonic approximation. Besides, the colored areas in the Fig.(2.13) also implies the oscillation of the state, which is mostly due to the quantum tunnelling between the states, not the change of bias current. Because our energy state at a given effective bias energy is not close enough to flux state such that there is still a small oscillation of the state at the same frequency of 1GHz and our numerical simulation prefers the flux-basis representation.

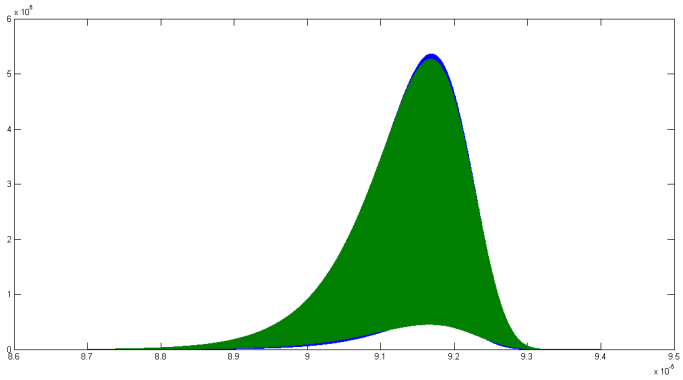

Figure 2.12: The numerical result of current switching probability according to Eq.(2.42) for qubit starting with either flux state and the parameters based on the NTT static experiments except $\Delta = 10^9$Hz, $\frac{dy}{dt} = 10^4$, and $\frac{0L - E_{0R}}{2} = 0$ only at the maximum switching probability. Here the X-axis and Y-axis correspond to the current ramping time $t\,(\text{sec})$ and switching amplitude $P\left(\text{sec}^{-1}\right)$ respectively. The two distributions are almost overlapped and have the same distribution peak. Especially, the large colored area implies the fast oscillation(at rate about 1GHz) between the maximum and the minimum switching probabilities respectively corresponding to two qubit flux states. That's because our flux state is not stationary and the truncated model of Eq.(2.42) is intrinsically based on the flux-state representation where the escape probability is evaluated by $P = \Gamma_{0L} \left|a_1\right|^2 + \Gamma_{0R} \left|a_2\right|^2$. The pattern here is totally different from what in Fig.(2.10), which start with energy state instead, but the corresponding switching currents at the peak of probability in both cases are the same. Besides, if we take the average of the maximum and minimum values, it will gives the same curve as shown in the Fig.(2.10)

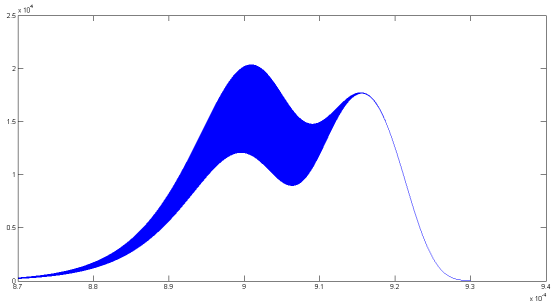

Figure 2.13: The numerical result of current switching probability according to Eq.(2.42) with the same parameter as the NTT static experiment except $\frac{dy}{dt} = 5 \times 10^3$Hz, $\Delta = 10^9$Hz, and effective bias energy equal to 5Δ. Here the X-axis and Y-axis correspond to the current ramping time $t\,(\text{sec})$ and switching amplitude $P\left(\text{sec}^{-1}\right)$ respectively. We only show the switching distribution of qubit starting with $\frac{1}{\sqrt{2}}\left|L\right\rangle + \frac{1}{\sqrt{2}}\left|R\right\rangle$ and it clearly has two separated peaks, where each peak approximately corresponds to the switching events for the flux state. The presence of blue area here also implies the oscillation of the qubit state. That's because our energy state at large bias energy is not exactly equal to the flux state, though they are close each other.

2.6 Discussion

Based on the conventional understanding of von Neumann measurement, the σ_z coupling between qubit and dcSQUID implies the projection of qubit energy state stochastically onto either $|R\rangle$ or $|L\rangle$ after the current switching if the corresponding current distributions of $|R\rangle$ and $|L\rangle$ are distinguishable, i.e. the separation between two current distributions centred at I_R and I_L are large enough in comparison to the width of each distribution. Actually, the experimental results give a different answer (especially for static experiment): after the NTT group successfully improved the resolution of the switching current of the dcSQUID [24], their raw data of switching currents for flux qubit being in its ground state clearly shows a single peak of the current distribution which continuously shifts from I_R to I_L(depending on the qubit applied flux); the existence of such intermediate distribution staying between I_R and I_L gives a direct evidence of the entanglement between dcSQUID wave function and qubit energy state, otherwise the entanglement of dcSQUID to the qubit flux state should give two current distributions respectively at I_R and I_L after measurement. Furthermore, they also do the simulation with a reasonable coupling strength [21] and give the same result, namely a single-peak switching current distribution, for the measurement of qubit in the ground state under various external fluxes Φ_q. Therefore it looks like the coupled system prefer to escape as qubit being projected onto energy state instead of flux state in static experiments(with small current ramping rate), which is different from our conventional understanding of von Neumann measurement. To solve this puzzle we have investigated the escape physics in different parameter regimes in previous sections and give a very consistent result, namely that the measurement basis tend to be the energy basis in the small escape rate limit but tend to be the flux basis in large escape rate limit.

As we know that in most static experiments the current sweeping rate is as slow as $10^3 \sim 10^4$Hz, it generally gives the scenario of small escape rate limit $\Gamma \ll \Delta/\hbar$ (or $|\Gamma_{0L} - \Gamma_{0R}| \ll \Delta/\hbar$) for dcSQUID. That's why we use our harmonic approximation to deal with the escape dynamics in section 3, where it gives consistent result with the NTT's static experiments. Besides, the two-channel escape dynamics after the harmonic approximation help us to see why the current switching measurement of flux qubit prefer to work as a wave collapsing into energy eigenstates $|+\rangle$ and $|-\rangle$ instead of the flux states $|R\rangle$ and $|L\rangle$ [36]; our measurement of qubit behaves as an energy-basis-preferred measurement in the small escape rate limit. At same time, if we consider the dependence of the qubit effective bias energy on the SQUID bias current, the energy basis of each channel actually rotates during the current ramping. Besides, because of the slow current ramping rate in static experiment, which is much smaller than the plasma frequency of the SQUID potential, the state evolution of coupled system with the bias current can be considered in the adiabatic limit. Therefore if we don't take into account the conditional evolution of density matrix according to the

measurement outcome, ideally the weight for each channel should be preserved from its starting value to the end. But in fact the weight for each channel(i.e. the diagonal components in density matrix) should depend on the measurement outcome via the Bayes' rule[37]. Even there is no switching event taking place during the current ramping, it still provides some information about the measurement of qubit; the density matrix still evolves conditionally with the negative outcome measurement.

In the following, we are going to analyze how the density matrix evolves according to the Bayes's rule under the negative outcome measurement. Because of the large back-action from the dcSQUID, we are not interested in the qubit density matrix for SQUID being in the voltage mode.

2.6.1 The qubit density matrix evolution under the negative outcome measurement

According to previous analysis of static experiments(in the slow current ramping rate limit), the harmonic approximation already told us that the SQUID prefers to escape in two energy channels. Therefore we can assume the eigenstates for two escape channels are $|\psi_+\rangle|+\rangle$ and $|\psi_-\rangle|-\rangle$, where $|\psi_+\rangle$ and $|\psi_-\rangle$ are the corresponding dcSQUID ground state wave functions, and any state $|\psi\rangle$ of our coupled system under the condition that the dcSQUID stays in its ground state can be decomposed into these eigenstates, which gives

$$|\psi\rangle = a_+|\psi_+\rangle|+\rangle + a_-|\psi_-\rangle|-\rangle \tag{2.48}$$

with $|a_-|^2+|a_+|^2=1$; the corresponding density matrix elements of the qubit are $\sigma_{++}(0)=|a_+|^2$, $\sigma_{--}(0)=1-\sigma_{++}(0)$, and $|\sigma_{-+}(0)|=\sqrt{\sigma_{++}(0)\,\sigma_{--}(0)}$ respectively. As we mentioned before, if the dcSQUID does not switch to the voltage mode during the measurement time t, we can consider it as a measurement with negative outcome, which happens with the probability $W(y_t)$. Consequently, after the negative outcome measurement we still can get useful information from the system; the diagonal part of density matrix σ_{++}, σ_{--} should change accordingly based on the standard Bayes' formula for a posteriori probability, which is similar to the analysis by Korotkov [37].

As an example, let's first consider an ideal case where we only observe the measurement result with negative outcome at $y=y_t$; the negative outcome measurement is operated in a black box until we open the box at time t. As we know, for given SQUID state $|\psi_+\rangle$ and $|\psi_-\rangle$ between the time interval $0<t'<t$, where $0<y'<y_t$, the corresponding probabilities of the SQUID staying in the well (not escaping) are

evaluated by

$$W_{\pm}(t) \equiv \exp\left[-\frac{1}{dy/dt}\int_0^{y_t} dy' \Gamma_{\pm}(y')\right] \tag{2.49}$$

, which strictly depend on how bias current ramps and $\frac{dy}{dt}$ can change with time. According this formula for given state as in Eq.(2.48), the total probability W of observing the dcSQUID being not switched during $0 < t' < t$ is given by

$$W(t) = \sigma_{++}(0) W_{+}(t) + \sigma_{--}(0) W_{-}(t) \tag{2.50}$$

Therefore, based on the conditional probability of observing the SQUID being not switched at $y = y_t$, the diagonal elements of density matrix after observation should be modified by

$$\sigma_{++}(t) = \sigma_{++}(0)(W_{+}(t))\{W(t)\}^{-1} \tag{2.51}$$

$$\sigma_{--}(t) = 1 - \sigma_{++}(t) \tag{2.52}$$

On the other hand, for the off-diagonal density matrix elements, because there is no tunnelling energy between the two escape channels, if we assume that our measurement suffers no de-coherence [38] we can follow the same procedure as Korotkov's [37] to give the formula of $\sigma_{+-}(t)$:

$$|\sigma_{+-}(t)| = \sqrt{\sigma_{++}(t)\sigma_{--}(t)} \tag{2.53}$$

and

$$\sigma_{+-}(t) = \exp\left(i\int_0^t \frac{\varepsilon_{+-}(t)}{\hbar} dt\right)\sqrt{\sigma_{++}(t)\sigma_{--}(t)}. \tag{2.54}$$

Here $\varepsilon_{+-}(t)$ is the energy difference between two states $|\psi_{+}\rangle|+\rangle$ and $|\psi_{-}\rangle|-\rangle$. Basically, the Equations (2.51) and(2.54) describe how density matrix evolves after we observe the measurement result in the ideal case. This is our first type of negative outcome measurement.

But in the real experiment we actually observe the measurement continuously at every moment. Therefore, to analyze the problem in the real case, we will consider the second type of measurement, where the time interval $0 < t' < t$ is divided into N segments of length $\tau = \frac{t}{N}$, and then rewrite the Eq.(2.49) as

$$W_{\pm}\left(y_t\right) \approx \prod_{n=1}^{N} w_{\pm}\left(n\right) \tag{2.55}$$

. Here we have

$$w_{\pm}\left(n\right) \equiv \exp\left[-\int_{n\tau}^{(n+1)\tau} dt' \Gamma_{\pm}\left(y_{t'}\right)\right] \tag{2.56}$$

as the probability of SQUID not escaping during the time segment $n\tau < t' < (n+1)\tau$. Similarly, according to the formula of $w_{\pm}$ we can claim the total probability $w\left(n\right)$ of observing the dcSQUID being not switched during $n\tau < t' < (n+1)\tau$ is given by

$$\begin{aligned} w\left(n\right) &= \sigma_{++}\left(n\tau\right) w_{+}\left(n\right) \\ &+ \sigma_{--}\left(n\tau\right) w_{-}\left(n\right) \end{aligned} \tag{2.57}$$

Here $\sigma_{++}\left(n\tau\right)$ and $\sigma_{--}\left(n\tau\right)$ are the diagonal density matrix elements at $t' = n\tau$. Because we disclose the measurement result at every moment in the scheme for real case, according to Bayes' rule we can derive evolution of diagonal elements of density matrix after each observation of the time segment, which gives the formulas in differential form:

$$\sigma_{++}\left(\left(n+1\right)\tau\right) = \sigma_{++}\left(n\tau\right)\left(w_{+}\left(n\right)\right)\left\{w(n)\right\}^{-1} \tag{2.58}$$

$$\sigma_{--}\left(\left(n+1\right)\tau\right) = 1 - \sigma_{++}\left(\left(n+1\right)\tau\right) \tag{2.59}$$

or equivalently

$$\sigma_{++}\left(t+\tau\right) = \sigma_{++}\left(t\right)\left(w_{+}\left(t\right)\right)\left\{w(t)\right\}^{-1} \tag{2.60}$$

$$\sigma_{--}\left(t+\tau\right) = 1 - \sigma_{++}\left(t+\tau\right). \tag{2.61}$$

Similarily, corresponding to Eq.(2.54), we have replacing formula for the off diagonal density matrix

element, i.e.

$$\sigma_{+-}(t+\tau)=\sigma_{+-}(t)\,e^{\frac{i}{\hbar}\varepsilon_{+-}(t)\tau}\sqrt{\frac{\sigma_{++}(t+\tau)\,\sigma_{--}(t+\tau)}{\sigma_{++}(t)\,\sigma_{--}(t)}}. \tag{2.62}$$

Moreover, it's not hard to derive the Langevin-type equations for σ_{++} and σ_{+-}, which are

$$\dot{\sigma}_{++}(t)=-\sigma_{++}(t)\,\sigma_{--}(t)\left(\Gamma_{+}(y_t)-\Gamma_{-}(y_t)\right) \tag{2.63}$$

$$\dot{\sigma}_{+-}(t)=\frac{i\varepsilon_{+-}}{\hbar}\sigma_{+-}+\frac{\sigma_{+-}}{2}\left(\sigma_{++}-\sigma_{--}\right)\left(\Gamma_{+}(y_t)-\Gamma_{-}(y_t)\right) \tag{2.64}$$

In sum, for the second type of measurement scheme, the equations (2.60) and (2.62) describe how the qubit density matrix evolves before the dcSQUID switches to the voltage mode, especially for negative outcome measurement in the slow current ramping rate limit. More general representation of these equations is given in appendix G.

Although the two types of measurement schemes are intrinsically different, we can prove that the equations (2.60) and (2.62) give the same evolution as what of the equations (2.51) and (2.54), see Appendix F. It is because the two measurement types are equivalent only when there is no dynamical transition between two channels, e.g., no Landau-Zener transition occurs during the sudden change of bias current. Therefore, the differential form of equations, that's Eq.(2.60) and Eq.(2.62), in the real scheme are more appropriate to describe the evolution of the qubit density matrix. We will see its advantages in the following analysis of generalized evolution formulas of density matrix, which is not restricted to small escape rate limit and also includes the dynamical transition between two channels.

Next, to generalize the density matrix analysis of negative outcome measurement (especially for Eq.(2.57) and (2.60)) to the other limits, we also need to consider the possible conditions in dynamic experiments where the current ramping rate can be as fast as 10GHz and $|\Gamma_{0L}-\Gamma_{0R}|$ can be comparable to or much larger than $\Delta/\hbar$ which can be as low as 1MHz. As we discussed in previous sections, even though the effective bias energy is small by comparing to the qubit tunnelling energy no matter how the bias current changes, each energy basis of escape channel still can rotate to flux basis in the end if the escape rate reaches the limit $|\Gamma_{0L}-\Gamma_{0R}|\gg\Delta/\hbar$ at higher bias current. This implies that the escape energy also contributes to the

rotation of the eigenbasis though the related mechanism is not as simply as what we have in small escape rate limit[39]. Consequently, we can generalize the idea of basis rotation and extend it to all range of bias current, where it usually requires higher current ramping rate to reach higher range of bias current. Besides, we believe that our two-channel picture for escape dynamics still works at regime other than small escape rate and large escape rate limits [40]. Hence we generalize the application of two-channel picture to all range of bias current. Based on above assumptions of universal two-channel picture with generalized basis rotation, we can justify that, as long as the excitations to higher energy levels of dcSQUID are negligible, the Eq.(2.48) of wave function being decomposed into two channels is generally true even at higher current ramping rate, and then each element of density matrix in two channel representation is meaningful. Theoretically we can derive the intrinsic evolution of composite system(including the basis rotation with bias current) before considering the "observation" effect that will induce the conditional probability on the evolution of the system's density matrix. To identify this intrinsic evolution, let's assume that the evolution from $\sigma_{++}(t)$ to $\sigma_{++}^{(0)}(t+\tau)$(or from $\sigma_{--}(t)$ to $\sigma_{--}^{(0)}(t+\tau)$) is purely based on the dynamics of our composite system between t' and $t'+\tau$. Next, it's ready for us the generalize Eq.(2.57) and Eq.(2.60) by merging them with the pure dynamical evolution of density matrix. We can use $\sigma_{++}^{(0)}(t+\tau)$ and $\sigma_{--}^{(0)}(t+\tau)$ to claim that the total probability $w(t+\tau)$ of observing the dcSQUID being not switched during $t<t'<t+\tau$ is given by

$$\begin{aligned} w(t+\tau) &= \sigma_{++}^{(0)}(t+\tau)\, w_{+}(t+\tau) \\ &+ \sigma_{--}^{(0)}(t+\tau)\, w_{-}(t+\tau). \end{aligned} \tag{2.65}$$

Then we can use Eq.(2.65) to derive the evolution of the density matrix under Bayes' rule after the observation of negative outcome measurement during $t<t'<t+\tau$, which gives

$$\sigma_{++}(t+\tau) = \sigma_{++}^{(0)}(t+\tau)\left(w_{+}(t+\tau)\right)\left\{w(t+\tau)\right\}^{-1}. \tag{2.66}$$

$$\sigma_{+-}(t+\tau) = \sigma_{+-}^{(0)}(t+\tau)\sqrt{\frac{\sigma_{++}(t+\tau)\,\sigma_{--}(t+\tau)}{\sigma_{++}^{(0)}(t+\tau)\,\sigma_{--}^{(0)}(t+\tau)}}. \tag{2.67}$$

Once we have $\sigma_{++}(t+\tau)$ from Eq.(2.66), we can use it to generate $\sigma_{++}^{(0)}(t+2\tau)$ according to the dynamical evolution of composite system and then bring $\sigma_{++}^{(0)}(t+2\tau)$ back to Eq.(2.65) for repeating steps, and so forth.(Similar for the $\sigma_{+-}(t+\tau)$ of Eq.(2.67)) The Eq.(2.65), Eq.(2.66), and Eq.(2.67) are our general evolution formulas for density matrix, which already include both the system's dynamics and the conditional

probability based on the observation of measurement result. Their corresponding Langevin-type equations are

$$\dot{\sigma}_{++}(t) = \dot{\sigma}^{(0)}_{++}(t) - \sigma_{++}(t)\,\sigma_{--}(t)\,(\Gamma_+(y_t) - \Gamma_-(y_t)) \tag{2.68}$$

$$\dot{\sigma}_{+-}(t) = \dot{\sigma}^{(0)}_{+-} + \frac{\sigma_{+-}}{2}(\sigma_{++} - \sigma_{--})\,(\Gamma_+(y_t) - \Gamma_-(y_t)) \tag{2.69}$$

For more general representation of these equations please see the appendix G.

To understand the evolution of the qubit density matrix described by Equations (2.68) and (2.69), let's investigate their nonlinear terms, which represent the conditional evolution due to the negative outcome after the measurement and are all proportional to $(\Gamma_+ - \Gamma_-)$. As an example, let's assume that we are performing the negative outcome measurement for $-$ state, i.e., we require $\Gamma_+ > \Gamma_-$ such that the probability of the qubit staying in the $-$ state increases after the negative outcome measurement. Because now we have $\Gamma_+ > \Gamma_-$, the nonlinear term in Eq.(2.68) should be negative. Hence, without considering the terms of intrinsic dynamics $\dot{\sigma}^{(0)}_{++}(t)$ and $\dot{\sigma}^{(0)}_{+-}(t)$, we expect $\sigma_{++}(t)$ should always decrease to 0 (as the orange "-.-" line in Fig. (2.14)) and $\sigma_{--}(t)$ should increase to 1, which is consistent with our assumption of the negative outcome measurement for $-$ state. Besides, the nonlinear term in Eq.(2.68) is proportional to σ_{++} and σ_{--}, hence its effect is negligible near $\sigma_{++} = 1$ or $\sigma_{++} = 0$ but reaches maximum at $\sigma_{++} = \frac{1}{2}$. Also, if we take σ_{++} as the role of velocity v in the equation of motion of an object, then the Eq.(2.68) looks like $\dot{v} = \dot{v}^{(0)} - v\,(1-v)\,(\Gamma_+ - \Gamma_-)$, where $\dot{v}^{(0)}$ is the original trajectory before the measurement, and then the nonlinear term in Eq.(2.68) works as a dissipative force.

Furthermore, if we take the terms $\dot{\sigma}^{(0)}_{++}(t)$ and $\dot{\sigma}^{(0)}_{+-}(t)$ back into account in the Eq. (2.68) and (2.69), the evolution will be more complicated and there will be a quantum Zeno effect or anti-Zeno effect depending on the dynamics in different conditions and limits(we will show them soon). As mentioned before, our composite system is ideally diagonalized into two energy states("+" and "-") and the escape rate $(\Gamma_\pm)$ only defined for each energy state in the two-channel picture. Therefore, we expect that a possible way to induce a dynamical transition between two energy states is by a Landau-Zener-type transition due to non-adiabatic current ramping. In general, the bias current and the dynamical transition between two states can be any possible function of time. Therefore, as example, we will focus on two typical transition behaviors of density matrix (before considering the measurement effect) to illustrate how these behaviors change after

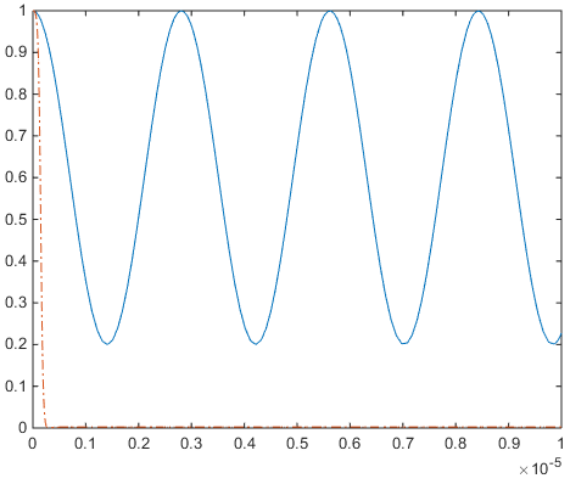

Figure 2.14: The numerical result for σ_{++} under $\varepsilon' = 10^6$Hz, $\Delta' = 10^6$Hz, and $\Gamma_+ - \Gamma_- = 4 \times 10^7$Hz. The blue line represents the oscillating motion of σ_{++} starting at $\sigma_{++} = 1$ before the measurement effect takes place. The orange line represents the evolution of σ_{++} after considering the negative measurement effect. Here we can see, due to the strong measurement effect when $\alpha \ll |\Gamma_+ - \Gamma_-|$, the σ_{++} decays from 1 much faster than the original motion and then goes to 0 in the end, which works as a strong Anti-Zeno measurement.

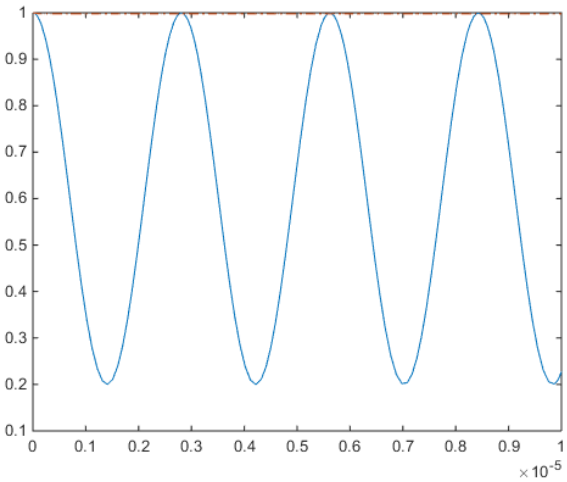

Figure 2.15: The numerical result for σ_{--} under $\varepsilon' = 10^6$Hz, $\Delta' = 10^6$Hz, and $\Gamma_+ - \Gamma_- = 4 \times 10^7$Hz. The blue line represents for the oscillating motion of σ_{--} starting at $\sigma_{--} = 1$ before the measurement effect takes place. The orange line represents the evolution of σ_{--} after the negative measurement effect. Here we can see, due to the strong measurement effect when $\alpha \ll |\Gamma_+ - \Gamma_-|$, the σ_{--} decays from 1 much slower than the original motion and keeps staying around 1, which works as a strong Zeno measurement.

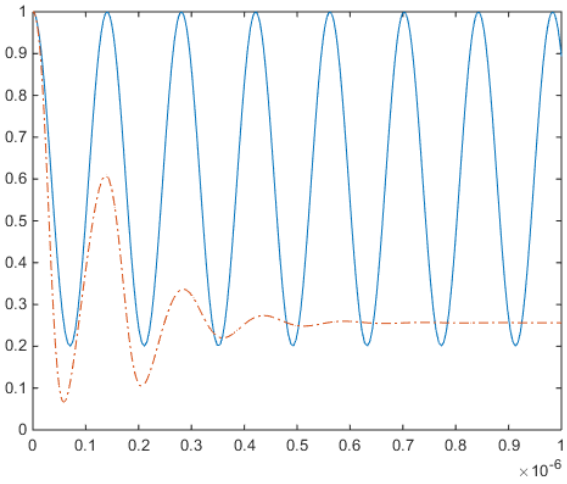

Figure 2.16: The numerical result for σ_{++} under $\varepsilon' = 2\times10^7$Hz, $\Delta' = 2\times10^7$Hz, and $\Gamma_+ - \Gamma_- = 4\times10^7$Hz. The blue line represents the oscillating motion of σ_{++} starting at $\sigma_{++} = 1$ before the measurement effect takes place. The orange line represents the evolution of σ_{++} after considering the negative measurement effect. Here we can see, due to the measurement effect under $\alpha \approx |\Gamma_+ - \Gamma_-|$, the σ_{--} decays from 1 faster than its original oscillating motion thought it no longer goes to 0 in the end. Besides, the oscillation keeps damping and reaches a new equilibrium $\sigma_{++} \approx 0.25$, where we still can see its tendency of Anti-Zeno effect.

the measurement.

The first effective behavior we are interested in is the simple oscillation between "+" and "−" energy states, which is briefly described by $\dot{\sigma}^{(0)} = -\frac{i}{\hbar}[H_e, \sigma]$ with $H_e = \begin{pmatrix} \varepsilon' & \Delta' \\ \Delta' & -\varepsilon' \end{pmatrix}$ in the energy basis representation. The oscillation of σ_{++} should follow $\sigma_{++} = \frac{1}{2}\left(1 + \frac{\varepsilon'^2}{\varepsilon'^2+\Delta'^2}\right) + \frac{1}{2}\frac{\Delta'^2}{\varepsilon'^2+\Delta'^2}\cos(\alpha t)$ with $\alpha = 2\frac{\sqrt{\varepsilon'^2+\Delta'^2}}{\hbar}$ (for σ_{++} starting from 1 before taking the measurement effect into account). Please note that the σ_{++} decaying behavior in the $t \to 0$ limit is similar to the standard quantum Zeno problem. The second one is the exponential decaying from one state to another, i.e., $\sigma_{++} = e^{-\beta t}$ or $\dot{\sigma}^{(0)}_{++} = -\beta\sigma_{++}$ which gives $\sigma_{++} = 1-\beta t$ in $t \to 0$ limit. These basically are the evolutions of interest before the measurement effective is considered, the corresponding detail analysis of how they change under the measurement effect (in different conditions and limits) will be discussed in the follows.

In the limit $\alpha \ll |\Gamma_+ - \Gamma_-|$ in the first case and $\beta \ll |\Gamma_+ - \Gamma_-|$ in the second case, the so called quantum zeno and anit-Zeno effect is very strong; if we start with $\sigma_{++} = 1$ then the σ_{++} will be forced to go zero at a rate about $|\Gamma_+ - \Gamma_-|$, which gives the strong anti-Zeno effect, but if we start with $\sigma_{--} = 1$ then the σ_{--} will keep staying at 1, which gives the strong Zeno effect. Please see Fig. (2.15) and Fig. (2.14).

In the limit of α being comparable to $\Gamma_+ - \Gamma_-$ of the first case, if we start with $\sigma_{++} = 1$ we can see the σ_{++} will be forced to decay faster than its original oscillating motion until it bounces back by the oscillation.

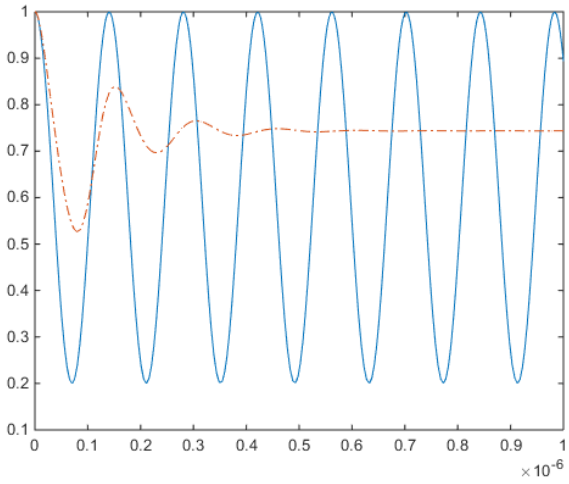

Figure 2.17: The numerical result for σ_{--} under $\varepsilon' = 2 \times 10^7$Hz, $\Delta' = 2 \times 10^7$Hz, and $\Gamma_+ - \Gamma_- = 4 \times 10^7$Hz. The blue line represents the oscillating motion of σ_{--} starting at $\sigma_{--} = 1$ before the measurement effect takes place. The orange line represents the evolution of σ_{--} after the negative measurement effect. Here we can see, due to the measurement effect under $\alpha \approx |\Gamma_+ - \Gamma_-|$, the σ_{--} decays from 1 slower than its original oscillating motion thought it no more stays around 1 in the end. In addition, the oscillation keeps damping and reaches a new equilibrium $\sigma_{--} \approx 0.75$, where we still can see the tendency of Zeno effect.

Besides, the oscillation keeps damping due to the measurement effect and it will reach a new equilibrium determined by the competition between the oscillation force and measurement effect, which still gives the tendency of the anti-Zeno effect. Please see Fig. (2.16). On the other hand, if we start with $\sigma_{--} = 1$ then the σ_{--} will decay slower than its original motion and keep damping in oscillation until it reaches a equilibrium which is determined by the competition between the oscillation force and measurement effect and therefore different from 1, which also reveals the tendency of Zeno effect. Please see Fig. (2.17). Similarly, under the condition of $\beta \approx \Gamma_+ - \Gamma_-$ in the second case, we still can see the so called quantum zeno(for σ_{++} starting from 1) and anit-Zeno effect(for σ_{++} starting from 1); if we start with $\sigma_{++} = 1$ then the σ_{++} will be forced to decrease faster by the measurement until it reaches 0, which corresponds to the anti-Zeno effect, but if we start with $\sigma_{--} = 1$ then the σ_{--} will decay first at the rate slower than β until it reaches $\beta = \sigma_{++}(\Gamma_+ - \Gamma_-)$, which corresponds to the Zeno effect.

In the limit of $\alpha \gg |\Gamma_+ - \Gamma_-|$ of the first case and $\beta \gg |\Gamma_+ - \Gamma_-|$ of the second case, the so called quantum zeno and anit-Zeno effect is negligible because we are also in the relative weak measurement limit. The trivial case is that when $|\Gamma_+ - \Gamma_-| = 0$ our negative measurement works as no measurement at all.

There are two special cases we also need to consider. The first one is under the condition of $\Delta' = 0$ and either σ_{++} or σ_{--} start at 1, where there is no change of σ_{++} or σ_{++} at all. It's because the decay term in the Eq.(2.68) is always zero except we make $\Delta' \neq 0$ to change this situation. The second one is the

condition of $\varepsilon' = 0$, which may show the periodic oscillation without damping on amplitude depending on the ration $\frac{\Delta'}{|\Gamma_+ - \Gamma_-|}$; if $\frac{\Delta'}{|\Gamma_+ - \Gamma_-|}$ is greater than the critical value the density matrix will show the periodic behavior forever. In this case the measurement (with decaying rate difference between two channels) still changes the behavior and the period of the density matrix though no more damping on amplitude.

2.6.2 The scenario related to the weak measurement

Because of the inherent stochastic property of quantum tunnelling, the switching probability has a certain width ΔI_{sw} such that the displacement($\delta \bar{I}_{sw}$) between two peaks of switching current distribution of qubit states $|-\rangle$ and $|+\rangle$ may be relatively small. Therefore we need to repeat the experiment tens of thousands of times to get the change of average value and read out the qubit's state; a single measurement is not enough to get any useful information about the qubit. This situation(with $\frac{\delta \bar{I}_{sw}}{\Delta I_{sw}} \ll 1$) is similar to the "weak measurement" scheme of Albert et al. [16](though no post selection step is made in our measurement) and hereafter we call it the "weak measurement limit". In addition, based on the Equations (2.65), (2.66), and (2.67) in the "weak measurement limit", the density matrix will not show any clear change from its initial value due to the strong overlap between $P_+(I)$ and $P_-(I)$. On the contrary, the "von Neumann limit" requires the condition $\frac{\delta \bar{I}_{sw}}{\Delta I_{sw}} \gg 1$. Although a single measurement is still not enough to uniquely characterize the original state of the qubit, at least we can tell, in this "von Neumann limit", into which energy state does the qubit collapse after each measurement, which means that our measurement is a projective measurement into $|-\rangle$ and $|+\rangle$. Correspondingly, the density matrix described by our equations shows good localization in one or other of the two states after the current switching measurement. In the more general case, while no complete collapse takes place due to the strong overlap between the two switching-current distributions, at least we can analyze the qubit density matrix according to equations (2.65), (2.66), and (2.62) to give probabilities of two states after the current switching.

In the Rabi experiments [18], because a^+ and a^- in Eq.(2.48) should oscillate between 0 and 1 alternatively by applying microwave of correct frequency that is equal to the energy difference between the two states $|\psi_+\rangle|+\rangle$ and $|\psi_-\rangle|-\rangle$, the total switching probability $P = |a^+|^2 P_+ + |a^-|^2 P_-$ should oscillate between P_+ and P_-. Usually, experimentalists pick up the current at which the difference between P_+ and P_- is maximized, therefore, the Rabi or Ramsey diagram should oscillate with the amplitude $|P_+ - P_-|$. In essence, the evolution of the density matrix also follows equations (2.65), (2.66), and (2.62) under the specified current-ramping-up scheme for dynamic experiments. Similarly, the larger $|P_+ - P_-|$ can make the density matrix more localized onto either of two states.

2.6.3 The sudden change of state due to fast current ramping

As a part of dynamical analysis, we need to notice that the state of composite system in static experiments evolves adiabatically under the slow bias current ramping, but if we instead increase the current ramping rate to the regime of $r \geq 10\Delta/h$, the state of composite system can evolve suddenly, where the initial state is preserved with bias current. In general, it's similar to the Landau-Zener problem and more detail analysis is shown in Appendix I. All of these properties will be useful for our discussion in the next section of "the extension to ideal negative outcome measurement for testing TBI".

2.6.4 The entanglement between qubit and dcSQUID

Because of the limitation of qubit-SQUID coupling, the SQUID wave functions within the well for the two qubit states may not be much different even at large bias current [44], but this does not imply that the switching current distributions for two states can not be distinguishable. Actually, if we take the SQUID wave function outside the well into account we will clearly see how does the SQUID become entangled with the qubit as time evolves; the SQUID wave function can gradually become entangled with the qubit if the SQUID wave function of one qubit state escapes faster than the other one such that two SQUID wave functions have significant difference on distribution. And that's why we can have distinct switching distributions for two qubit states.

To illustrate the entanglement of our composite system, let's consider again our system being in the state of

$$|\psi\rangle = a_+ |\psi_+\rangle |+\rangle + a_- |\psi_-\rangle |-\rangle \tag{2.70}$$

with $|a_-|^2 + |a_+|^2 = 1$. Here we have assume that the state of the system can be decomposed into two escape channels of bases $|\pm\rangle$ in which the corresponding SQUID states $|\psi_\pm\rangle$ decay at the rates $\Gamma_\pm$ respectively. Besides, similar to the behaviour of $|\psi\rangle$, the density matrix $\rho = |\psi\rangle \langle\psi|$ changes with bias current and time. In principle, we can trace out the SQUID part to obtain the reduced density matrix on qubit, which gives

$$\rho_{\mathrm{q}} = \begin{pmatrix} |a_+|^2 & a_+^* a_- \langle\psi_+ \mid \psi_-\rangle \\ a_+ a_-^* \langle\psi_- \mid \psi_+\rangle & |a_-|^2 \end{pmatrix} \tag{2.71}$$

in the representation of bases $|\pm\rangle$. Based on this, we can derive the entanglement entropy of the composite

system

$$\begin{aligned} S &= -\mathrm{Tr}\left(\rho_{\mathrm{q}} \log_2 \rho_{\mathrm{q}}\right) \\ &= -\lambda_1 \log_2 \lambda_1 - \lambda_2 \log_2 \lambda_2 \end{aligned} \tag{2.72}$$

with $\lambda_1, \lambda_2 = \frac{1}{2} \pm \frac{1}{2}\sqrt{1 - 4\left|a_+\right|^2 \left|a_-\right|^2 \left(1 - \left|\langle \psi_+ \mid \psi_- \rangle\right|^2\right)}$. As an example, according to Eq.(2.72) for $\left|a_+\right|^2 = \left|a_-\right|^2 = \frac{1}{2}$ we can have the maximum entanglement entropy of our composite system as a function of $r \equiv \left|\langle \psi_+ \mid \psi_- \rangle\right|$, that is

$$S_{\max} = 1 - \frac{1}{2}(1+r)\log_2(1+r) - \frac{1}{2}(1-r)\log_2(1-r). \tag{2.73}$$

At the beginning of lower bias current, we have $\left|\langle \psi_+ \mid \psi_- \rangle\right| \approx 1$ [44] and $S_{\max} \approx 0$, where qubit and SQUID are not entangled, because the wave functions $|\psi_\pm\rangle$ are all distributed within the well and they are almost identical to each other. But if we start increasing the bias current to the higher value of $\Gamma_+ \gg \Gamma_-$ such that after waiting long enough we may have $|\psi_+\rangle$ distributed mostly different from $|\psi_-\rangle$ which still stays in the well, then ideally we can make $\left|\langle \psi_+ \mid \psi_- \rangle\right|$ approaching zero and $S_{\max}$ close to one, where the qubit-SQUID system becomes entangled and the switching measurement gives the distinct distributions for two qubit states. This gives us a rough picture of entanglement formation for switching measurement on flux qubit by SQUID.

Because the mutual inductance between the qubit and the dcSQUID already exists by experimental design, we need to consider the qubit and the dcSQUID together as a quantum system where energy levels evolve with bias current. Therefore, at first glance, we may think the measurement mechanism of qubit-dcSQUID composite system is different from the standard weak-measurement assumption that the interaction between system and apparatus is only turned on at measuring time. But, according to above analysis of entanglement, if we regard the fact that in the weak-coupling limit the qubit and the dcSQUID are not entangled until I_b approaches a certain value with a given time, it will be more appropriate to think of using the development of a certain degree of entanglement between the system and apparatus as defining the "turning on" time of the interaction or measurement.

2.6.5 Other considerations

The conclusion of two current distributions reflecting two qubit energy states in static experiments is true only when the de-coherence effect from the measurement is small(in comparison with Δ [21]) such that the behavior of the eigenstates of the coupled Hamiltonian in Eq.(2.6) is good enough to describe the escape

dynamics in the measurement process; this situation is similar to the "Hamiltonian-dominated regime" in the review of [45], if we consider the qubit-dcSQUID together as a quantum system. The opposite limit is the decoherence-dominated regime in which the two parallel switching current distributions correspond to two qubit "flux" states instead [25] and our coupled Hamiltonian can not give a complete picture to catch the real dynamics [36]. Usually, in a static experiment the qubit density matrix automatically evolves to a statistical mixture before the switching event is detected [21].

Note added: When this thesis was in the final stages of preparation, we received an updated and expanded version of ref.[21], which treats some of the same issues which are discussed above. While we do not disagree with any of the conclusions of this paper, we want to emphasize our belief that even in the complete absence of the decoherence an experiment starting from a non-trivial superposition of energy eigenstates will yield a two-peak distribution of switching currents.

2.7 The extension to ideal negative outcome measurement for testing TBI

In order to design an ideal negative result measurement for the TBI, we need to appropriately control the bias current such that we can accurately collect the ensemble of system being in the claimed flux state under the condition of no escape happening during the whole process of the measurement. The basic current operation scheme follows the steps of first ramping up the bias current fast to I_1 at t_1, then keeping the same current value till t_2(the platform of height I_1 from t_1 to t_2), and finally fast decreasing the bias current to zero. Here the bias current is required to be ramped up fast enough such that the qubit initial state is preserved till the current reaches the platform regime, and the (flux) state of system right after the current platform is also required to be preserved to the end by fast decreasing bias current to zero. Because we want to construct a flux basis preferred measurement the height of the current platform, that is I_1, is required to be high enough to make sure that the SQUID reaches the large escape rate limit and prefers to escape in flux basis. Ideally we wish that most of the evolution of the density matrix under the conditional probability of negative outcome measurement takes place during the current platform from t_1 to t_2 because any uncontrollable density matrix evolution (before t_1 or after t_2) based on the wrong state will increase the error(or venality) of the measurement. Besides, the value of I_1 also needs to satisfy the requirement that the escape rate of the SQUID under the desired flux state is much slower than the opposite one such that after the (negative) conditional evolution of density matrix between t_1 and t_2 the diagonal matrix element of the opposite flux state is close to zero. Therefore the system only has the probability of staying in the

claimed state after the current operation if there is no escape taking place; we exactly perform a negative measurement of the required flux state on the system. To complete the ideal negative outcome measurement, we also need to perform the negative measurement on the opposite state and integrate them to evaluate the probabilities of the two states.

As an example, for negative measurement of R state we require the escape rate $\Gamma_L(I_1)$ for the L state at given bias current I_1 is much faster than $\Gamma_R(I_1)$ for the R state such that we have

$$w_L \approx e^{-\tau\Gamma_L(I_1)} \ll w_R \approx e^{-\tau\Gamma_R(I_1)} \tag{2.74}$$

$$W_L \approx e^{-(t_2-t_1)\Gamma_L(I_1)} \ll W_R \approx e^{-(t_2-t_1)\Gamma_R(I_1)} \tag{2.75}$$

right after the whole process of bias current operation. Although the starting basis of each channel at zero bias current is not the flux basis, we still can have the initial density matrix elements based on flux states, which are $\sigma_{RR}(0)$ and $\sigma_{LL}(0)$. Hence there are only

$$w \approx \sigma_{RR}(t_1) w_R + \sigma_{LL}(t_1) w_L \simeq \sigma_{RR}(t_1) \delta W_R \tag{2.76}$$

$$W \approx \sigma_{RR}(t_1) W_R + \sigma_{LL}(t_1) W_L \simeq \sigma_{RR}(t_1) W_R \tag{2.77}$$

of the total number of experiment remaining as the ensemble of negative outcome measurement, where it's more accurate to use $\sigma_{RR}(t_1)$ and $\sigma_{LL}(t_1)$ instead of $\sigma_{RR}(0)$ and $\sigma_{LL}(0)$ but ideally we wish $\sigma_{RR}(t_1) \approx \sigma_{RR}(0)$ and $\sigma_{LL}(t_1) \approx \sigma_{LL}(0)$ if the current ramps to I_1 fast enough. As an illustration, the two color lines in Fig.2.18 respectively show how $\sigma_{RR}(0) W_R(t)$ and $\sigma_{LL}(0) W_L(t)$, which are the probabilities of the SQUID remaining in the relevant flux channel, evolve under our current operation with starting density elements $\sigma_{RR}(0) = \sigma_{LL}(0) = 0.5$. At the same time because the density matrix elements evolve eventually to

$$\sigma_{RR} \approx \sigma_{RR}(t_1) W_R \{W\}^{-1} \approx 1 \tag{2.78}$$

and

$$\sigma_{LL} \approx \sigma_{LL}(t_1) W_L \{W\}^{-1} \approx 0 \tag{2.79}$$

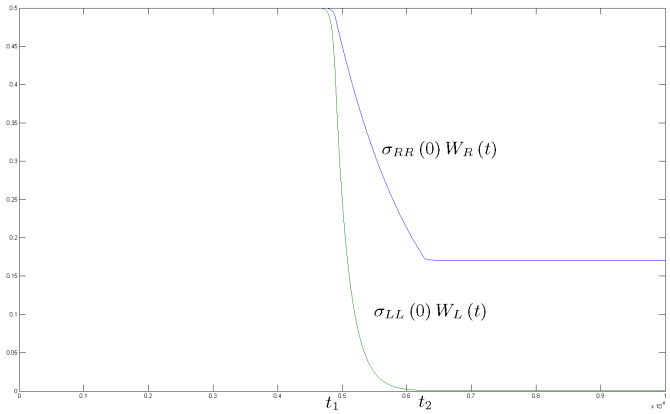

Figure 2.18: The blue line and green line respectively represent for the evolution of $\sigma_{RR}(0) W_R(t)$ and $\sigma_{LL}(0) W_L(t)$ for negative measurement of R state. Here we start with $\sigma_{RR}(0) = \sigma_{LL}(0) = 0.5$ as an example. Both lines have obvious drop between t_1 and t_2, during which the bias current is constantly I_1, but have different decay rates $\Gamma_R(I_1)$ and $\Gamma_L(I_1)$. Finally, $\sigma_{LL}(0) W_L(t)$ go to zero and $\sigma_{RR}(0) W_L(t) \approx \sigma_{RR}(t_1) e^{-(t_2-t_1)\Gamma_R(I_1)}$ according to Eq.(2.75) and Eq.(2.77).

as shown in the Fig.2.19, where only the systems being in the R state left after the current operation without escape taking place, we can claim that we are exactly performing a negative outcome measurement on R state, though only a fraction W of the total tests is left as the required ensemble. According to Eq.(2.77), we

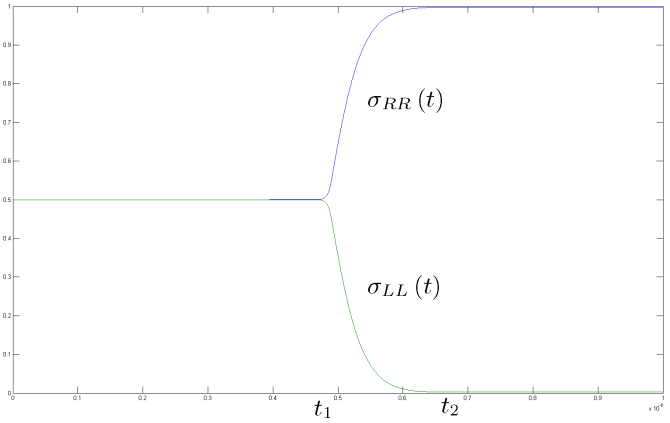

Figure 2.19: The evolutions of the density matrix elements $\sigma_{RR}(t)$ and $\sigma_{LL}(t)$ are respectively represented by blue line and green line under the negative measurement of R state. As an example, both starting at value 0.5 and then have obvious change between t_1 and t_2. Finally, $\sigma_{RR}(t)$ approaches 1 and $\sigma_{LL}(t)$ approaches 0 as described in Eq.(2.78) and Eq.(2.79) .

can estimate $\sigma_{RR}(0)$ by $\sigma_{RR}(t_1)$ if we can correctly measure W and W_R. Similarly, for negative measurement of L state, we need construct a situation where the escape rate $\Gamma'_R(I'_1)$ for the R state at given bias current is much faster than $\Gamma'_L(I'_1)$ for the L state such that we have

$$W'_L \approx \exp^{-\left(t'_2-t'_1\right)\Gamma'_L\left(I'_1\right)} \gg W'_R \approx \exp^{-\left(t'_2-t'_1\right)\Gamma'_R\left(I'_1\right)}. \tag{2.80}$$

in the end and then we can claim that the systems after negative outcome measurement are all in the L state. Here we use the prime notation to denote the difference between R and L measurement. Also the portion of negative outcome ensemble relative to the total number of tests is

$$W' = \sigma_{RR}\left(t_1'\right) W_R' + \sigma_{LL}\left(t_1'\right) W_L' \simeq \sigma_{LL}\left(t_1'\right) W_L' \tag{2.81}$$

, and we can use this formula to estimate $\sigma_{LL}\left(0\right)$.

Let's consider the other possibility of constructing the flux basis preferred measurement if we instead increase and decrease the bias current adiabatically during the measurement. Because in the adiabatic limit the evolution of the weight for each channel follows its initial value, which is based on the energy basis not flux basis, the only information we can get after the negative outcome measurement is just the density matrix elements based on energy basis at zero bias current. Therefore our negative outcome measurement in the adiabatic limit of bias current is the energy basis preferred measurement. If we want to change it to a flux basis preferred measurement, we can make a sudden increase of the qubit bias energy right before the adiabatic ramping of bias current on dcSQUID such that the eigen basis at zero bias current is exactly the flux basis and what we measure in the end are the components of qubit initial state in flux basis.

2.8 Summary

The "two-channel" picture based on energy basis after Harmonic approximation captures most of the physics in static experiments. On the other hand, the "two-channel" picture based on flux basis also works well in the large escape rate limit of dynamic experiment. Therefore, we generalized the idea of "two-channel" escape to all of the parameter regime for the qubit-SQUID system and conclude that our coupled system tends to behave as an energy-basis measurement in the small escape rate limit but as a flux-basis measurement in the large escape rate limit. In sum we have studied the escape physics of the qubit-SQUID coupled system in varies limits. Furthermore, we use these results to analyze the qubit density matrix evolution before the current switching happens, the entanglement of the qubit-SQUID system, and the weak measurement behavior of our experiment. In the end, we discussed the possible ways to realize the flux-basis projective measurements with our qubit-SQUID system for the preparation of the TBI test.

Chapter 3

Possibilities of a test of the Temporal Bell inequalities(TBI) using a flux qubit coupling to a dcSQUID

3.1 Introduction

In this chapter we have two main objectives; the first is to discuss the realization of an ideal negative result (INR) measurement on our qubit-dcSQUID system, and the second is to quantify the measurement invasiveness in the ancillary test and use it to improve the TBI experiment. In Section 2, we will give a quick review of our motivations which have been discussed in Chpater 1, and introduce briefly the overall structure of Knee's experiment for testing TBI. The core structure of the INR measurement implemented by Knee's group will be discussed in detail in Section 3. Also, we will show how to generalize the structure to our qubit-dcSQUID composite system. Our goal in this section is to set up a projective INR measurement on a macroscopic object with flux basis such that we can achieve the prototype measurement mentioned in ref.[1] for TBI. This is our first main objective. The second main objective of this chapter will be discussed in sections 4-6. In Section 4, the ancillary test is reviewed in greater detail. Furthermore, we also take into account the idea of Wilde and Mizel [3] in the quantification of the measurement invasiveness so that we can give a more concrete protocol of the ancillary test that cooperates with our new arrangement of the TBI test, which is itself given in Section 5. A new lower bound for TBI will be given based on the ancillary test from Section 4 and the modified TBI main experiment described in Section 5 such that the loophole will be narrowed. Next, we will give an idealized analysis of the boundary of TBI in Section 6. As there does not yet exist any experimental implementation of the ancillary test, it is uncertain how large the measurement invasivity will be. Therefore, we try to estimate the measurement invasivity based on an INR measurement. We assume that the ensemble of negative outcome is perfectly non-invasive by measurement, but it it possible to mistakenly measure a positive outcome ensemble as a negative outcome ensemble. Therefore, a mis-assignment of any portion of the positive ensemble will effectively introduce measurement invasivity. Here the mistaken ratio can be described by the term measurement venality ζ, which is exactly the probability of having a measurement error (this term will be described in detail later). Based on this simplified model, we can find a venality-dependent TBI lower bound, and use it to determine

the feasibility of the ancillary test. In other words, we will determine the maximum tolerated measurement error within which the TBI experiment will be meaningful.) In Section 7, we discuss the possible sources that can cause measurement error using our implementation of INR measurement given in Section 3.

3.2 The Motivation (review)

As we know from Chapter 1, the purpose of the TBI experiment is to see whether we can rule out MR, thereby supporting quantum mechanics at the macroscopic scale. The TBI is given by

$$L\left(t_1,t_2,t_3\right) \equiv \left\langle Q_1Q_2\right\rangle_{1,2} + \left\langle Q_2Q_3\right\rangle_{2,3} + \left\langle Q_1Q_3\right\rangle_{1,3} + 1 \geq 0. \tag{3.1}$$

(Please read Chapter 1 Section 1 for detailed definitions.) It is based on the three postulates: (1) macroscopic realism (MR), (2) noninvasive measurability (or measurement) (NIM), and (3) induction. To implement the NIM, the INR measurement was suggested by Leggett and Garg [1]. Recently, Knee et al. [4] successfully realized the INR measurement on a nuclear-electron coupled system in the high field limit (we will discuss their detailed implementation in the next section). More critically, in order to rule out MR we need to make sure these postulates (especially the NIM) are satisfied in the TBI experiment; the ancillary test [9] is introduced to check the measurement invasivity to avoid a possible loophole [3] of ruling out MR. Therefore, one of our most important tasks in this chapter is designing an applicable way to quantify the measurement invasivity for improving TBI by avoiding the NIM loophole.

With the help of nuclear-electron-pair based INR measurement, Knee et al. [4] first performed the TBI test on a microscopic system using projective measurement of electron (or nuclear) spin. A family of three experiments (each corresponding to a set of runs of the same operating times $\{t_i,t_j\}$) are implemented to get three two-time correlators $K_{ij} = \left\langle Q\left(t_i\right)Q\left(t_j\right)\right\rangle$ for $i<j(i,j=1,2,3)$. Every experimental run always has the arrangement of an INR measurement (the 1st measurement at t_i) followed by a normal measurement (the 2nd measurement at t_j). In addition, between two measurements at t_i and t_j there should be an unitary operation U to perform a coherent control on the system (nuclear) between two energy states to set up the required two-time correlation of system. The results of Knee et al. indeed show the violation of TBI and are close to quantum mechanical prediction, but they did not consider the ancillary test to ensure the non-invasiveness of their INR measurement. Therefore, the experiment still is subject to the loophole problem [3] and may not be used to rule out the MR assumption; their TBI experiment is not complete. To solve this problem, we will study the ancillary test in Section 4 and Section 5. Before that, in Section 3 we will discuss the adaptation of the core structure of INR measurement used by Knee et al. to our

qubit-dcSQUID composite system. Basically, we apply the properties of energy states of the qubit-dcSQUID composite system given in Chapter 2 to the protocol of INR measurement used by Knee et al.

3.3 The realization of INR measurement with the qubit-SQUID coupled system

So far there is no experiment indeed testing TBI based on Leggett-Garg proposal[1] of projective measurement on macroscopic quantum coherent flux states; Palacios-Laloy et al. [5] only perform a weak measurement on transmon type superconducting qubit, and Knee et al. [4] only realize projective INR measurement on microscopic system. (Please note that some of these motivations may not be true anymore because during the preparation of my thesis writing new experiments related to macroscopically testing TBI is published, see ref. [50],[51].) The quantum theory as applied to macroscopic objects is still questionable. In order to construct an INR measurement on a macroscopic object, we are going to generalize Knee's INR measurement by replacing nuclear-electron system with qubit-dcSQUID system. Basically, the core structure of our INR measurement is very similar to Knee's for the transition of system size from microscopic to macroscopic.

In Knee's experiment, the core structure of INR measurement is based on nuclear-electron(system-ancilla) pair, where the four possible energy eigen states of the coupled system are $|\uparrow\uparrow\rangle, |\uparrow\downarrow\rangle, |\downarrow\downarrow\rangle,$ and $|\downarrow\uparrow\rangle$ in the spin representation of $|system, ancilla\rangle$(see Fig.3.1). Because the two possible excited energies (MW1 and MW2) of electron depend on nuclear spin, when the frequency of the applied microwave matches one of the two possible electron excited energies, the electron will flip its spin from ground energy level to excited energy level and we can identify the nuclear spin via the measurement of electron state if the electron is correctly prepared in the ground level $|\downarrow\rangle$. Therefore, an INR measurement on nuclear spin up and spin down states can be realized by post-selecting the runs of electron spin being not excited by microwave of frequency MW2 and MW1 respectively, which are also called the CNOT gate and the antiCNOT gate in Knee's paper.

In our experiment, the qubit's two energy states correspond to the nuclear spin of Knee's experiment, and the lowest two energy states of dcSQUID together can act as the electron spin. Furthermore, if we want the excited energy between two dcSQUID states to depend on the qubit state, the flux qubit needs to interact with dcSQUID such that they can behave exactly like a nuclear-electron pair in Knee's experiment. Because the induced flux from the qubit states can effectively change dcSQUID phase potential, as required, the excited energy of lowest two energy levels of dcSQUID indeed depends on the qubit state. Therefore, by solving the energy levels of qubit-dcSQUID coupled system, we can exactly show how energy levels of

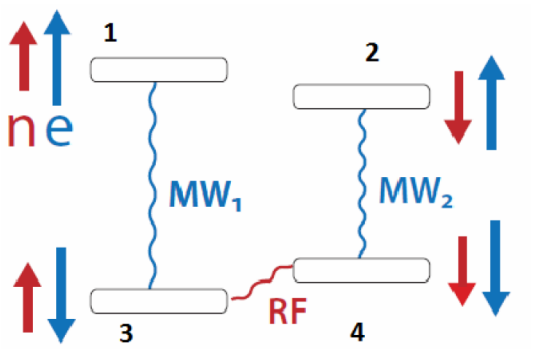

Figure 3.1: the four energy levels in Knee's INR measurement

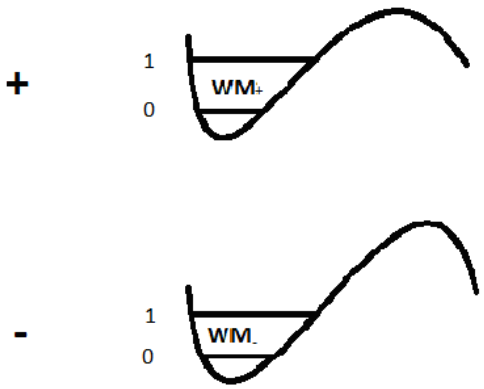

Figure 3.2: the four energy levels in our INR measurement

dcSQUID change with qubit state.

Please note that the work in this section is different from the tasks in Chapter 2. The analysis in Chapter 2 of whether the escape dynamics of the SQUID is better described in terms of energy or flux channels can be considered as the preparartion for the work in this section; the relative knowledge can help us to pick up the right channels and setup energy levels of qubit-SQUID so that we can construct an INR measurement similar to Knee's experiment based on our qubit-SQUID system.

Let's consider the qubit-dcSQUID coupled system with simplified Hamiltonian

$$\begin{aligned} H &= H_q + H_{\mathrm{SQ}} + H_{\mathrm{coupling}} \\ H_q &= \varepsilon\sigma_z + \Delta\sigma_x \\ H_{\mathrm{SQ}} &= \frac{-\hbar^2}{2m}\partial_\phi^2 - 2E_{J0}\cos\left[\pi f_{SQ}\right]\cos\left[\phi\right] + \frac{\hbar I_b}{2e}\phi \\ H_{\mathrm{coupling}} &\simeq 2\pi M E_{J0}\sin\left[\pi f_{SQ}\right]\cos\left[\phi\right]\sigma_z = \varepsilon_{\mathrm{int}}\left(\phi\right)\sigma_z \end{aligned}$$

, where 2ε and Δ are respectively the energy difference and tunneling energy between the two flux states of the qubit. For the dcSQUID, E_{J0} and C_0 are the Josephson energy and capacitance of one junction, $m = 2C_0\left(\frac{\hbar}{2e}\right)^2$ is the effective mass of the average phase ϕ of the junctions, and I_b is the bias current. We have $f_{SQ} = \frac{\Phi_{SQ}}{\Phi_0}$ representing for the SQUID applied flux and $M = \frac{\Phi_q}{\Phi_0}$ being the coupling strength between qubit and dcSQUID with Φ_q being the qubits induced flux on dcSQUID.

Based on our previous analysis of qubit-dcSQUID coupled system , we can effectively diagonalize our Hamiltonian into the following form by new spin basis $|+\rangle$ and $|-\rangle$ of the coupled system:

$$H = \begin{pmatrix} H_+ & 0 \\ 0 & H_- \end{pmatrix} \tag{3.2}$$

, where

$$H_\pm = \frac{-\hbar^2}{2m}\partial_\phi^2 + U_\pm(\phi) \tag{3.3}$$

with $U_+(\phi)$ and $U_-(\phi)$ being the effective SQUID potentials corresponding to new spin basis $|+\rangle$ and $|-\rangle$ respectively. Based on these effective potentials of dcSQUID, we can easily estimate the excited energy and escape rates of lowest two energy levels($|0\rangle$ and $|1\rangle$) of each potential. Ideally, we can consider the dynamics of our coupled system as two-channel-escaping physics(without tunneling between the channels) as shown in Fig.3.2; and similar to Knee's experiment, the states $|+,0\rangle, |+,1\rangle, |-,0\rangle,$ and $|-,1\rangle$ are the corresponding four energy levels, and the required excited energies(or frequencies) are

$$\mathrm{MW1} \equiv (E_{+1} - E_{+0}) \approx (E_1 - E_0) + \left(\sum_{k\neq 1}\frac{|\varepsilon_{1k}|^2}{E_1 - E_k} - \sum_{k\neq 0}\frac{|\varepsilon_{0k}|^2}{E_0 - E_k}\right) + \left(\sqrt{\varepsilon_{11}^2 + \Delta^2} - \sqrt{\varepsilon_{00}^2 + \Delta^2}\right) \tag{3.4}$$

$$\mathrm{MW2} \equiv (E_{-1} - E_{-0}) \approx (E_1 - E_0) + \left(\sum_{k\neq 1}\frac{|\varepsilon_{1k}|^2}{E_1 - E_k} - \sum_{k\neq 0}\frac{|\varepsilon_{0k}|^2}{E_0 - E_k}\right) - \left(\sqrt{\varepsilon_{11}^2 + \Delta^2} - \sqrt{\varepsilon_{00}^2 + \Delta^2}\right) \tag{3.5}$$

$$\mathrm{E_U} \equiv E_{+0} - E_{-0} = 2\sqrt{\varepsilon_{00}^2 + \Delta^2} + O\left(M^3\right) \tag{3.6}$$

Here we have defined $\varepsilon_{mn} \equiv \langle m|\,\varepsilon + \varepsilon_{\mathrm{int}}(\phi)\,|n\rangle$, and E_n and $|n\rangle$ are eigen energy and eigen state of the dcSQUID Hamiltonian in Eq.(3.2) respectively. In Eq. (3.4) and (3.5), the first terms are the SQUID energy difference before coupling to qubit, the second terms are the perturbation corrections to the SQUID energy, and the last one is the qubit energy diffence in our two-channel representation. Please see Eq. (B.12) and (B.13) for detailed analysis. The energy $\mathrm{E_U}$ in Eq.(3.6) corresponds to the transition between

$|+,0\rangle$ and $|-,0\rangle$, which gives the microwave frequency for uniatry operation U on qubit system between any two measuring times. The other two equations describe the excited energy between $|+,0\rangle$ and $|+,1\rangle$, and the excited energy between $|-,1\rangle$ and $|-,0\rangle$, which respectively take place of the MW1 and MW2 of the Knee's experiment. As we can see that the difference between Eq. (3.4) and Eq. (3.5) is contributed by their last terms, which is $2\left(\sqrt{\varepsilon_{11}^2+\Delta^2}-\sqrt{\varepsilon_{00}^2+\Delta^2}\right)$ and related to the effective bias energy and qubit tunneling energy. Theoretically, we justified that our qubit-SQUID system has similar energy structure as nuclear-electron system in Knee's experiment for INR measurement. We can either numerically calculate these energy levels, or experimentally test their excited energies to get the correct resonance frequencies.

After figuring out the required excited energies between the states, it is not hard to control our system coherently with microwaves. Besides, with appropriate bias current, once the dcSQUID is excited to $|1\rangle$ it should switch to voltage mode immediately due to the large escape rate Γ_1 for dcSQUID in $|1\rangle$. By contrast, the dcSQUID in $|0\rangle$ is supposed to stay in superconducting mode by its relatively small escape rate Γ_0, which corresponds to negative result of measurement because there is no voltage signal measured. Therefore, we can operate an INR measurement with qubit-dcSQUID system by applying microwave of selected frequency on coupled system under appropriate current control of dcSQUID. Also, an unitary operation on qubit(primary system) can be realized by conherent control of coupled system between $|+,0\rangle$ and $|-,0\rangle$ with microwave frequency of energy E_U. Practically, this unitary operation will be affected by relaxation and dephasing physics.

Entirely, the core structure of each INR measurement requires appropriately controlled bias current I_b such that the escape rate Γ_1 of dcSQUID state $|1\rangle$ can be much greater than Γ_0 of state $|0\rangle$, γ_{10} , and γ_φ, where γ_{10} and γ_φ are the relaxation rate and the dephasing rate between $|1\rangle$ and $|0\rangle$ (for more detail analysis, please see Section 6). Besides, the system needs to wait for a certain time longer than $\frac{1}{\Gamma_1}$ to prepare dcSQUID in its ground state $|0\rangle$, then we can perform the INR measurement of states $|+\rangle$ and $|-\rangle$ by applying the microwave MW_- and MW_+ respectively to equal number of experimental runs and keeping only the systems of negative runs where dcSQUID does not switch to the voltage mode. Finally, the ratio between two types of negative runs reveals the information of the system under the INR measurement.

3.4 Quantifying measurement invasiveness in the ancillary test

The main logic of the ancillary test is quite simple: if we don't want the violation of TBI to be ascribed to the untested measurement invasiveness, we need to implement a test to justify the non-invasiveness of the measurements or at least measure and quantify the measurement invasiveness such that we can use these

measured classical invasivities to adjust the boundary of TBI. Of course, if the measurement invasivities are too large such that the new boundary of TBI is outside the range of the quantum limit, then it is hopeless to claim anything. But, if we can set up the experiment appropriately such that the new boundary of TBI is still within the quantum limit, then it may be possible to rule out macroscopic realism by our use of the TBI experiment.

In this section, we will introduce the principles of the ancillary test, analyze how to quantify the measurement invasiveness in a more practical way based on two-time correlators, and construct our protocol for the ancillary test. We hope to use the test results to modify the lower bound of TBI in Eq.(1.3) such that the possible violation of TBI due to the "classical" measurement invasiveness is already considered and the loophole of arguing the invalidity of macroscopic realism per se becomes narrower.

In principle, it has been mentioned by A. J. Leggett in 1988 [9] that a complete experiment of TBI should include such an ancillary test in order to justify the noninvasive measurability in the experiment. After that, Wilde and Mizel [3] gave a more detailed theoretical analysis of measurement invasiveness in the ancillary test. Consequently, the whole experiment has following stages:

I. Ancillary test:

I-A. Preparation of quantum state This is the standard experimental protocol of quantum mechanics; we can operate and adjust the standard von Neumann measurement(VNM) repeatedly to ensure the agreement between experimental result and quantum mechanical prediction so that we can correctly prepare our system in a specific state.

I-B. Test for classical invasivity This is the main stage of the ancillary test used to check the NIM. The NIM postulate is considered in the context of the postulate of (macro) realism; the argument goes that the system must (according to MR) be in a definite state right before measurement in TBI experiment, and thus in the ancillary test, we only need to determine whether the system, when known (independently of MR) to be in a definite state, is perturbed (invasively) by measurements or not, and we define the degree of invasiveness under these conditions as 'classical' invasivity. Therefore, to check the 'classical' invasivity of the measurement in TBI, we need to prepare the system in a definite state right at the measurement time to guarantee the' classical' behavior of the system such that we can test the NIM postulate 'classically'; any scenario inducing wave collapse mechanics should be excluded in the ancillary test because the measurement in such a scenario will be invasive in quantum fashion. For example, if we want to test the invasiviness of measurement $Q(t_2')$, we need to prepare the system in such a manner that the measurement always gives $Q(t_2') = +1$ whenever we operate it at t_2', where the preparation step is given by stage I-A. Next, once we set

up our system state at t_2', we can compare the system's behaviors at $t' > t_2'$ under the condition A that the measurement is performed at t_2' and condition B that no measurement is performed at t_2'. The discrepancy between these two system's behaviors indicates how invasive the measurement $Q(t_2')$ is.

II. Main experiment: The purpose of this stage is to test the TBI. Based on Eq.(3.1), three core measurements are implemented to get the three possible two-time correlators $K_{ij} = \langle Q_i Q_j \rangle$(for $1 \leq i < j \leq 3$) and to give the Leggett-Garg function.

To quantify the measurement invasivity, Wilde and Mizel [3] give a concrete definition for the discrepancy between the system's behaviors under two different measurement conditions, though they do not focus on the required classical preparation of state as described in stage I-B of the ancillary test. Wilde and Mizel define a measurable quantity ϵ which is based on the change in joint probability distribution of the two measurements' outcomes (at t_1 and t_3) due to the operation of the measurement (at t_2' in our case).

$$\sum_{a.c} |P(a, c\,|\mathrm{A}) - P(a, c\,|\mathrm{B})| \leq \epsilon \tag{3.7}$$

Here a and c respectively represent the possible measurement outcomes of the 1st(at t_1) and the 3rd(at t_3) measurements. In addition, "A" denotes a the condition where "the 2nd measurement is performed" and "B" denotes a the condition where "the 2nd measurement is not performed", where the 2nd measurement is the main measurement to be tested for its invasiveness. Therefore, $P(a, c\,|\mathrm{A})$ and $P(a, c\,|\mathrm{B})$ can be read as the measured joint probabilities of two given outcomes (a and c) of the 1st and the 3rd measurements, respectively, under the conditions of being with and without the operation of the 2nd measurement.

To provide a more practical scheme for the ancillary test, we need to convert the idea of Wilde and Mizel to a more useful representation for quantifying the invasiveness of measurement tested in the stage I-B, so that we can easily use these quantified invasivities to modify the lower bound of TBI. Therefore, in the following paragraph we will discuss further details of how to quantify the measurement invasivities.

Based on the protocol of the TBI experiment, in principle, there should be three possible structures of invasivities according to the relative order between the measurement to be tested and the two-time correlator used as an indicator, where the arrangement is similar to the analysis of non-invaded correlations(NIC) in ref.[46]. For example, we can consider a situation in which the measurement to be tested(at t_1) always appears before the times(t_2 and t_3) of two-time correlator and see how does the two-time correlator change due to the operation of that measurement, which is denoted as the type I invasivity. In order to fulfill the

requirement of ancillary test in I-B stage, we need to prepare the system in either "Q_{1+}" condition or "Q_{1-}" condition, where the "$Q_{1\pm}$" condition means that the outcome always shows $Q = \pm$ whenever we perform a VNM at t_1. Besides, we will need the conditions $A_1 \equiv$ "the measurement at t_1 is performed" and $B_1 \equiv$ "the measurement at t_1 is not performed".

Based on above definitions, if we consider $P_{+-}\left(t_2, t_3 \left| Q_{1+}, A_1 \right.\right)$ as the joint probability of $Q\left(t_2\right) = +1$ and $Q\left(t_3\right) = -1$ under the conditions Q_{1+} and A_1, then the corresponding two-time correlator under the same conditions is

$$\begin{aligned} K\left(t_2, t_3 \left| Q_{1+}, A_1 \right.\right) &= P_{+,+}\left(t_2, t_3 \left| Q_{1+}, A_1 \right.\right) + P_{-,-}\left(t_2, t_3 \left| Q_{1+}, A_1 \right.\right) \\ &- P_{+,-}\left(t_2, t_3 \left| Q_{1+}, A_1 \right.\right) - P_{-,+}\left(t_2, t_3 \left| Q_{1+}, A_1 \right.\right). \end{aligned} \tag{3.8}$$

Accordingly, the change of the two-time correlator between measurements at t_2 and t_3 due to the operation of the measurement at t_1 is given by

$$\Delta K_{23}\left(Q_{1+}\right) \equiv \Delta K\left(t_2, t_3 \left| Q_{1+} \right.\right) \equiv K\left(t_2, t_3 \left| Q_{1+}, A_1 \right.\right) - K\left(t_2, t_3 \left| Q_{1+}, B_1 \right.\right). \tag{3.9}$$

On the other hand, we can also consider $\Delta K_{23}\left(Q_{1-}\right)$ for the "Q_{1-}" condition. In principle, we can use $\Delta K_{23}\left(Q_{1+}\right)$ and $\Delta K_{23}\left(Q_{1-}\right)$ to quantify the type I invasivity. Please note that for utilizing our formula of type I invasivity to the analysis of TBI in Eq.(1.3), in TBI main experiment we just need to specify the initial state at t_1 by considering the "$Q_{1\pm}$" condition so that we can set t_1, t_2, and t_3 here to be exactly equal to the time sequence in the main experiment of TBI.

Next, we can also consider another type of invasivity, called the type II invasivity, where the measurement to be tested appears within the time period of two-time correlator; the three measurements respectively appear at t_1, t_2', and t_3, where the ones at t_1 and t_3 belong to the two-time correlator and the one at t_2' is going to be tested its invasiveness. In principle, similar to the Type I invasivity, we wish our time sequence t_1, t_2', and t_3 here to agree with what in the TBI main experiment. However, the choice of t_2' in the I-B stage of ancillary test should satisfy the classical condition $Q_{2\pm}$ that "the system is prepared definitely in $\pm$ state before we take any measurement at t_2'". Therefore the t_2' for type II invasivity test is not the same as the t_2 in the TBI main experiment.

If we define $A_2 \equiv$ "the measurement at t_2' is performed" and $B_2 \equiv$"no measurement at t_2'", similarly, we also can have the change of the two-time correlator of measurements at t_1 and t_3 due to the operation of

the measurement at t_2', i.e.

$$\Delta K_{13}\left(Q_{2+}\right) \equiv \Delta K\left(t_1, t_3\left|Q_{2+}\right.\right) \equiv K\left(t_1, t_3\left|Q_{2+}, A_2\right.\right) - K\left(t_1, t_3\left|Q_{2+}, B_2\right.\right) \tag{3.10}$$

Also, the corresponding change of two-time correlator K_{13} due to the measurement at t_2' under the condition Q_{2-} is given by $\Delta K_{13}\left(Q_{2-}\right) \equiv \Delta K\left(t_1, t_3\left|Q_{2-}\right.\right)$. Basically, we use $\Delta K_{13}\left(Q_{2+}\right)$ and $\Delta K_{13}\left(Q_{2-}\right)$ to quantify the type II invasivity.

Because we believe the postulate of induction rather than the MR and NIM, we don't consider the type III invasivity test in which the measurement to be tested always appears after the times of two-time correlator. Basically we just set the type III invasivity equal to zero by hypothesis.

Once we measure the quantified type I and type II invasivities, we can use them to modify the lower bound of TBI under certain initial condition at t_1. The detailed analysis will be discussed in next section. In general, the measurements in TBI experiment can be any type, e.g., the VNM or the INR measurement. However, if we want to reduce the values of type I and type II invasivities, the first measurement (at t_1) and the second measurement(at t_2) are needed be the INR measurement. Please notice that even though the type I invasivity (defined by $\Delta K_{23}\left(Q_{1+}\right)$ or $\Delta K_{23}\left(Q_{1-}\right)$) is expected to be zero in the quantum theory, the ancillary test for type I invasivity is still required based on the macrorealism.

As we mentioned before, because of the $Q_{2\pm}$ condition, only the choice of t_2' in type II invasivity test is not equal to t_2 in TBI experiment. Therefore, in order to make our ancillary test applicable to the improvement of TBI, at least we can make the choice of t_1 and t_3 in ancillary test are the same as that(t_1 and t_3) in the TBI main experiment, which should be based on the requirement of maximum violation in TBI experiment ($\theta_{13} = \frac{4n\pi}{3}$ for n being integer). Here θ_{ij} represents the evolution phase of system between t_i and t_j for quantum mechanical two-time correlator $\langle Q_i Q_j \rangle_{i,j} = \cos\theta_{ij}$. Next, we require that t_2' should stay between t_1 and t_3 so that we can check the type II inavsivity in ancillary test for estimating the measurement invasivity at t_2 in main TBI experiment. Accordingly, we can find the required minimum θ_{13} between t_1 and t_3 satisfies $\theta_{13} = \frac{4\pi}{3}$ for t_2' satisfying $Q_{2\pm}$ with $\theta_{12'} = 0$ or $\frac{\pi}{2}$.

3.5 The arrangement of main TBI experimental based on the invasivities measured in ancillary test

To reduce the type I and type II invasivities, the INR measurement would be good candidates for measurements Q_1 and Q_2. Therefore, we can set up a new arrangement of TBI experiment with Q_1 and Q_2

being the INR measurements for $\langle Q_1 Q_2 \rangle_{1,2}$, Q_2 and Q_3 respectively being INR measurement and VNM for $\langle Q_2 Q_3 \rangle_{2,3}$, and Q_1 and Q_3 respectively being INR measurement and VNM for $\langle Q_1 Q_3 \rangle_{1,3}$. Besides, in order to make the ancillary test more applicable to the TBI experiment, we also require the $Q_{1\pm}$ condition in TBI experiment.

If we make the postulates of MR and induction and assign values of type I and type II invasivities, we can estimate the new lower bound of Eq.(3.1) by extrapolating the ensemble in TBI experiment to another ideal ensemble of sequence of three measurements ordered by INR measurement, INR measurement, and VNM respectively at t_1, t_2, and t_3 (under the same initial condition at t_1). Of course, all extrapolations are under the classical picture. For example, because of the assumption of induction, which gives zero type III invasivity, the presence of the measurement at t_3 has nothing to do with the correlator $\langle Q_1 Q_2 \rangle_{1,2}$ and therefore we can simply extrapolate $\langle Q_1 Q_2 \rangle_{1,2}$ in Eq.(3.1) to $\langle Q_1 Q_2 \rangle_{1,2,3}$ without any invasivity correction, where the subscripts $1, 2, 3$ on the pointed bracket represent the new ensemble of system with three measurements ordered by INR measurement, INR measurement, and VNM respectively at t_1, t_2, and t_3. Next, for the extrapolation from $\langle Q_2 Q_3 \rangle_{2,3}$ to $\langle Q_2 Q_3 \rangle_{1,2,3}$ we need to consider the change of $\langle Q_2 Q_3 \rangle$ due to the "classical" invasivity of the INR measurement at t_1, which is exactly described by the type I invasivity $\Delta K\left(t_2, t_3 \,|Q_{1+}\right)$. Here we have considered the "Q_{1+}" condition that the system is prepared in "$Q = +$" state at t_1. Consequently we can replace $\langle Q_2 Q_3 \rangle_{2,3}$ by $\langle Q_2 Q_3 \rangle_{1,2,3}$ in Eq.(3.1) with the correction from $\Delta K\left(t_2, t_3 \,|Q_{1+}\right)$. Similarly, with a knowledge of type II invasivity, that is $\Delta K\left(t_1, t_3 \,|Q_{1+}, Q_{2\pm}\right)$, we can do the extrapolation from $\langle Q_1 Q_3 \rangle_{1,3}$ to $\langle Q_1 Q_3 \rangle_{1,2,3}$. Please note that because the system at t_2 in main TBI experiment does not satisfy the "reality" requirement for the ancillary test, we can not directly measure the "classical" inavaisity of the measurement Q_2 at t_2. Therefore, we can only measure $\Delta K\left(t_1, t_3 \,|Q_{2+}\right)$ and $\Delta K\left(t_1, t_3 \,|Q_{2-}\right)$ at t_2' in ancillary test and use them to estimate the classical measurement invasivity at t_2 for main experiment, where we emphasize that $\Delta K\left(t_1, t_3 \,|Q_{2\pm}\right)$ is defined by Eq. (3.10) with $Q_\pm$ condition on t_2'. Here we have assumed that the measurement invasivity of Q_2 only depends on the state of the system. The estimated formula for the classical invasivity of Q_2 at t_2 is given by

$$\max \Delta K\left(t_1, t_3 \,|Q_{2\pm}\right) \geq \Delta K_{cl}\left(t_1, t_3 \,|Q_2 \text{ at } t_2\right) \tag{3.11}$$

. Here $\Delta K_{cl}\left(t_1, t_3\left|Q_2 \text{ at } \mathrm{t}_2\right.\right)$ is the imaginary type II invasivity of the measurement Q_2 at t_2 in TBI experiment. Finally, we can extrapolate Eq.(3.1) to the following equation:

$$\begin{aligned} L\left(t_1, t_2, t_3\right) \geq & \left\langle Q_1 Q_2\right\rangle_{1,2,3}+\left\langle Q_2 Q_3\right\rangle_{1,2,3}+\left\langle Q_1 Q_3\right\rangle_{1,2,3}+1 \\ & -\Delta K\left(t_2, t_3\left|Q_{1+}\right.\right)-\max \Delta K\left(t_1, t_3\left|Q_{1+}, Q_{2 \pm}\right.\right) \\ \geq & -\Delta K\left(t_2, t_3\left|Q_{1+}\right.\right)-\max \Delta K\left(t_1, t_3\left|Q_{1+}, Q_{2 \pm}\right.\right) . \end{aligned} \tag{3.12}$$

Here we have applied the previous result of $\left\langle Q_1 Q_2\right\rangle_{1,2,3}+\left\langle Q_2 Q_3\right\rangle_{1,2,3}+\left\langle Q_1 Q_3\right\rangle_{1,2,3}+1 \geq 0$ for the second inequality. It is bounded by our type I and type II invasivities, which are measurable quantity in the ancillary test. Because the above analysis only considers the case of initial condition where the system is prepared in "$Q=+$" state at t_1, to complete the analysis we also need to consider the condition where the system is prepared in "$Q=-$" state at t_1:

$$\begin{aligned} L\left(t_1, t_2, t_3\right) \geq & \left\langle Q_1 Q_2\right\rangle_{1,2,3}+\left\langle Q_2 Q_3\right\rangle_{1,2,3}+\left\langle Q_1 Q_3\right\rangle_{1,2,3}+1 \\ & -\Delta K\left(t_2, t_3\left|Q_{1-}\right.\right)-\max \Delta K\left(t_1, t_3\left|Q_{1-}, Q_{2 \pm}\right.\right) \\ \geq & -\Delta K\left(t_2, t_3\left|Q_{1-}\right.\right)-\max \Delta K\left(t_1, t_3\left|Q_{1-}, Q_{2 \pm}\right.\right) . \end{aligned} \tag{3.13}$$

As we mentioned, although the type I invasivity is ideally zero in quantum theory, the value of $\Delta K\left(t_2, t_3\left|Q_{1 \pm}\right.\right)$ is still required during the extrapolation to TBI by macrorealism. Please note that if we apply the $Q_{1 \pm}$ condition to TBI main experiment we can have the equality $\Delta K\left(t_2, t_3\left|Q_{1 \pm}\right.\right)=\left\langle Q_2 Q_3\right\rangle_{1,2,3}-\left\langle Q_2 Q_3\right\rangle_{2,3}$, where $\Delta K\left(t_2, t_3\left|Q_{1 \pm}\right.\right)$ are measured in ancillary test but $\left\langle Q_2 Q_3\right\rangle_{1,2,3}$ and $\left\langle Q_2 Q_3\right\rangle_{2,3}$ are measured in the main experiment. This equality happens only when we specify the $Q_{1 \pm}$ initial condition on main experiment, in general we don't specify such 'classical' condition on TBI experiment. Therefore, we can conclude that the only contribution to TBI violation comes from the difference between type II invasivity and $\left\langle Q_1 Q_3\right\rangle_{1,2,3}-\left\langle Q_1 Q_3\right\rangle_{1,3}$. Here we have introduced the induction postulate to set the type III invasivity equal to zero. In sum, by appropriate choose of initial condition we can make all TBI violation related to $\left\langle Q_1 Q_3\right\rangle_{1,3}$.

In fact, there is a way to realize the noninvasive measurement(NIM) in our new TBI experiment setup; if we simply specify "macrorealism", in words, as the hypothesis that the macroscopic system with two macroscopically distinct states, described by measurement outcome $Q \in\{+1,-1\}$, available to it will at all times be in one of these states. Suppose we can prepare our (macro-realistic by hypothesis) system

at t_1 so that whenever we start from the prescribed initial condition at t=0 and operate a measurement at t_1, we always find it has $Q = +$; based on the specified "macrorealism" assumption, even if we don't measure the system at t_1, we still know its state of "$Q = +$" at t_1. Therefore, we can claim that we already perform a NIM at t_1 even though we do not actually measure the system at t_1, because no invasive action is performed to tell the state of the system. This imaginary NIM at t_1 helps us to get rid of the type I invasivity during the extrapolation to the temporal Bell inequality. With this imaginary NIM at t_1, our TBI experiment can be rearranged with the core structures of Q_1 and Q_2 being NIM and INR measurements respectively for $\langle Q_1 Q_2 \rangle_{1,2}$, Q_2 and Q_3 being INR measurement and VNM respectively for $\langle Q_2 Q_3 \rangle_{2,3}$, and Q_1 and Q_3 being NIM measurement and VNM respectively for $\langle Q_1 Q_3 \rangle_{1,3}$. Similarly, we can extrapolate ensemble of TBI experiment to another ensemble with sequence of three measurements ordered by NIM, INR measurement, and VNM respectively at t_1, t_2, and t_3. Because the type I invaisivity for NIM should be zero, i.e. $\Delta K\left(t_2, t_3 \left| Q_{1+} \right.\right) = 0$, the new extrapolated inequality corresponding to Eq. (3.12) is

$$L\left(t_1, t_2, t_3\right) \geq -\max \Delta K\left(t_1, t_3 \left| Q_{1+}, Q_{2\pm} \right.\right). \tag{3.14}$$

Similarly, we also need to consider the NIM under the condition of "$Q = -$" at t_1 to complete the whole TBI analysis. There the corresponding extrapolated formula is

$$L\left(t_1, t_2, t_3\right) \geq -\max \Delta K\left(t_1, t_3 \left| Q_{1-}, Q_{2\pm} \right.\right). \tag{3.15}$$

With the help of our imaginary NIM, there is only one INR measurement required(at t_2) in the new arrangement of main TBI experiment, then it is relatively easier to perform the experiment; we don't need to operate two adjacent INR measurements to get the two-time correlator $\langle Q_1 Q_2 \rangle_{1,2}$.

3.6 The estimation of type II invasivity $\Delta K\left(t_1, t_3 \left| Q_{2\pm} \right.\right)$ of INR measurement (by simple venality model)

In principle, we consider the INR measurement as a system-ancilla coupled system[4], where the purpose of the ancilla is to indicate the state of the system. In Knee's experiment, due to the possibility of an incorrectly initialized ancilla in an INR measurement, the measurement venality [4] is defined and analyzed. Instead of using Knee's definition of venality, we want to generalize the definition as the fraction of the ensemble of which the ancilla cannot correctly indicate the system state; we introduce ζ to denote the venality, which

is simply a measurement error of the INR measurement. In principle, the measurement venality and the measurement invasivity are two different things; the venality can be understood as any improper indication of the system state by the ancilla but the measurement invasivity is the direct measuring perturbation on the behavior of system. Although the venality is different from the invasivity, as we will see in the analysis of this section, the venality is able to provide a possible way of introducing the measurement invasivity under a simplified assumption that the measurement invasiveness only comes from the interaction with system at the 'positive' state. (Equivalently, we assume that there is no invasivity if the venality is reduced to zero.) Here the 'positive' state is claimed to be the only state that can interact with the (INR) measurement, giving a positive outcome. Statistically, the venality can change the interpretation of the experimental result by mistaking the runs intended give a positive outcome for runs intended to give a negative outcome. For example, in the INR measurement the venality can induce a false negative case, where a state which is really 'positive' may instead to give a negative measurement outcome. Therefore, according to the assumption that the measurement invasiveness only comes from the interaction on the 'positive' state, the system will become more invasive by the measurement as the venality ζ increases. The venality can mix the invasive part of the system ensemble into the noninvasive part so that we unable to guarantee the non-invasiveness of our system ensemble even when we have a negative outcome. Due to the inappropriate preparation of the ancilla and other detailed physical reasons, it is inevitable to consider measurement error (or fidelity) of the INR measurement.

Motivated by the discussion above, if the measurement error is too large so that we already know the system is heavily invasive by measurement, the TBI becomes meaningless and there is no need for the ancillary test anymore. The purpose of the section is to estimate the maximum tolerated venality (or measurement error) for making the TBI experiment feasible, so that we still have a to do the ancillary test for TBI experiment. As we will see, the type II invasivity of the ancillary test is ideally quantified in terms of the venality under our simplified venality model, which gives us an easy way to estimate part of the measurement invasivity. In general, there are many other models which can establish the relationship between invasivity and venality. Furthermore, in a different model, the system can be invasive by measurement even at zero venality, which may be related to the issue of from the 'negative' state and is additional to our results, but this is not our main concern here. Our priority is to find the maximum tolerated measurement error (or the minimum fidelity of measurement) that can make the TBI experiment meaningful.

Before a detailed theoretical analysis, we first need to classify some possible physical situations and give corresponding notations for them.

1. The measured probability under zero venality In (macro)realism, if the measurement have venality (or error), the results may not correctly reflect the "real" behavior (or state) of the system. Therefore, to make a distinction between the "real" behavior of the system, which can be measured by $\zeta = 0$ measurement, and the measured behavior under $\zeta \neq 0$, we use $P_{i^0_+}$ and $P_{i^0_-}$ to represent the "real" probability of the system being respectively in the state '+' and state '−' at t_i, where 0 denote the system's "real" behavior right before the measurement and it should equal to the measured behavior if $\zeta = 0$. For example, in a realistic picture 1^0_+ represents the system being in + state at t_1, which should be read from the outcome of $\zeta = 0$ measurements. Practically, we take the most reliable($\zeta = 0$) measurement to "describe" the "real" state of system, e.g. we take the von Neumann measurement(VNM) as the $\zeta = 0$ measurement. Although the values of the real behavior and ($\zeta = 0$)measured behavior are exactly the same, the ($\zeta = 0$)measured behavior requires the operation of measurement to read out the 'real' behavior. Therefore, to make a distinction between these two concepts, we use "M" to denote measured behavior under ($\zeta = 0$) measurement. As we will see (especially for the INR measurement in the following analysis), the "real" probability can help us clearly to represent how the measured correlation changes with the nonzero venality.

2. The measured probability based on the INR measurement We use p and n to represent the positive and negative outcomes of INR measurement. Therefore, P_{2_p} and P_{2_n} respectively describe the measured probability of INR measurement with positive outcome and negative outcome at t_2. Based on Knee's experimental analysis, the INR experiment can be decomposed into two sub-measurements: the CNOT gate and antiCNOT gate; one is designed to give the negative outcome (or not response) with + state and the other is designed to give the negative outcome with − state, which are respectively called R measurement and L measurement in the following analysis. Consequently, if we use R and L respectively as the R measurement and the L measurement, then we can take 2^R_n and 2^L_n for the system with negative outcome respectively in R measurement and L measurement at t_2, 2^R_p and 2^L_p for the system of positive outcome respectively in R measurement and L measurement at t_2, and $P_{2^R_n}$ and $P_{2^L_n}$ for the probabilities of system with negative outcome respectively in R measurement and L measurement at t_2. Besides, we may use the term "negative state" for the state for which the INR measurement is supposed to give negative outcome. For example, in R(L) measurement, the $+(-)$ qubit state is the corresponding negative state.

To give a proper estimation of type II invasivity, we will use a simple model of venality by assuming that in the INR measurement the measurement invasiveness only comes from the interaction with the negative state and the venalities of L measurement and R measurement are the same. Especially, we consider the arrangement of Q_1, Q_2, and Q_3 in TBI main experiment being NIM, INR measurement, VNM respectively.

Besides, in ancillary test we require that the system is prepared in + state at t_1, which is $P_{1_+^0}=1$, and is predicted to be in − state at t_2', which is $P_{2_-'^0}=1$, though there is no measurement operated at t_1 and t_2'. Therefore, if we perform an INR measurement (Q_2 with venality ζ) at t_2', we suppose to have $P_{2_n'^L}=(1-\zeta)\,P_{2_-'^0}=1-\zeta$ for L measurement and $P_{2_n'^R}=\zeta P_{2_-'^0}=\zeta$ for R measurement; $(1-\zeta)$ of ensemble correctly indicate the system state according to the definition of venality. Consistently, if there is no venality, we should observe $P_{2_n'^L}=P_{2_-'^0}=1$ and $P_{2_n'^R}=P_{2_+'^0}=0$.

Furthermore, we have $P_{2_-'^0,3_+^M}$ as the joint probability of system in the condition of $2_-'^0$ and 3_+^M, where the system is predicted to stay in − state at t_2' without performing a measurement and shown to be in + state at t_3 by a VNM. The other joint probabilities can be read in similar way. However, because the system of − state could be invasive by R measurement, we use double primes on joint probabilities ($P''_{2_-'^0,3_+^M}$ and $P''_{2_-'^0,3_-^M}$) to indicate the perturbed behavior of the system after the measurement at t_2'. Similarly, we use $P'_{2_+'^0,3_+^M}$ and $P'_{2_+'^0,3_-^M}$ to indicate the invasive behavior of system after the L measurement. Next, to evaluate the joint probabilities between Q_2 and Q_3 , we put all above arguments together to give the following equations:

$$\begin{aligned}
&\mathrm{L}-\text{measurement}: P_{2_n'^L}=(1-\zeta)\,P_{2_-'^0}\\
&\Rightarrow\begin{cases} P_{2_n'^L,3_+^M}=(1-\zeta)\,P_{2_-'^0,3_+^M}+\zeta P'_{2_+'^0,3_+^M},\\ P_{2_n'^L,3_-^M}=(1-\zeta)\,P_{2_-'^0,3_-^M}+\zeta P'_{2_+'^0,3_-^M}.\end{cases}\\
&\mathrm{R}-\text{measureemnt}: P_{2_R'^n}=\zeta P_{2_-'^0}\\
&\Rightarrow\begin{cases} P_{2_n'^R,3_+^M}=(1-\zeta)\,P_{2_+'^0,3_+^M}+\zeta P''_{2_-'^0,3_+^M},\\ P_{2_n'^R,3_-^M}=(1-\zeta)\,P_{2_+'^0,3_-^M}+\zeta P''_{2_-'^0,3_-^M},\end{cases}
\end{aligned}\tag{3.16}$$

Once we have set up above joint probabilities (for $\zeta\neq 0$) between the measurements, we can use them to evaluate the possible range of type II invasivity of the ancillary test in the following analysis so that we can estimate the lower bound of TBI. Please note that if we want to consider the invasivity even at zero venality, we should be aware of the terms proportional to $(1-\eta)$ in Eq.(3.16) and then expect there will be an additional term directly related to the invasity in Eq.(3.19). Based on the above analysis, we can have the two-time correlator between measurements at t_1 and t_3 with the INR measurement Q_2 at t_2' under Q_{2-} condition:

$$\begin{aligned}
K\left(t_1,t_3\,|Q_{2-},A_2\right)&=P_{2_n'^L,3_+^M}+P_{2_n'^R,3_+^M}-P_{2_n'^L,3_-^M}-P_{2_n'^R,3_-^M}\\
&=(1-\zeta)\,K\left(t_1,t_3\,|Q_{2-},B_2\right)+\zeta\left(P''_{2_-'^0,3_+^M}-P''_{2_-'^0,3_-^M}\right).
\end{aligned}\tag{3.17}$$

Here we have assumed $P'_{2_+'^0,3_+^M}=P'_{2_+'^0,3_-^M}=0$ because of Q_{2-} condition. At same time, the corresponding

two-time correlator between measurements at t_1 and t_3 without the presence of the INR measurement Q_2 is

$$K\left(t_1, t_3 \left| Q_{2-}, B_2 \right.\right) = P_{2'^0_-, 3^M_+} - P_{2'^0_-, 3^M_-} \tag{3.18}$$

, where we have $P_{1^0_+} = P_{2'^0_-} = P_{1^0_+, 2'^0_-} = 1$.

Finally, the difference between above two equations gives

$$\begin{aligned} &\Delta K\left(t_1, t_3 \left| Q_{1+}, Q_{2-} \right.\right) \\ &= K\left(t_1, t_3 \left| Q_{2-}, A_2 \right.\right) - K\left(t_1, t_3 \left| Q_{2-}, B_2 \right.\right) \\ &= \zeta \left\{ \left(P''_{2'^0_-, 3^M_+} - P''_{2'^0_-, 3^M_-} \right) - K\left(t_1, t_3 \left| Q_{2-}, B_2 \right.\right) \right\} \leq \frac{3}{2}\zeta \end{aligned} \tag{3.19}$$

, where we used the fact that $\left| P''_{2'^0_-, 3^M_+} - P''_{2'^0_-, 3^M_-} \right| \leq 1$ (for $P''_{2'^0_-, 3^M_+} + P''_{2'^0_-, 3^M_-} = 1$) and $K\left(t_1, t_3 \left| Q_{2-}, B_2 \right.\right) = -\frac{1}{2}$ (for the parameter setting in the TBI main experiment). The result shows us that the estimated bound of the type II invasivity $\Delta K\left(t_1, t_3 \left| Q_{1+}, Q_{2-} \right.\right)$ in our simplified venality model should be limited by $\frac{3}{2}\zeta$. Similarly, we can show $\Delta K\left(t_1, t_3 \left| Q_{1+}, Q_{2+} \right.\right)$ and $\Delta K\left(t_1, t_3 \left| Q_{1-}, Q_{2\pm} \right.\right)$ are also smaller than $\frac{3}{2}\zeta$. By applying this results to the right sides of Eq.(3.14) and Eq.(3.15), we can get the estimated lower bound of TBIs.

$$L\left(t_1, t_2, t_3\right) \geq -\frac{3}{2}\zeta \tag{3.20}$$

So far, we just use the simplified venality model (of the assumption that the measurement invasiveness only comes from the interaction with positive state) to estimate the possible value of type II invasity in the ancillary test, and then plug it into our new TBI formula and give Eq.(3.20). Next, we are going to estimate the three two time correlators in TBI experiment from the quantum point of view. Because the venality of our INR measurement can make a wrong indication of the system state, it will give rise to a chance of sign change of the two-time correlator. Similar to the analysis in Knee's paper [4], quantum theory would predict that each two-time correlator ($K_{1,2}$ or $K_{2,3}$) with INR measurement Q_2 in it will be replaced by $(1-\zeta) K_{i,j} - \zeta K_{i,j}$ due to the the presence of venality ζ, which finally gives the quantum prediction of Leggett-Garg function (for $\cos\theta_{ij} = \frac{1}{2}$)

$$\begin{aligned} L_Q &= (1-2\zeta)\left(\cos\theta_{12} + \cos\theta_{23}\right) + \cos\theta_{13} + 1 \\ &\geq -0.5 + 2\zeta \end{aligned} \tag{3.21}$$

By comparing the lower bound of L_Q with the estimated TBI in Eq.(3.20), if we want to see the TBI violation in our experiment, we need to have the venality ζ satisfying $\zeta < \frac{1}{7}$. This gives us the maximum tolerated measurement error for satisfying the minimum requirement for testing TBI, in which we don't consider the general invasivity.

3.7 The possible sources of venality in our INR measurement with qubit-SQUID coupled system

Basically, the structure of our INR measurement is similar to what is in Knee's experiment by its system-ancilla composition, where the ground state and first excited state of dcSQUID together work as an electron spin(ancilla) and the purpose of the ancilla is to indicate the state of system. Since in last section we already generalized definition of venality to be the fraction of the ensemble of which the ancilla can not correctly indicate the system state, the inaccurate preparation of the dcSQUID state(ancilla) is not the only physical mechanism inducing the venality. Therefore, to figure out all the other possible mechanism that causes the venality in our experiment is the main topic of this section.

1. The inaccurate preparation of the dcSQUID state (ancilla) due to thermal fluctuation: In most of experiments like NTT's and Delft's [12],[17],[18],[24],[25],[36],[22], for given the temperature of dc-SQUID (about 25mK), and the energy difference between ground state and excited state for SQUID potential ($\omega_0\hbar \approx 75mK$), the population ratio between two SQUID states is $1:\alpha$ with $\alpha = \exp\left(-\omega_0\hbar/k_bT\right) = 0.055$, where ω_0 is the plasma frequency at the minimum of the SQUID potential. The corresponding venality contribution $\zeta = \frac{\alpha}{1+\alpha}$ is about 5%, and we denote this kind of venality as ζ_0 .

2. Non-efficient pumping between two states of dcSQUID: Due to the relaxation and escape process, the pumping mechanics from ground state to excited state should be modified [47]. By solving the Liouville equation in the limit of $\Gamma_1 > \gamma_{10} > \gamma_\varphi > \Gamma_0$ [49], we can estimate the probability of dcSQUID staying in excited state $|1\rangle$ by the formula $\rho_{11}(t) = e^{-\Gamma t}\frac{\Omega_0^2}{|\Omega|^2}\left|\sin\left(\frac{\Omega t}{2}\right)\right|^2$ [47]. Here Γ_0 and Γ_1 are the escape rates of ground and excited states of dcSQUID, and γ_φ and γ_{10} are dephasing(not decoherence) and relaxation rates between ground state and excited state. Besides, $\Omega \equiv \sqrt{\Omega_0^2 - \left(\Gamma - i\overline{\Delta}\right)^2}$, Ω_0 is the on resonance Rabi frequency; $\Gamma \equiv \frac{1}{2}\left(\Gamma_1 + \Gamma_0 + \gamma_{10}\right) + \gamma_\varphi$, and $\overline{\Delta} = \left(E_1 - E_0\right)/\hbar - \omega$ is the detuning. Considering the maximum pumping at which $\rho_{11}(t)$ reaches its maximum, we have

$$\rho_{11} = 1 - \frac{\pi\Gamma}{2\Omega_0} = 1 - \zeta_0$$

with $\zeta_0 \equiv \frac{\pi\Gamma}{2\Omega_0}$(see Appendix J) in which we have required $\Omega_0 \gg \Gamma$ such that $\zeta_0 \ll 1$. Because Γ_1 corresponds to the dcSQUID escaping to the voltage mode and gives positive outcome of measurement, we ignore Γ_1 in the formula of Γ directly and only keep γ_φ and γ_{10} such that $\zeta_0 \approx \frac{\pi(\gamma_{10}+2\gamma_\varphi)}{4\Omega_0}$.

3. Non-perfect escape process due to the relaxation of dcSQUID from excited state to ground state [48]: Once the qubit is not in negative state the dcSQUID will be pumped to excited state and immediately escapes to voltage mode to give positive outcome due to large Γ_1. However, it is still possible for dcSQUID to stay in superconducting mode if the dcSQUID is released to its ground state before escape process. Basically, in this case, we can use probability of dcSQUID relaxing to its ground state as the evaluation of our new venality.

Given $\rho_{11} = 1 - \zeta_0$ right after pumping stage of previous discussion, in the limit of $\Gamma_1 \gg \gamma_{10} \gg \Gamma_0$, the probability of the SQUID remaining in zero voltage state is [48]

$$\begin{aligned} P(t) &= (1-\gamma)\, e^{-\Gamma_0 t} + \gamma e^{-\Gamma' t} \\ &\approx (\zeta_0 + \zeta_1)\, e^{-\Gamma_0 t} + (1 - \zeta_0 - \zeta_1)\, e^{-\Gamma_1 t} \end{aligned} \tag{3.22}$$

Here $\Gamma' = \Gamma_1 + \gamma_{10}$, $\zeta_1 \equiv \gamma_{10}/\Gamma_1$, and we have defined

$$\begin{aligned} \gamma &\equiv \rho_{11}(0)\,[1 - \gamma_{10}/(\Gamma' - \Gamma_0)] \approx (1-\zeta_0)\,[1 - \gamma_{10}/\Gamma_1] \\ &\approx (1 - \zeta_0 - \zeta_1) \end{aligned} \tag{3.23}$$

with $\rho_{11}(0) \approx (1-\zeta_0)$ being the population of excited state right after microwave resonance pumping.

Roughly speaking, the $e^{-\Gamma_1 t}$ term will vanish after certain time and only the term of $e^{-\Gamma_0 t}$ (≈ 1 for $\Gamma_1 \gg \gamma_{10} \gg \Gamma_0$) is left in $P(t)$ Finally, we can have $P(t) \approx (\zeta_0 + \zeta_1)$, where ζ_1 is our new venality due to the non-perfect escape of SQUID excited state.

4. The off-resonance pumping of dcSQUID for the qubit in the negative state [47] Even if the qubit is in the negative state during the INR measurement, its ancilla (i.e. the dcSQUID) still has a chance to be excited by off-resonance pumping.

Again, let's consider the formula $\rho_{11}(t) = e^{-\Gamma t}\frac{\Omega_0^2}{|\Omega|^2}\left|\sin\left(\frac{\Omega t}{2}\right)\right|^2$ in the limit of large detuning $\overline{\Delta}^2 \gg \Omega_0^2 \gg \Gamma^2$, then we will evaluate the incorrect pumping of dcSQUID for the qubit being in negative state: $\rho_{11}(t_{\max}) \approx \frac{\Omega_0^2}{\overline{\Delta}^2} \equiv \zeta_2$ (see Appendix K).

Based on the dynamical analysis of qubit-dcSQUID coupled system, the escape rates for first excited

state of dcSQUID would depend on qubit state. Therefore, if we can distinguish or enlarge such first-excited-state escape rate difference between two qubit states it is still possible to elimate the venality of unwanted off-resonance pumping.

Actually, ζ_0 and ζ_1 correspond to the venalities of mistaking the positive state as the negative state, and ζ_2 corresponds to the venality of mistaking the negative state as the positive state. Therefore, only the venality ζ_0 almost contributes equally to both positive and negative states, and the others behave differently in R and L measurements.

3.8 The parameter analysis:

Basically, if we want our estimated venality to be small enough, that is

$$\zeta_0 = \frac{\pi\left(\gamma_{10} + 2\gamma_\varphi\right)}{4\Omega_0} \ll 1 \tag{3.24}$$

$$\zeta_1 = \gamma_{10}/\Gamma_1 \ll 1 \tag{3.25}$$

$$\zeta_2 = \frac{\Omega_0^2}{\overline{\Delta}^2} \ll 1 \tag{3.26}$$

, the parameter constraints $\Omega_0 \gg \gamma_{10}$ and γ_φ, $\overline{\Delta}^2 \gg \Omega_0^2$, and $\Gamma_1 \gg \gamma_{10}$ are required. Please note that $\overline{\Delta} = \left(E_1 - E_0\right)/\hbar - \omega$ is the detuning.

We can estimate the off resonance detuning by the difference between two SQUID excited energies corresponding to two qubit states :

$$\overline{\Delta} = \text{MW1} - \text{MW2} = \delta\omega \simeq 2M\omega = 0.1 \; to \; 1GHz \tag{3.27}$$

Here MW1 and MW2 are the resonance frequencies of dcSQUID corresponding to two qubit states, and ω_0 is the harmonic frequency at minimum of the potential of dcSQUID. Typically, we estimate $\omega_0 \sim 100GHz$ and the coupling strength between qubit and dcSQUID $M \equiv \frac{\Phi_{qubit}}{\pi\Phi_0} \sim 0.01$ to 0.001. Here $2\Phi_{qubit}$ is the flux difference on dcSQUID induced by two qubit states and Φ_0 is the flux quantum.

According to the relation $\overline{\Delta}^2 \gg \Omega_0^2$, we estimate that $\frac{\Omega_0}{\overline{\Delta}} \sim 0.3$ and then the corresponding on resonance Rabi frequency

$$\Omega_0 = (0.3GHz) \sim (30MHz) \tag{3.28}$$

Similarly, based on the relation $\Omega_0 \gg \gamma_{10}$, we require $\frac{\gamma_{10}}{\Omega_0} \sim 0.1$ and γ_{10} can be $(30MHz) \sim (3MHz)$. Finally, they totally give $\frac{\overline{\Delta}}{\gamma_{10}} \sim 30$.

Next, based on the relation $\Omega_0 \gg \Gamma_1$ we require

$$\Gamma_1 = (30MHz) \sim (3MHz) \tag{3.29}$$

(possible? $\Gamma_1 \sim 0.4MHz$ in ref. [47]). Because we require $\Gamma_1 \gg \gamma_{10}$, we also have

$$\gamma_{10} = (3MHz) \sim (0.3MHz)\,. \tag{3.30}$$

The corresponding relaxation time $\tau_d = 1/\gamma_{10} = 300ns \sim 3000ns$. Based on current technology, $\tau_d = 300ns$ may be possible but the corresponding coupling M is larger than the standard ones; that implies we need to reach a balance between τ_d and M based on technical consideration such that we can minimize the measurement venalities.

Using the formula $\gamma_{10}(=\Gamma_d) \approx 2\pi\omega\frac{R_Q}{R}$ [48] with $R_Q = h/4e^2$ being the resistance quantum and R being the resistance of RCJ model of junction in dcSQUID, basically, we can have the following relation

$$\bar{\Delta} \simeq 2M\omega \gg \gamma_{10} \approx 2\pi\frac{R_Q}{R}\omega \tag{3.31}$$

, and estimate the minimum required ratio between the parameters based on the above analysis:

$$\bar{\Delta}/\gamma_{10} = \frac{MR}{\pi R_Q} > 30 \tag{3.32}$$

According to this inequality, our experimental setup needs to increase the coupling strength M and junction resistance R in dcSQUID. If the current achievable parameter values cannot give such a large ratio, then we can't guarantee a low enough venality for the TBI experiment to refute MR even if the measurements are NIM. Therefore, how to increase this ratio is a really important technical problem in the future development of TBI experiment.

3.9 Conclusion

In sum, we give a complete protocol for the ancillary test, which makes a consistent cooperation between invasivity test and TBI experiment to give a more rigorous bound for TBI; our new arrangement of TBI experiment successfully improves the Knee's experiment to narrow its possible loophole for arguing the failure of MR postulate. In addition, our classification of measurement invasivity is convenient for identifying the properties of measurement invasiveness. Especially, under appropriate initial condition we can claim that

only the difference between the type II invasivity and $\langle Q_1 Q_3 \rangle_{1,2,3} - \langle Q_1 Q_3 \rangle_{1,3}$ contributes to TBI violation.

Chapter 4

Summary

In Chapter 2, for the escape dynamics of qubit-SQUID composite system, we generalize the idea of "two-channel" escape to all of the parameter regime of the qubit-SQUID system and conclude that our coupled system tends to behave as an energy-basis measurement in the small escape rate limit but as a flux-basis measurement in the large escape rate limit. Furthermore, we used these results to analyze the qubit density matrix evolution before the current switching happens, the entanglement of the qubit-SQUID system, and the weak measurement behavior of our experiment. To extend the application to NIM measurement in TBI experiment, we also discussed a possible parameter setup to realize the flux-basis projective measurements with our qubit-SQUID system.

In Chapter 3, we use a practical way to quantify the measurement invasisveness to improve the ancillary test. Furthermore, we set up the best arrangement of TBI main experiment consistent with the ancillary test and give the modified lower bound of TBI. On the other hand, we give a elegant protocol of how to implement the INR measurement with qubit-SQUID composite system so that we can really test MR by performing a TBI experiment on "macroscopic" system. In the end, we roughly estimated the feasibility of the proposed experiment based on the design of our INR measurement; the estimation gives the most tolerable measurement error (venality) for making TBI experiment meaningful.

Recently, working with G.Knee and the NTT group, we applied the idea of the ancillary test to the TBI experiment on flux qubit-SQUID composite system[50]. We believe that this is the first fully satisfactory test of realism versus QM at the 'macroscopic' level[52]. In our new paper[50], we try to test a new type of TBI which is different from conventional one. The new TBI only needs to measure the time behavior of the third measurement Q_3, which is going to see the violation of the non-disturbance condition NDC:

$$\langle Q_3 \rangle_G - \langle Q_3 \rangle_{\bar{2}} = 0. \tag{4.1}$$

Here 'G' means the ensemble in which all three measurements Q_1, Q_2, Q_3 are operated, and '$\bar{2}$' means that only Q_2 is not performed in the ensemble. There is a detailed discussion of the relation between the

conventional TBI and NDC in the supplementary material of that paper[50]; according to the invasivity analysis for conventional TBI, we do ancillary test for type II invasivity to narrow the loophole in the test of NDC; please note that NIM measurement is not used in this new TBI test.

Appendix A

The perturbation correction to our Harmonic approximation

To deal with the Hamiltonian given in Eq.(2.20), in which $H^H = H_d^H + V^H$ and $V^H = -\left(\varepsilon^H(R)\sin\chi + \Delta\cos\chi\right)\tau_x$, we can treat the last term, that is V^H, perturbatively. Here we have $\varepsilon^H(R) = \varepsilon + \pi g\tan[\pi f_{SQ}]\left(k - 3\frac{k}{R_c}R - \frac{k}{2}R^2\right)$, see Eq. (2.17). As we know that the lowest two eigenstates of H_d^H are denoted as $\left|0'_+\right\rangle$ and $\left|0'_-\right\rangle$, the corresponding eigenenergies in H_d^H are E_+ and E_-. Following the steps of perturbation theory, we can calculate correction to the eigenenergy E_+, namely

$$\Delta E_+ = \frac{\left|\left\langle 0'_+\right| V^H \left|0'_-\right\rangle\right|^2}{E_+ - E_-}. \tag{A.1}$$

Because the first order term $\left\langle 0'_+\right| V^H \left|0'_+\right\rangle$is zero automatically, we keep the second order term here. Besides, according to Eq.(18) and (20) we have

$$E_+ - E_- \approx \delta\omega\hbar = 2g\omega\hbar\cos\chi\tan[\pi f_{SQ}]\left(1 + \left(\frac{3}{R_c}\right)^2\right)$$

On the other hand, we can evaluate $\left\langle 0'_+\right| V^H \left|0'_-\right\rangle$ in the harmonic approximation:

$$\begin{aligned}
&\left\langle 0'_+\right| V^H \left|0'_-\right\rangle \\
&= -\left[\left\langle \psi_{0_+}\right| \varepsilon^H(R) \left|\psi_{0_-}\right\rangle \sin\chi + \left\langle \psi_{0_+} \mid \psi_{0_-}\right\rangle \Delta\cos\chi\right] \\
&= \frac{\Delta\left\langle \psi_{0_+} \mid \psi_{0_-}\right\rangle}{\sqrt{\varepsilon_{00}^{H2} + \Delta^2}}\left[\frac{\left\langle \psi_{0_+}\right| \varepsilon^H(R) \left|\psi_{0_-}\right\rangle}{\left\langle \psi_{0_+} \mid \psi_{0_-}\right\rangle} - \varepsilon_{00}^H\right] \\
&= \frac{\Delta\left\langle \psi_{0_+} \mid \psi_{0_-}\right\rangle}{\sqrt{\varepsilon_{00}^{H2} + \Delta^2}}\frac{gk}{2}\frac{\hbar}{m}\tan[\pi f_{SQ}]\left(\left(\frac{1}{\omega_+ + \omega_-}\right) - \frac{1}{2\omega}\right)
\end{aligned}$$

$$= \frac{g^3}{16}\omega\hbar\tan^3[\pi f_{SQ}]\left\langle \psi_{0_+} \mid \psi_{0_-}\right\rangle \sin\chi\left(\cos\chi\left(1 + \left(\frac{3}{R_c}\right)^2\right)\right)^2$$

(Here we have given only the critical steps). $\left|\psi_{0_+}\right\rangle$ and $\left|\psi_{0_-}\right\rangle$ are the corresponding SQUID harmonic

(ground state) wavefunctions of $\left|0'_+\right\rangle$ and $\left|0'_-\right\rangle$. Then ω_+ and ω_- are the corresponding harmonic frequencies.

Plugging all the above formulae into Eq.(A.1), we get

$$\begin{aligned}\Delta E_+ &\approx \frac{\left|\left\langle 0'_+\right| V^H \left|0'_-\right\rangle\right|^2}{[2\delta\omega\hbar]} \\ &\approx (\omega\hbar)\,\frac{g^5}{1024}\tan^5[\pi f_{SQ}]\cos\chi\sin^2 2\chi \sim 10^{-34}J\end{aligned}$$

Appendix B

More general perturbation analysis of qubit-SQUID composite system

B.1 The energy levels of qubit-SQUID composite system

In this appendix we give a more detailed study of the splitting of the lowest two energy levels of the qubit-dcSQUID system, including the effects of the deviation of the SQUID wave functions from the pure harmonic form. While this more detailed analysis does not by itself allow us to improve the formulae for the escape rates Γ_+ and Γ_- calculated in the main text, it is useful in a slightly different context, namely the practical implementation of a test of the temporal Bell inequalities[1] at the macroscopic level[34]. Our calculation is based on a perturbative treatment of the complete Hamiltonian in Eq.(2.6), and its output will be a more accurate value χ_{00} of the "spin rotation angle" χ introduced in Eq.(2.19) of the main text.

Please note that, for simplicity, from now on we use $|n\rangle$ to represent the eigenstate of $H_{\rm SQ}$ instead of simple harmonic wave function, i.e. $H_{\rm SQ}|n\rangle = E_n|n\rangle$. Thus, if we approximate the SQUID potential by Eq.(2.10), then the cubic correction to the simple harmonic wave function already contribute to the eigenstate here (except that we ignore the small escape energy to simplify the analysis). We will also require $E_n \gg \varepsilon_{mn}$, Δ, where ε_{mn} is defined in Eq.(B.3); this condition is satisfied for most experimental set-ups.

We can rewrite our total Hamiltonian in the spin representation:

$$H = \begin{pmatrix} H_{\rm SQ}(x) + \varepsilon + \varepsilon_{\rm int}(x) & \Delta \\ \Delta & H_{\rm SQ}(x) - \varepsilon - \varepsilon_{\rm int}(x) \end{pmatrix}. \tag{B.1}$$

Here $H_{SQ}(x)$ and $\varepsilon_{\rm int}(x)$ are defined in Eq.(3.2)and Eq.(2.5). The basis for this representation is $|x,\sigma\rangle$, where $|x\rangle$ and $|\sigma\rangle$ ($\sigma \in \{R, L\}$) represent the SQUID phase state and qubit flux state respectively. Furthermore, in terms of the energy representation with $|n,\sigma\rangle$ as basis , we can alternatively represent the total

Hamiltonian by

$$H = \begin{pmatrix} h_{00} & h_{01} & h_{02} & . \\ h_{10} & h_{11} & h_{12} & . \\ h_{20} & h_{21} & h_{22} & . \\ . & . & . & . \end{pmatrix} \tag{B.2}$$

where $h_{nn} = \begin{pmatrix} E_n + \varepsilon_{nn} & \Delta \\ \Delta & E_n - \varepsilon_{nn} \end{pmatrix}$ and $h_{\substack{mn \\ (m \neq n)}} = \begin{pmatrix} \varepsilon_{mn} & 0 \\ 0 & -\varepsilon_{mn} \end{pmatrix}$, where

$$\varepsilon_{mn} \equiv \langle m | \, \varepsilon + \varepsilon_{\text{int}} \, | n \rangle \, . \tag{B.3}$$

Each element of the diagonal part of Eq.(B.2) can be rearranged into the form

$$h_{nn} = E_n + \sqrt{\varepsilon_{nn}^2 + \Delta^2} \cdot \begin{pmatrix} \cos\chi_{nn} & \sin\chi_{nn} \\ \sin\chi_{nn} & -\cos\chi_{nn} \end{pmatrix} \tag{B.4}$$

with

$$\cos\chi_{nn} \equiv \frac{\varepsilon_{nn}}{\sqrt{\varepsilon_{nn}^2 + \Delta^2}}, \ \sin\chi_{nn} \equiv \frac{-\Delta}{\sqrt{\varepsilon_{nn}^2 + \Delta^2}}. \tag{B.5}$$

Next, we can divide the total Hamiltonian into a diagonal part (H_D) and an off-diagonal part ($H - H_D$)

$$\begin{aligned} H &= \begin{pmatrix} h_{00} & 0 & 0 & . \\ 0 & h_{11} & 0 & . \\ 0 & 0 & h_{22} & . \\ . & . & . & . \end{pmatrix} + \begin{pmatrix} 0 & h_{01} & h_{02} & . \\ h_{10} & 0 & h_{12} & . \\ h_{20} & h_{21} & 0 & . \\ . & . & . & . \end{pmatrix} \\ &= H_D + (H - H_D) \end{aligned} \tag{B.6}$$

In the diagonal part H_D, each element h_{nn}(, which is the 2×2 diagonal block in H,) can be further diagonalized into

$$
\begin{aligned}
h'_{nn} &= \begin{pmatrix} E_n + \sqrt{\varepsilon_{nn}^2 + \Delta^2} & 0 \\ 0 & E_n - \sqrt{\varepsilon_{nn}^2 + \Delta^2} \end{pmatrix} \\
&= \begin{pmatrix} E_{n+} & 0 \\ 0 & E_{n-} \end{pmatrix}
\end{aligned} \tag{B.7}
$$

with an appropriate new spin basis $|n, \sigma'\rangle$ $(\sigma' \in \{+, -\})$, where $\begin{cases} |n,+\rangle = \cos\frac{\chi_{nn}}{2}|n,R\rangle + \sin\frac{\chi_{nn}}{2}|n,L\rangle \\ |n,-\rangle = -\sin\frac{\chi_{nn}}{2}|n,R\rangle + \cos\frac{\chi_{nn}}{2}|n,L\rangle \end{cases}$.
In other words, the Hamiltonian H_D can be exactly diagonalized by $|n, \sigma'\rangle$; $H_D|n, \sigma'\rangle = E_{n,\sigma'}|n, \sigma'\rangle$. Also, the elements in $(H - H_D)$ can be rewritten as

$$
h'_{mn} = \varepsilon_{mn} \begin{pmatrix} \cos\frac{\chi_{mm}+\chi_{nn}}{2} & -\sin\frac{\chi_{mm}+\chi_{nn}}{2} \\ -\sin\frac{\chi_{mm}+\chi_{nn}}{2} & -\cos\frac{\chi_{mm}+\chi_{nn}}{2} \end{pmatrix} \tag{B.8}
$$

in this new basis $|n, \sigma'\rangle$. Hereafter, instead of using $|\sigma'\rangle$, we denote $|\sigma\rangle$ $(\sigma \in \{+, -\})$ as our new spin basis for convenience.

In the following, we will consider the off diagonal part $(H - H_D)$ as a perturbation, and argue that the correction to the energy due to it is much smaller than any difference between eigenenergies of H_D. Therefore, we can neglect its effect on eigenenergies and effectively evaluate the energy spectrum of the coupled system.

Let's consider the perturbation correction for the energy levels of H_D up to second order.

$$
\begin{aligned}
E_{n\sigma}^{\text{new}} &= E_{n\sigma} + \langle n\sigma|(H - H_D)|n\sigma\rangle \\
&+ \sum_{k\sigma' \neq n\sigma} \frac{|\langle k\sigma'|(H - H_D)|n\sigma\rangle|^2}{E_{n\sigma} - E_{k\sigma'}} + O\left(g^3\right)
\end{aligned} \tag{B.9}
$$

Here σ' and σ all stand for the new spin basis of H_D, where $\sigma, \sigma' \in \{+, -\}$. Because of the off-diagonal property of $(H - H_D)$, the first order term is exactly zero, $\langle n\sigma|(H - H_D)|n\sigma\rangle = 0$, and the second order term with the summation $k = n$, which implies $\sigma' \neq \sigma$, also vanishes, $\langle n\sigma'|(H - H_D)|n\sigma\rangle = 0$. Then we can further simplify the equation to

$$E_{n\sigma}^{\text{new}} = E_{n\sigma} + \sum_{k\neq n,\sigma'} \frac{\left|\langle k\sigma'|\left(H - H_D\right)|n\sigma\rangle\right|^2}{E_{n\sigma} - E_{k\sigma'}} + O\left(M^3\right) \tag{B.10}$$

Also, the approximation $\sum_{k\neq n,\sigma'} \frac{\left|\langle k\sigma'|(H-H_D)|n\sigma\rangle\right|^2}{E_{n\sigma}-E_{k\sigma'}} \approx \sum_{k\neq n} \frac{|\varepsilon_{kn}|^2}{E_n - E_k}$ is correct to the second order in M . Finally, we obtain the new eigenenergies:

$$E_{n\pm}^{\text{new}} = E_{n\pm} + \sum_{k\neq n} \frac{|\varepsilon_{nk}|^2}{E_n - E_k} + O\left(M^3\right) \tag{B.11}$$

According to Eq.(B.11), the excitation energies (from $n = 0$ to $n = 1$) for $\sigma = +$ and $\sigma = -$ channels can be derived.

$$\begin{aligned}
\Delta \mathrm{E}_+ &= (\mathrm{E}_1 - \mathrm{E}_0) + \left(\sum_{\mathrm{k}\neq 1} \frac{|\varepsilon_{1\mathrm{k}}|^2}{\mathrm{E}_1 - \mathrm{E}_\mathrm{k}} - \sum_{\mathrm{k}\neq 0} \frac{|\varepsilon_{0\mathrm{k}}|^2}{\mathrm{E}_0 - \mathrm{E}_\mathrm{k}} \right) + \left(\sqrt{\varepsilon_{11}^2 + \Delta^2} - \sqrt{\varepsilon_{00}^2 + \Delta^2} \right) + \mathrm{O}\left(\mathrm{M}^3\right) \\
\Delta \mathrm{E}_- &= (\mathrm{E}_1 - \mathrm{E}_0) + \left(\sum_{\mathrm{k}\neq 1} \frac{|\varepsilon_{1\mathrm{k}}|^2}{\mathrm{E}_1 - \mathrm{E}_\mathrm{k}} - \sum_{\mathrm{k}\neq 0} \frac{|\varepsilon_{0\mathrm{k}}|^2}{\mathrm{E}_0 - \mathrm{E}_\mathrm{k}} \right) - \left(\sqrt{\varepsilon_{11}^2 + \Delta^2} - \sqrt{\varepsilon_{00}^2 + \Delta^2} \right) + \mathrm{O}\left(\mathrm{M}^3\right)
\end{aligned} \tag{B.12}$$

It's easy to see that the first two terms of $\Delta \mathrm{E}_+$ are the same as the corresponding terms of $\Delta \mathrm{E}_-$, and the third terms of $\Delta \mathrm{E}_+$ and $\Delta \mathrm{E}_-$ are just different by a sign. This is consistent with the property that the states $|0, \pm\rangle$ have the same energy correction $\sum_{k\neq 0} \frac{|\varepsilon_{0k}|^2}{E_0 - E_k}$, and the states $|1, \pm\rangle$ have the same energy correction $\sum_{k\neq 1} \frac{|\varepsilon_{1k}|^2}{E_1 - E_k}$, which are always true for states on the same energy level n. Based on this property, we can easily derive the difference of excited energy between spin + and spin − channels.

$$\begin{aligned}
&\Delta \mathrm{E}_+ - \Delta \mathrm{E}_- = (E_{1+} - E_{0+}) - (E_{1-} - E_{0-}) \\
&= (E_{0+} - E_{0-}) - (E_{1+} - E_{1-}) \\
&= 2\sqrt{\varepsilon_{00}^2 + \Delta^2} - 2\sqrt{\varepsilon_{11}^2 + \Delta^2}
\end{aligned} \tag{B.13}$$

In general, Eq.(B.13) is a very good estimation for the difference of resonance frequencies between two spin channels because we can eliminate the perturbation correction from $(H - H_D)$ and only need to consider the energy spectrum of H_D.

If we want to get rid of the second term on right side of Eq.(B.12), which is $\sum_{k\neq 1}\frac{|\varepsilon_{1k}|^2}{E_1-E_k}-\sum_{k\neq 0}\frac{|\varepsilon_{0k}|^2}{E_0-E_k}$, we have to require it to be much smaller than the last term of the formula, $\left(\sqrt{\varepsilon_{11}^2+\Delta^2}-\sqrt{\varepsilon_{00}^2+\Delta^2}\right)$. Then it gives

$$\frac{\left|\sum_{k\neq 1}\frac{|\varepsilon_{1k}|^2}{E_1-E_k}-\sum_{k\neq 0}\frac{|\varepsilon_{0k}|^2}{E_0-E_k}\right|}{\left|\sqrt{\varepsilon_{11}^2+\Delta^2}-\sqrt{\varepsilon_{00}^2+\Delta^2}\right|}\ll 1 \tag{B.14}$$

Typically, we expect $(E_n-E_m)\sim E_n\gg\varepsilon_{mn}\sim\varepsilon_{nn}$, and we can estimate that $\frac{|\varepsilon_{kn}|^2}{E_n-E_k}\sim\frac{|\varepsilon_{kn}|^2}{E_n}\sim\frac{|\varepsilon_{nn}|^2}{E_n}\ll|\varepsilon_{nn}|$. Therefore, with appropriate dcSQUID bias current I_b and qubit's bias energy ε, Eq.(B.14) usually can be satisfied such that we can have the simpler formulae,

$$\begin{aligned}\Delta\mathrm{E}_+&=(E_1-E_0)+\left(\sqrt{\varepsilon_{11}^2+\Delta^2}-\sqrt{\varepsilon_{00}^2+\Delta^2}\right)\\ \Delta\mathrm{E}_-&=(E_1-E_0)-\left(\sqrt{\varepsilon_{11}^2+\Delta^2}-\sqrt{\varepsilon_{00}^2+\Delta^2}\right).\end{aligned} \tag{B.15}$$

Here $\left(\sqrt{\varepsilon_{11}^2+\Delta^2}-\sqrt{\varepsilon_{00}^2+\Delta^2}\right)$ can be further simplified by [35]

$$\begin{aligned}\sqrt{\varepsilon_{11}^2+\Delta^2}-\sqrt{\varepsilon_{00}^2+\Delta^2}&\simeq\frac{\varepsilon_{00}(\varepsilon_{11}-\varepsilon_{00})}{\sqrt{\varepsilon_{00}^2+\Delta^2}}\\ &=\cos\chi_{00}\,(\varepsilon_{11}-\varepsilon_{00})\end{aligned} \tag{B.16}$$

Next, to evaluate ε_{11} and ε_{00} by Eq.(B.3), we can use the approximate formula in Eq.(2.13) to replace ε_{int}, and use the approximate potential in Eq.(2.10) to find the energy levels $|n\rangle$. After some calculations with the above elements, we finally get the result in Eq.(B.17). Actually, the first term in Eq.(B.17) is contributed by the square and cubic terms in Eq.(2.13) and can be equivalently derived from the change of energy levels of potential in Eq.(2.10) due to the small variation in parameter k by $\delta k=M\pi\cos\chi_{00}\tan[\pi f_{SQ}]\,k$, and the second term in Eq.(B.17) can be understood from the non-vanishing ground state expectation value of linear term in Eq.(2.13) due to the an-harmonic behaviour of SQUID ground state $|0\rangle$ (see Appendix B.2).

$$\begin{aligned}&\sqrt{\varepsilon_{11}^2+\Delta^2}-\sqrt{\varepsilon_{00}^2+\Delta^2}\\ &=\tfrac{\pi}{2}M\omega\hbar\tan[\pi f_{SQ}]\cos\chi_{00}\left(1+\left(\tfrac{3}{R_c}\right)^2\right)\end{aligned} \tag{B.17}$$

To justify our harmonic-approximation analysis in the section 3, we need to compare the frequencies in Eq.(2.25) and (2.23) with those in Eq.(B.15) and (B.17) respectively and the result shows that they are indeed consistent except for a replacement of χ by χ_{00}, where χ_{00} is evaluated by using the dcSQUID ground state wave function instead of the simple harmonic ground state for χ. This slight difference could be more significant when the bias current is approaching its critical value where the anharmonic effect from the cubic term of dcSQUID potential becomes more important. Therefore, if we want to ignore the effect of escape and efficiently diagonalize the whole wave function within the well, instead of a pure harmonic wave function, the SQUID wave function $|n\rangle$ is a more appropriate basis to start with, and the spin angle χ_{nn} defined in Eq.(B.5) seems better than χ in Eq.(2.19). Finally, we can improve and simplify our harmonic approximation by replacing it by rewriting the coupled Hamiltonian of Eq.(2.14) in terms of the new spin basis defined by χ_{00} and then keeping the diagonal part only. Then it gives an equation corresponding to Eq.(2.21), namely

$$H_d = \frac{-\hbar^2}{2m}\partial_R^2 + v\left(R\right) + \left(\varepsilon\left(R\right)\cos\chi_{00} - \Delta\sin\chi_{00}\right)\sigma_z^{00}. \tag{B.18}$$

Here we have defined $\sigma_z^{00} = \cos\chi_{00}\sigma_z^{00} - \sin\chi_{00}\sigma_x^{00}$. The new parameters corresponding to Eq.(2.22) are

$$\begin{aligned}
&\overline{k}_{\pm} = k\left(1 \pm \pi M\cos\chi_{00}\tan\left[\pi f_{SQ}\right]\left(1 + \left(\tfrac{3}{R_c}\right)^2\right)\right)\\
&\overline{R}_{c\pm} = R_c\left(1 \pm \left(\tfrac{3}{R_c}\right)^2 \pi M\cos\chi_{00}\tan\left[\pi f_{SQ}\right]\right)\\
&k_0^{\pm} = \mp\left(\sqrt{\varepsilon_{00}^2 + \Delta^2} + \tfrac{\pi M}{4}\omega\hbar\cos\chi_{00}\tan\left[\pi f_{SQ}\right]\right.\\
&\left.\times\left(1 + \left(\tfrac{3}{R_c}\right)^2\right)\right).
\end{aligned} \tag{B.19}$$

Comparing the Eq.(B.19) with Eq.(2.22), the only changes are the replacement of χ by χ_{00} and the small correction to $k_0^{\pm}$. Finally, we have the same decay rate formula as in Eq.(2.26) except that each parameter is modified by the replacement of χ by χ_{00}.

In brief, according our spectrum analysis in this section, once we find the "new spin basis" to diagonalize the H_{nn} in Eq.(B.7)(we called it the "first step" here) we can treat the "new off-diagonal part"$(H - H_D)$ perturbatively as shown in Eq.(B.10) and Eq.(B.11)(the "second step"). Therefore the only condition required is that $\omega\hbar \gg \varepsilon_{00}^H$ (or $\varepsilon_{\mathrm{mn}}$) if we want the perturbation formula Eq.(B.11) to be accurate to the second order; the assumption of $\omega\hbar \gg \Delta$ seems not necessary. Basically, it may be difficult to diagonalize the terms ∂_R^2, $\varepsilon\left(R\right)\sigma_z$, and $\Delta\sigma_x$ simultaneously, but we can instead deal with the terms ∂_R^2, $\varepsilon\left(R\right)\sigma_z$(that is called the "diagonal terms" in the flux-state representation) first and then treat $\Delta\sigma_x$(the "off-diagonal term") perturbatively, which only requires the smallness of the "off-diagonal term" to guarantee the correctness of

perturbation method. To generalize this (perturbation) method, we can also deal with our total Hamiltonian H in similar way but within "new spin representation" where the purpose of choosing the "new spin basis" is to appropriately divide the whole Hamiltonian H into the "diagonal part" and "off-diagonal part" such that we can minimize the "off-diagonal part" in the "new basis" [41], that is exactly what we do in the "first step". Although the way to determine the "new spin basis" here is a little bit different from that used in the harmonic approximation in the section 3, their principal ideas are the same.

B.2 The calculation of the SQUID's lowest two energy levels

To analyze the energy levels of the dcSQUID, we start with the approximate Hamiltonian

$$H = \frac{P^2}{2m} + \frac{k}{2}R^2 - \beta R^3 \tag{B.20}$$

with $\beta \equiv \frac{k}{2R_c}$ and $\alpha \equiv \sqrt{\frac{\hbar}{2m\omega}}$, and treat the cubic term $-\beta R^3$ perturbatively. Besides, we use $|n\rangle$ for representing energy state of Hamiltonian in Eq.(B.20) and $|n'\rangle$ for corresponding simple harmonic state. Then the dcSQUID's ground state wave function $|0\rangle$ can be constructed from the simple harmonic wave function $|n'\rangle$ by perturbation analysis,

$$\begin{aligned} |0\rangle &= |0'\rangle - \beta\frac{\langle 1'|\, R^3\, |0'\rangle}{E_{0'} - E_{1'}}\,|1'\rangle - \beta\frac{\langle 3'|\, R^3\, |0'\rangle}{E_{0'} - E_{3'}}\,|3'\rangle \\ &= |0'\rangle + \frac{3\alpha^3\beta}{\omega\hbar}\,|1'\rangle - \frac{\sqrt{6}\alpha^3\beta}{3\omega\hbar}\,|3'\rangle\,. \end{aligned}$$

Similarly, we also have the first excited state

$$|1\rangle = |1'\rangle - \frac{3\alpha^3\beta}{\omega\hbar}\,|0'\rangle + \frac{\sqrt{72}\alpha^3\beta}{\omega\hbar}\,|2'\rangle + \frac{\sqrt{24}\alpha^3\beta}{3\omega\hbar}\,|4'\rangle\,,$$

and the second excited state

$$|2\rangle = |2'\rangle - \frac{\sqrt{72}\alpha^3\beta}{\omega\hbar}\,|1'\rangle + \frac{\sqrt{243}\alpha^3\beta}{\omega\hbar}\,|3'\rangle + \frac{\sqrt{60}\alpha^3\beta}{3\omega\hbar}\,|5'\rangle\,.$$

The expectation value of R in these energy levels is

$$\begin{aligned}
\langle 0|\, R\, |0\rangle &= \frac{3\alpha^3\beta}{\omega\hbar}\left(\langle 1'|\, R\, |0'\rangle + \langle 0'|\, R\, |1'\rangle\right) = \frac{6\alpha^4\beta}{\omega\hbar}, \\
\langle 1|\, R\, |1\rangle &= \frac{-3\alpha^3\beta}{\omega\hbar}\left(\langle 1'|\, R\, |0'\rangle + \langle 0'|\, R\, |1'\rangle\right) \\
&+ \frac{\sqrt{72}\alpha^3\beta}{\omega\hbar}\left(\langle 2'|\, R\, |1'\rangle + \langle 1'|\, R\, |2'\rangle\right) = \frac{18\alpha^4\beta}{\omega\hbar}, \\
\langle 2|\, R\, |2\rangle &= \frac{-\sqrt{72}\alpha^3\beta}{\omega\hbar}\left(\langle 2'|\, R\, |1'\rangle + \langle 1'|\, R\, |2'\rangle\right) \\
&+ \frac{\sqrt{243}\alpha^3\beta}{\omega\hbar}\left(\langle 3'|\, R\, |2'\rangle + \langle 2'|\, R\, |3'\rangle\right) = \frac{30\alpha^4\beta}{\omega\hbar}.
\end{aligned}$$

Therefore, the difference between the two expectation values of the linear term in Eq.(2.13) is

$$\begin{aligned}
&\pi M \tan\left[\pi f_{SQ}\right]\left(\tfrac{3k}{R_c}\langle 1|\, R\, |1\rangle - \tfrac{3k}{R_c}\langle 0|\, R\, |0\rangle\right) \\
&= \pi M \tan\left[\pi f_{SQ}\right]\tfrac{3k}{R_c}\tfrac{12\alpha^4\beta}{\omega\hbar} = \tfrac{\pi M}{2}\omega\hbar\tan\left[\pi f_{SQ}\right]\left(\tfrac{3}{R_c}\right)^2.
\end{aligned}$$

According to the definition of ε_{mn} in Eq.(B.3), we can insert this result into Eq.(B.16), and give the second term in Eq.(B.17). On other hand, we can also calculate all the other terms in ε_{00} and ε_{11} by Eq.(B.3), and as a result we have

$$\begin{aligned}
\varepsilon_{00} &= \tfrac{\pi M}{2}\omega\hbar\tan\left[\pi f_{SQ}\right]\left(\tfrac{1}{2} + \tfrac{1}{2}\left(\tfrac{3}{R_c}\right)^2\right) + \varepsilon - \pi M k \tan\left[\pi f_{SQ}\right] \\
\varepsilon_{11} &= \tfrac{\pi M}{2}\omega\hbar\tan\left[\pi f_{SQ}\right]\left(\tfrac{3}{2} + \tfrac{3}{2}\left(\tfrac{3}{R_c}\right)^2\right) + \varepsilon - \pi M k \tan\left[\pi f_{SQ}\right]
\end{aligned}$$

Appendix C

The behavior of maximum switching point with the current ramping rate

Here we are going to analyze how does the maximum switching probability point change and how does its corresponding escape rate behave with the change of the current ramping rate. Roughly, the escape rate at maximum switching probability is increased with current ramping rate, but its detailed behaviour still need to be investigated.

Let's consider the formula of current switching probability, namely

$$P(y) = \frac{\Gamma(y)}{dy/dt} \exp\left[-\frac{1}{dy/dt}\int_0^y \Gamma(y')\,dy'\right] \tag{C.1}$$

If we take the y derivative of Eq. (C.1) and set it equal to zero then we get an equation for the value y_{max} of y corresponding to the maximum switching probability:

$$\Gamma^{-2}\frac{d\Gamma}{dy} = \frac{1}{\frac{dy}{dt}} \tag{C.2}$$

It can be rewritten as

$$\Gamma(y) = \frac{d\ln\Gamma}{dy}\frac{dy}{dt}. \tag{C.3}$$

In principle, we need to find the solution $y = y_{max}$ for the equation, and insert it in the formula for Γ to give the escape rate Γ_{max} at the maximum switching point. But if $\frac{d\ln\Gamma(y)}{dy}$ does not change a lot within a small range of y we may consider it as a constant(it's about 200 for $0.9 < y < 0.92$ for $10^3\text{Hz} < \frac{\text{dy}}{\text{dt}} < 10^4\text{Hz}$ (for static experiment) and all other parameters being the same as in the NTT experiments, see Fig.C.1) and we will approximately see that the escape rate at maximum switching probability increases with the current ramping rate, e.g., $\Gamma(y_{max}) \approx 200\frac{dy}{dt}$ for y_{max} satisfying Eq.(C.3) under the condition $10^3\text{Hz} < \frac{\text{dy}}{\text{dt}} < 10^4\text{Hz}$.

If this approximation is not accurate enough, we need to attack the problem in another way. Before that, we need to review how Γ depends on y. In general, we have the escape formula as

$$\Gamma(y) = \omega 60^{1/2}\left(\frac{B}{2\pi\hbar}\right)^{1/2}\exp -[(B/\hbar)\left(1+\frac{0.87}{Q}\right)]. \tag{C.4}$$

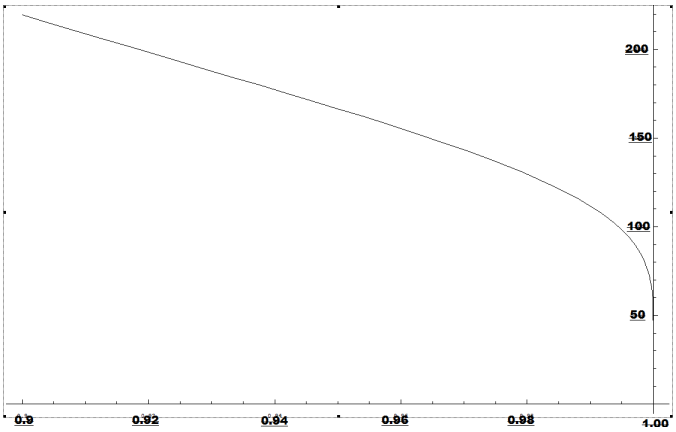

Figure C.1: The diagram shows the behavior of $\frac{d\ln\Gamma(y)}{dy}$ over the range $0.9 < y < 1$. Here the X-axis and Y-axis correspond to the bias current parameter y and $\frac{d\ln\Gamma}{dy}$ respectively. Based on the NTT parameters for the static experiments, we have $y_{max} \approx 0.9$(according to Eq.(C.3) numerically) for the current ramping rate of $\frac{dy}{dt} = 10^3$Hz, and the corresponding $\left.\frac{d\ln\Gamma(y)}{dy}\right|_{y=y_{max}} = 220$. If we increase the ramping rate to $\frac{dy}{dt} = 10^4$Hz we will have $y_{max} \approx 0.92$(according to Eq.(C.3) numerically) and the corresponding $\left.\frac{d\ln\Gamma(y)}{dy}\right|_{y=y_{max}} = 200$. That means the change of $\left.\frac{d\ln\Gamma(y)}{dy}\right|_{y=y_{max}}$ is less than 10 % if we raise the ramping by a factor of 10 from $\frac{dy}{dt} = 10^3$Hz. Therefore, if we can tolerate such small change of $\left.\frac{d\ln\Gamma(y)}{dy}\right|_{y=y_{max}}$ and consider it as a constant then we approximately have $\Gamma(y_{max}) \approx 200\frac{dy}{dt}$ for $10^3\text{Hz} < \frac{\text{dy}}{\text{dt}} < 10^4\text{Hz}$.

, where $\text{B} = \frac{8}{15}m\omega R_c^2$ is the decay bounce action and $Q = \omega R_s C_0$ is the damping factor with net resistance R_s [30]. We expect Γ depends on y because B, Q, and ω are y dependent, as follows:

$$R_c = 3\frac{\sqrt{1-y^2}}{y} \tag{C.5}$$

$$\omega = \omega_0\left(1-y^2\right)^{\frac{1}{4}} \tag{C.6}$$

$$B = B_0\frac{\left(1-y^2\right)^{\frac{5}{4}}}{y^2} \tag{C.7}$$

$$Q = Q_0\left(1-y^2\right)^{\frac{1}{4}} \tag{C.8}$$

Then we have the following formula for Γ as a function of y:

$$\Gamma(y) = \omega_0 60^{1/2}\left(\frac{B_0}{2\pi\hbar}\right)^{1/2}\frac{\left(1-y^2\right)^{\frac{7}{8}}}{y} \times \exp -[\frac{B_0\left(1-y^2\right)}{\hbar y^2}\left(\left(1-y^2\right)^{\frac{1}{4}} + \frac{0.87}{Q_0}\right)]. \tag{C.9}$$

Here we have $\text{B}_0 = \frac{36}{5}m\omega_0$ and $Q_0 = \omega_0 R_s C_0$. Now, we can start our analysis based on Eq.(C.9). Eq.(C.2) can be rewritten as

$$\frac{d\Gamma^{-1}}{dy} = \frac{-1}{\frac{dy}{dt}} \tag{C.10}$$

Let's assume y is close to 1 and let $z = 1 - y$, then

$$\frac{d\Gamma^{-1}}{dz} = \frac{1}{r} \tag{C.11}$$

Here we have defined $\frac{dy}{dt} = r$. Then we can derive $\Gamma(z)$ from Eq.(C.9), which now reads

$$\Gamma(z) \approx \omega_0 60^{1/2} \left(\frac{B_0}{2\pi\hbar}\right)^{1/2} (z)^{\frac{7}{8}} \times \exp -[\frac{B_0}{\hbar}\left(z^{\frac{5}{4}} + \frac{0.87z}{Q_0}\right)]. \tag{C.12}$$

The result is

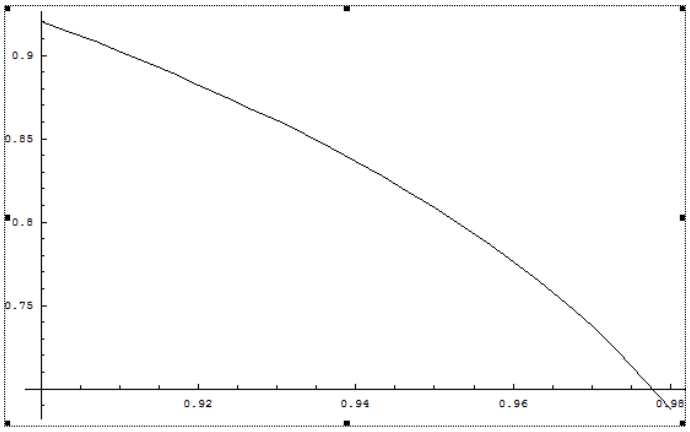

Figure C.2: The diagram shows the behavior of $\left(\frac{5}{4}z^{\frac{1}{4}} + \frac{0.87}{Q_0}\right)$ within the range $0.9 < y < 0.98$. Here the X-axis and Y-axis correspond to the bias current parameter y and $\left(\frac{5}{4}z^{\frac{1}{4}} + \frac{0.87}{Q_0}\right)$ respectively.

$$\frac{d\Gamma^{-1}}{dz}(z) \approx \omega_0^{-1} 60^{-1/2} \left(\frac{2\pi B_0}{\hbar}\right)^{1/2} z^{\frac{-7}{8}} \left(\frac{5}{4}z^{\frac{1}{4}} + \frac{0.87}{Q_0}\right) \times \exp[\frac{B_0}{\hbar}\left(z^{\frac{5}{4}} + \frac{0.87z}{Q_0}\right)] \tag{C.13}$$

$$\approx \Gamma^{-1}(z) \frac{B_0}{\hbar}\left(\frac{5}{4}z^{\frac{1}{4}} + \frac{0.87}{Q_0}\right) = \frac{1}{r}. \tag{C.14}$$

To simplify the analysis, lets assume there is a base point called z_0 where the maximum switching probability takes place at certain ramping rate, e.g. we may choose $z_0 = 0.9$ in our case. Because the term $\left(\frac{5}{4}z^{\frac{1}{4}} + \frac{0.87}{Q_0}\right)$ changes relatively little within the range around z_0, we take it as a constant $\left(\frac{5}{4}z_0^{\frac{1}{4}} + \frac{0.87}{Q_0}\right)$ instead and preserve the z dependence of the other terms. Then formula (C.14) can be rewritten as

$$\frac{d\Gamma^{-1}}{dz}(z) \approx \Gamma^{-1}(z) \frac{B_0}{\hbar}\left(\frac{5}{4}z_0^{\frac{1}{4}} + \frac{0.87}{Q_0}\right) = \frac{1}{r} \tag{C.15}$$

That gives the simple form

$$\Gamma_{max} \equiv \Gamma\left(z_{max}\right) \quad \approx \quad r\frac{B_0}{\hbar}\left(\frac{5}{4}z_0^{\frac{1}{4}} + \frac{0.87}{Q_0}\right) \tag{C.16}$$

More accurately, it should be

$$\Gamma\left(z_{max}\right) \quad \approx \quad r\frac{B_0}{\hbar}\left(\frac{5}{4}z_{max}^{\frac{1}{4}} + \frac{0.87}{Q_0}\right) \tag{C.17}$$

Because the behaviour of the $\exp[\frac{B_0}{\hbar}z^{\frac{5}{4}}]$ in Eq.(C.13) is most dramatic one by comparing to other z dependent terms with z around z_0, therefore we can solve z_{max} by taking others as constant with $z = z_0$ and preserving the z dependence of the term $\exp[\frac{B_0}{\hbar}z^{\frac{5}{4}}]$ in formula..

Hence, we have an approximated form of z_{max}

$$\frac{d\Gamma^{-1}}{dz}\left(z\right) \approx \omega_0^{-1}60^{-1/2}\left(\frac{2\pi B_0}{\hbar}\right)^{1/2}\left(\frac{5}{4}z_0^{\frac{-5}{8}} + \frac{0.87z_0^{\frac{-7}{8}}}{Q_0}\right)\exp[\frac{B_0}{\hbar}\frac{0.87z_0}{Q_0}]\exp[\frac{B_0}{\hbar}z^{\frac{5}{4}}] = \frac{1}{r}. \tag{C.18}$$

or

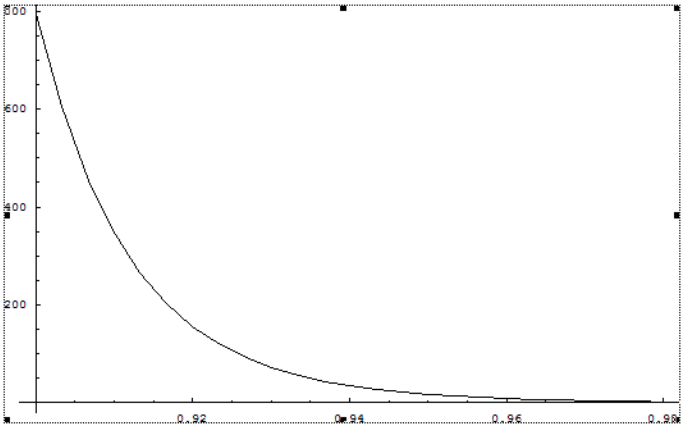

Figure C.3: The diagram shows the behavior of $\exp[\frac{B_0}{\hbar}z^{\frac{5}{4}}]$ within the range $0.9 < y < 0.98$. Here the X-axis and Y-axis correspond to the bias current parameter y and $\exp[\frac{B_0}{\hbar}z^{\frac{5}{4}}]$ respectively.

$$z_{max} = \left(-\frac{0.87z_0}{Q_0} - \frac{\hbar}{B_0}\ln\left(r\left(\frac{\pi B_0}{30\omega_0^2\hbar}\right)^{\frac{1}{2}}\left(\frac{5}{4}z_0^{\frac{-5}{8}} + \frac{0.87z_0^{\frac{-7}{8}}}{Q_0}\right)\right)\right)^{\frac{4}{5}}. \tag{C.19}$$

Insertion of (C.19) into (C.17) gives

$$\Gamma_{max} \approx r\frac{B_0}{\hbar}\left(\frac{0.87}{Q_0}+\frac{5}{4}\left(-\frac{0.87z_0}{Q_0}-\frac{\hbar}{B_0}\ln\left(r\left(\frac{\pi B_0}{30\omega_0^2\hbar}\right)^{\frac{1}{2}}\left(\frac{5}{4}z_0^{\frac{-5}{8}}+\frac{0.87z_0^{\frac{-7}{8}}}{Q_0}\right)\right)\right)^{\frac{1}{5}}\right) \tag{C.20}$$

Appendix D

The matrix elements of time evolution operator of qubit-SQUID system

Here we are going to derive the matrix elements of the evolution operator for the qubit-SQUID composite system. For the Hmiltonian $H = H_0 - \Delta\sigma_x$, the matrix elements of its time evolution operator $e^{-iHT/\hbar}$ are given by

$$
\begin{aligned}
&K \equiv \langle 0_{\sigma'}, \sigma' |\, e^{-iHT/\hbar} \,| 0_\sigma, \sigma \rangle = \langle 0_{\sigma'}, \sigma' |\, e^{-i(H_0 - \Delta\sigma_x)T/\hbar} \,| 0_\sigma, \sigma \rangle \\
&= \langle 0_{\sigma'}, \sigma' |\, e^{-iH_0 T/\hbar} \,| 0_\sigma, \sigma \rangle + \tfrac{i\Delta}{\hbar} \int_0^T \langle 0_{\sigma'}, \sigma' |\, e^{-iH_0(T-T_1)/\hbar} \sigma_x e^{-iH_0(T_1)/\hbar} \,| 0_\sigma, \sigma \rangle \, dT_1 \\
&+ \left(\tfrac{i\Delta}{\hbar}\right)^2 \int_0^T \int_0^{T_1} \langle 0_{\sigma'}, \sigma' |\, e^{-iH_0(T-T_1)/\hbar} \sigma_x e^{-iH_0(T_1-T_2)/\hbar} \sigma_x e^{-iH_0(T_2)/\hbar} \,| 0_\sigma, \sigma \rangle \, dT_1 dT_2 + O(\Delta^3)
\end{aligned}
$$

Here we have $\sigma', \sigma \in \{R, L\}$ and have expanded $e^{-iHT/\hbar}$ in a power series in Δ around $\Delta = 0$. Next, as we mentioned before, $|0_\sigma, \sigma\rangle$ evolves mostly to itself under the time evolution operator $e^{-iH_0 T_1/\hbar}$; the $\langle 0_\sigma, \sigma |\, e^{-iH_0 T/\hbar} \,| 0_\sigma, \sigma \rangle$ is the main contributing element of $e^{-iH_0 T/\hbar}$ if we start with $|0_\sigma, \sigma\rangle$. Thus

$$
\begin{aligned}
&\langle 0_{\sigma'}, \sigma' |\, e^{-iHT/\hbar} \,| 0_\sigma, \sigma \rangle \\
&= \langle 0_{\sigma'}, \sigma' |\, e^{-iH_0 T/\hbar} \,| 0_\sigma, \sigma \rangle \\
&+ \delta_{\sigma' \neq \sigma} \langle 0_{\sigma'} \,|0_\sigma\rangle \, \tfrac{i\Delta}{\hbar} \int_0^T \langle 0_{\sigma'}, \sigma' |\, e^{-iH_0(T-T_1)/\hbar} \,| 0_{\sigma'}, \sigma' \rangle \langle 0_\sigma, \sigma |\, e^{-iH_0(T_1)/\hbar} \,| 0_\sigma, \sigma \rangle \, dT_1 \\
&+ \delta_{\sigma' \neq \sigma''} \langle 0_{\sigma'} \,|0_{\sigma''}\rangle \delta_{\sigma'' \neq \sigma} \langle 0_{\sigma''} \,|0_\sigma\rangle \left(\tfrac{i\Delta}{\hbar}\right)^2 \int_0^T \int_0^{T_1} \langle 0_{\sigma'}, \sigma' |\, e^{-iH_0(T-T_1)/\hbar} \,| 0_{\sigma'}, \sigma' \rangle \langle 0_{\sigma''}, \sigma'' |\, e^{-iH_0(T_1-T_2)/\hbar} \,| 0_{\sigma''}, \sigma'' \rangle \\
&\times \langle 0_\sigma, \sigma |\, e^{-iH_0(T_2)/\hbar} \,| 0_\sigma, \sigma \rangle \, dT_1 dT_2 + O(\Delta^3)
\end{aligned}
$$

Next, we replace H_0 by its eigenenergy.

$$
\begin{aligned}
&\langle 0_{\sigma'}, \sigma' |\, e^{-iHT/\hbar} \,| 0_\sigma, \sigma \rangle \\
&= \delta_{\sigma=\sigma'} e^{-iE_{0\sigma}T/\hbar} + \delta_{\sigma \neq \sigma'} \langle 0_{\sigma'} \,|0_\sigma\rangle \, \tfrac{i\Delta}{\hbar} \int_0^T e^{-iE_{0\sigma'}(T-T_1)/\hbar} e^{-iE_{0\sigma}(T_1)/\hbar} dT_1 \\
&+ \delta_{\sigma=\sigma' \neq \sigma''} \left(\tfrac{i\Delta}{\hbar}\right)^2 |\langle 0_\sigma \,|0_{\sigma''}\rangle|^2 \int_0^T \int_0^{T_1} e^{-iE_{0\sigma}(T-T_1)/\hbar} e^{-iE_{0\sigma''}(T_1-T_2)/\hbar} e^{-iE_{0\sigma}T_2/\hbar} dT_1 dT_2 + O(\Delta^3)
\end{aligned}
\tag{D.1}
$$

Rearrange the integral formula.

$$K = \delta_{\sigma=\sigma'} e^{-iE_{0\sigma}T/\hbar} + \delta_{\sigma\neq\sigma'} e^{-iE_{0\sigma'}T/\hbar} \langle 0_{\sigma'} \, | 0_{\sigma} \rangle \, \frac{i\Delta}{\hbar} \int_0^T e^{-i\left(E_{0\sigma}-E_{0\sigma'}\right)T_1/\hbar} dT_1$$
$$+\delta_{\sigma=\sigma'\neq\sigma''} e^{-iE_{0\sigma}T/\hbar} \left|\langle 0_{\sigma} \, | 0_{\sigma''} \rangle\right|^2 \left(\frac{i\Delta}{\hbar}\right)^2 \int_0^T \int_0^{T_1} e^{-i\left(E_{0\sigma''}-E_{0\sigma}\right)T_1/\hbar} e^{i\left(E_{0\sigma''}-E_{0\sigma}\right)T_2/\hbar} dT_1 dT_2 + O(\Delta^3)$$

Integrate the first order and the second order terms.

$$= \delta_{\sigma=\sigma'} e^{-iE_{0\sigma}T/\hbar} + \delta_{\sigma\neq\sigma'} e^{-iE_{0\sigma'}T/\hbar} \langle 0_{\sigma'} \, | 0_{\sigma} \rangle \, \frac{\Delta}{\left(E_{0\sigma}-E_{0\sigma'}\right)} \left(1 - e^{-i\left(E_{0\sigma}-E_{0\sigma'}\right)T/\hbar}\right)$$
$$+\delta_{\sigma=\sigma'\neq\sigma''} e^{-iE_{0\sigma}T/\hbar} \left|\langle 0_{\sigma} \, | 0_{\sigma''} \rangle\right|^2 \left(\frac{i\Delta}{\hbar}\right)^2 \int_0^T e^{-i\left(E_{0\sigma''}-E_{0\sigma}\right)T_1/\hbar} \frac{\hbar}{i\left(E_{0\sigma''}-E_{0\sigma}\right)} \left(e^{i\left(E_{0\sigma''}-E_{0\sigma}\right)T_1/\hbar} - 1\right) dT_1$$
$$+O(\Delta^3)$$

Rearrange the first order term and continue to integrate the second order term.

$$= \delta_{\sigma=\sigma'} e^{-iE_{0\sigma}T/\hbar} + \delta_{\sigma\neq\sigma'} e^{-i\left(E_{0\sigma}+E_{0\sigma'}\right)T/2\hbar} \frac{\Delta 2i \langle 0_{\sigma'} \, | 0_{\sigma} \rangle}{\left(E_{0\sigma}-E_{0\sigma'}\right)} \sin\left(\left(E_{0\sigma} - E_{0\sigma'}\right) T/2\hbar\right)$$
$$+\delta_{\sigma=\sigma'\neq\sigma''} e^{-iE_{0\sigma}T/\hbar} \left|\langle 0_{\sigma} \, | 0_{\sigma''} \rangle\right|^2 \left(\frac{i\Delta}{\hbar}\right)^2 \int_0^T \frac{\hbar}{i\left(E_{0\sigma''}-E_{0\sigma}\right)} \left(1 - e^{-i\left(E_{0\sigma''}-E_{0\sigma}\right)T_1/\hbar}\right) dT_1 + O(\Delta^3) \qquad \text{(D.2)}$$

Finally we have

$$= \delta_{\sigma=\sigma'} e^{-iE_{0\sigma}T/\hbar}(1 + D_\sigma) + \delta_{\sigma\neq\sigma'} e^{-i\left(E_{0\sigma}+E_{0\sigma'}\right)T/2\hbar} \left(\frac{\Delta 2i \, \langle 0_{\sigma'} \, | 0_{\sigma} \rangle}{\left(E_{0\sigma} - E_{0\sigma'}\right)} \sin\left(\left(E_{0\sigma} - E_{0\sigma'}\right) T/2\hbar\right) + O(\Delta^3)\right) \text{(D.3)}$$

$$= \begin{pmatrix} e^{-iE_{0L}T/\hbar}(1 + D_L) & e^{-i\frac{(E_{0L}+E_{0R})T}{2\hbar}} \frac{\Delta 2i\langle 0_L \, | 0_R \rangle}{\left(E_{0R}-E_{0L}\right)} \sin\left(\frac{(E_{0R}-E_{0L})T}{2\hbar}\right) \\ e^{-i\frac{(E_{0L}+E_{0R})T}{2\hbar}} \frac{\Delta 2i\langle 0_R \, | 0_L \rangle}{\left(E_{0L}-E_{0R}\right)} \sin\left(\frac{(E_{0L}-E_{0R})T}{2\hbar}\right) & e^{-iE_{0R}T/\hbar}(1 + D_R) \end{pmatrix} + O\left(\Delta^3\right)$$

, where D_σ represents the higher order terms in an expansion in Δ of the diagonal term (with $\sigma'' \neq \sigma$).

$$D_\sigma = \delta_{\sigma\neq\sigma''} \left|\langle 0_{\sigma} \, | 0_{\sigma''} \rangle\right|^2 \left(\frac{i\Delta}{\hbar}\right)^2 \frac{\hbar}{i\left(E_{0\sigma''} - E_{0\sigma}\right)} \left(T - \frac{\hbar\left(e^{-i\left(E_{0\sigma''}-E_{0\sigma}\right)T/\hbar} - 1\right)}{-i\left(E_{0\sigma''} - E_{0\sigma}\right)}\right) + O\left(\Delta^4\right)$$

Appendix E

The formula for the switching current probability in different representations

The formula in Eq.(2.47), namely $P = \Gamma_{0L} |a_1|^2 + \Gamma_{0R} |a_2|^2$, seems not exactly correct; it is only true when the escape dynamics for the L and R channels are independent, that is $\Delta = 0$ in the dynamics equation Eq.(2.47). Therefore we need to find a correct formula for switching probability. Luckily, the general formula for the switching probability of single channel, namely

$$P(y) = \frac{\Gamma(y)}{dy/dt} \exp\left[-\frac{1}{dy/dt}\int_0^y \Gamma(y')\,dy'\right] \tag{E.1}$$

can be generalized to our truncated model so as to give a correct formula for the switching probability. To make it easier to understand the statistical meaning of Eq.(E.1), let's rewrite it as

$$\begin{aligned} P(y) &= -\frac{d}{dy} \exp\left[-\frac{1}{dy/dt}\int_0^y \Gamma(y')\,dy'\right] \\ &= -\frac{d}{dy} W(y) \end{aligned} \tag{E.2}$$

Here $W(y) = \exp\left[-\frac{1}{dy/dt}\int_0^y \Gamma(y')\,dy'\right]$ can be considered as the probability of SQUID remaining in the well or in the required state. Then we can say that the switching probability P is the -y derivative of this probability of the state. Motivated by this, we can follow the same idea by first finding the so called probability of remaining in the state of our truncated model (Eq.(2.42)), that gives $W(y) = |a_1(y)|^2 + |a_2(y)|^2$, and then applying it into Eq.(E.2). Eventually, we have the switching probability formula

$$P(y) = -\frac{d}{dy}\left(|a_1(y)|^2 + |a_2(y)|^2\right) \tag{E.3}$$

Usually, the two component a_1 and a_2 derived from numerical analysis of Eq.(2.42) are time dependent. Then the above formula can be written as

$$P(t) = \frac{-1}{\frac{dy}{dt}} \frac{d}{dt}\left(|a_1(t)|^2 + |a_2(t)|^2\right) \tag{E.4}$$

Please note that this formula is true only if the meaning of "probability"(of being in flux states) for $|a_1(t)|^2$ and $|a_2(t)|^2$ can be justified, and that's why we usually require $|a_1(t)|^2 + |a_2(t)|^2 = 1$ at the beginning.

Furthermore, if we claim

$$\begin{pmatrix} a_1(t) \\ a_2(t) \end{pmatrix} \equiv V(t) = U'V' = U' \begin{pmatrix} a_1'(t) \\ a_2'(t) \end{pmatrix} \tag{E.5}$$

, where $U^\dagger U = 1$ and a_1' a_2' are the corresponding components in the new basis, then we have

$$\sum_{i=1}^{2} |a_i(t)|^2 = V^\dagger V = V'^\dagger V' = \sum_{i=1}^{2} |a_i'(t)|^2$$

$$P(t) = \frac{-1}{\frac{dy}{dt}} \frac{d}{dt}\left(V^\dagger V\right) = \frac{-1}{\frac{dy}{dt}} \frac{d}{dt}\left(V'^\dagger V'\right) \tag{E.6}$$

The above formula implies that we can generalize Eq.(E.4) to the probabilities of any pair of states which are rotated unitarily from the two flux states such that the amplitude square of each component still preserve the meaning of "probability".

Therefore our naive guess in Chapter 2 of the formula

$$\begin{aligned} P &\equiv \Gamma_{0+} |a_+|^2 + \Gamma_{0-} |a_-|^2 \\ &= \frac{-1}{\frac{dy}{dt}} \frac{d}{dt}\left(|a_+(t)|^2 + |a_-(t)|^2\right) \end{aligned} \tag{E.7}$$

for the basis $|+\rangle$ and $|-\rangle$ after the diagonalization of Eq.(2.42) is not correct because the transformation U in Eq.(2.43) is not unitary; $|a_\pm|^2$ do not have the correct probabilistic meaning of staying in the $|\pm\rangle$ state. (Besides, $|\pm\rangle$ are not orthonormal either.)

Appendix F

The equivalence between the two measurement schemes in the zero transition limit

In this appendix, we are going to show that the two measurement schemes in Section (2.6) give the same qubit density matrix evolution if there is no dynamical transition between the channels.

According to Eq.(2.56), we get

$$\delta W_{\pm} \simeq e^{-\Gamma_{\pm}\tau} \simeq 1 - \tau\Gamma_{\pm}$$

for $\tau \to 0$. Therefore we can apply it to Eq.(2.60) and give

$$\begin{aligned} \sigma_{++}(t+\tau) &\simeq \frac{\sigma_{++}(t)(1-\Gamma_{+}\tau)}{\sigma_{++}(t)(1-\Gamma_{+}\tau)+\sigma_{--}(t)(1-\Gamma_{-}\tau)} \\ &\simeq \sigma_{++}(t)\left(1-\sigma_{--}(t)(\Gamma_{+}-\Gamma_{-})\tau\right) \end{aligned}$$

Here we have used $1-\sigma_{++}(t)=\sigma_{--}(t)$.

Then we can derive a Langevin - type equation:

$$\frac{\sigma_{++}(t+\tau)-\sigma_{++}(t)}{\tau} \simeq \frac{d\sigma_{++}}{dt} = -\sigma_{++}(t)\,\sigma_{--}(t)(\Gamma_{+}-\Gamma_{-})$$

Next, based on this formula, we can derive its solution. As we know, this formula can be rewritten in the form

$$\frac{d\sigma_{++}}{dt} = -\sigma_{++}(t)(1-\sigma_{++}(t))(\Gamma_{+}-\Gamma_{-})$$

, and it further gives the form

$$\frac{d\sigma_{++}}{\sigma_{++}(t)(1-\sigma_{++}(t))} = -(\Gamma_{+}-\Gamma_{-})\,dt.$$

After integration, this gives

$$\frac{\sigma_{++}(t)}{\sigma_{--}(t)}\frac{\sigma_{--}(0)}{\sigma_{++}(0)} = e^{-\int(\Gamma_+-\Gamma_-)dt}. \tag{F.1}$$

Finally, we get

$$\begin{aligned}
\sigma_{++}(t) &= \frac{\frac{\sigma_{++}(0)}{\sigma_{--}(0)}e^{-\int(\Gamma_+-\Gamma_-)dt}}{1+\frac{\sigma_{++}(0)}{\sigma_{--}(0)}e^{-\int(\Gamma_+-\Gamma_-)dt}} \\
&= \frac{\sigma_{++}(0)\,e^{-\int\Gamma_+dt}}{\sigma_{++}(0)\,e^{-\int\Gamma_+dt}+\sigma_{--}(0)\,e^{-\int\Gamma_-dt}} \\
&= \frac{\sigma_{++}(0)\,W_+(t)}{\sigma_{++}(0)\,W_+(t)+\sigma_{--}(0)\,W_-(t)}
\end{aligned}$$

, which is exactly the Eq.(2.51). Therefore, we conclude that these two types of measurement scheme give the same density matrix evolution.

Appendix G

Alternative description of qubit density matrix evolution under negative outcome measurement

Similar to the analysis of Eq.(2.58) and Eq.(2.62), we can instead represent the density matrix right after our negative measurement during the interval $n\tau < t' < (n+1)\tau$ by $P_n \sigma_n P_n$ on the basis of Bayes' rule, i.e.

$$\sigma_n \to \sigma_{n+1} = P_n \sigma_n P_n. \tag{G.1}$$

Here $P_n \equiv \sqrt{\frac{w_+(n)}{w(n)}} P_+ + \sqrt{\frac{w_-(n)}{w(n)}} P_-$ is the new projective operator corresponding to our negative outcome measurement, which automatically includes the Bayes' rule correction to the density matrix, and $P_\pm$ is the projective operator onto the $\pm$ state. To check the behavior of P_n in different limits, for $\Gamma_+ = \Gamma_- = 0$ we find it becomes the identity operator, which is $P_n = P_+ + P_- = I$, while for $\Gamma_+ = \infty$ and $\Gamma_- = 0$ we can see $P_n = \frac{1}{\sqrt{\sigma_{--}}} P_-$, which is the projective operator onto $-$ state with normalized factor $\frac{1}{\sqrt{\sigma_{--}}}$ due to the negative measurement; conversely in the opposite limit where $\Gamma_- = \infty$ and $\Gamma_+ = 0$ we will see $P_n = \frac{1}{\sqrt{\sigma_{++}}} P_+$, which is again the projective operator onto $+$ state with normalized factor $\frac{1}{\sqrt{\sigma_{++}}}$ due to the negative measurement.

Based on Eq.(G.1), we can formula the time derivative of the density matrix, where only the measurement effect is considered.

$$\frac{\sigma_{n+1} - \sigma_n}{\tau} = \left(\frac{P_n - I}{\tau} \right) \sigma_n + \sigma_n \left(\frac{P_n - I}{\tau} \right) \tag{G.2}$$

In the $\tau \to 0$ limit we will have

$$\dot{\sigma} = \left\{ \dot{P}(t), \sigma \right\} \tag{G.3}$$

Here $\dot{P}(t) = \lim_{\tau \to 0} \left(\frac{P_n - I}{\tau} \right)$ and it's not hard to prove

$$\dot{P}(t) = -\frac{1}{2}\sigma_{--}(\Gamma_+ - \Gamma_-) P_+ - \frac{1}{2}\sigma_{++}(\Gamma_- - \Gamma_+) P_-. \tag{G.4}$$

Next, after considering the intrinsic dynamical evolution of the density matrix, namely $\dot{\sigma}'$, we will get the full version of density matrix evolution, namely

$$\dot{\sigma} = \dot{\sigma}' + \left\{ \dot{P}(t), \sigma \right\}. \tag{G.5}$$

It's not hard to check that (G.5) is consistent with Eq.(2.68) and Eq.(2.69).

Appendix H

A pictorial way to understand the entanglement change during the measurement

We can understand how the entanglement (between qubit and SQUID) changes during the measurement by comparing two average "positions" of SQUID wave functions, $\bar{x}_{\pm} = \langle\psi_{\pm}| x |\psi_{\pm}\rangle$. Here $|\psi_{\pm}\rangle$ represent for SQUID wave functions corresponding to the two qubit states $|\pm\rangle$ and x is the SQUID phase. Please note that we have $\psi_{\pm}(x + 2\pi) = \psi_{\pm}(x)$. To simplify the analysis, let's assume that the wave functions inside and outside the well respectively are centered at 0 and l, where l can be larger than 2π and increases with time as long as the wave function outside the well keeps propagating. Moreover, as a further simplification we assume these centers are independent of the qubit states.(More accurately, l should depend on qubit states: $l = l_{\pm}$.) Then we can use these assumptions to derive the average position of SQUID wave function for qubit being in $\pm$ states, namely

$$\bar{x}_{\pm} = 0 \times W_{\pm} + l \times (1 - W_{\pm}) = l(1 - W_{\pm}). \tag{H.1}$$

Here $W_{\pm}$ are the probabilities of SQUID phase being in the well, which is defined in Eq.(2.49). Based on these formulas, we can obtain the difference between the two average positions of two qubit states:

$$\Delta\bar{x} = l(W_{+} - W_{-}). \tag{H.2}$$

Ideally, we wish $\Delta\bar{x}$ to be large if the two SQUID wave functions $|\psi_{\pm}\rangle$ are more entangled with qubit states $|\pm\rangle$. Although the change of the SQUID potential due to the qubit state is really small, so that the wave functions inside the well have negligible difference, the distance l can be very large and increases with time such that it can amplify the value of $(W_{+} - W_{-})$ and gives large $\Delta\bar{x}$. Basically, our strategy is to enlarge $(W_{+} - W_{-})$ and l at same time to give the maximum $\Delta\bar{x}$.

Because $(W_{+} - W_{-})$ increases at the beginning and then decreases to zero eventually as both W_{+} and W_{-} go to zero, we expect $\Delta\bar{x}$ will have a maximum value. To find the maximum value of $\Delta\bar{x}$ we need to

set its time derivative equal to zero, which gives

$$\frac{d\Delta\bar{x}}{dt} = \frac{dl}{dt}\left(W_+ - W_-\right) + l\frac{dy}{dt}\left(P_- - P_+\right) = 0 \tag{H.3}$$

Here we have applied the relation between the switching probability $P_\pm(y)$ and $W_\pm(y)$ as given by Eq.(E.2), namely

$$P_\pm(y) = -\frac{d}{dy}W_\pm(y). \tag{H.4}$$

If $\frac{dl}{dt} = 0$, then from Eq.(H.3) we can conclude that the maximum entanglement appears at the moment where the two switching probabilities are equal, that's $P_+ = P_-$ or $\Gamma_+ W_+ = \Gamma_- W_-$, and it's approximately around the middle between the two peaks of switching current distributions for qubit $\pm$ states. But actually we have $\frac{dl}{dt} \neq 0$. Therefore the maximum entanglement should appear after $P_- = P_+$, and its exact position depends on the experimental details of SQUID.

In principle, if $\Gamma_+ > \Gamma_-$ the peak of P_+ appears earlier than P_-'s, i.e. at a lower bias current, and the wave function $|\psi_+\rangle$ is distributed farther (from the well) than that of $|\psi_-\rangle$. As we know, the $\Delta\bar{x}$ increases until it reaches its maximum. After the maximum entanglement, $\Delta\bar{x}$ decreases and finally reaches an equilibrium value that depends on the terminal velocity of wave function outside the well. Here we assume that the two corresponding terminal velocities are the same. Of course, different terminal velocities can cause the increasing of $|l_+ - l_-|$.

Besides, we naively expect that a longer measurement time can induce larger entanglement between qubit and SQUID. Therefore we expect that the measurement at smaller bias current, which has smaller escape rate, will give larger maximum $\Delta\bar{x}$ of SQUID wave function after the measurement. Let's check it in the special case where $\frac{dl}{dt} = 0$ and the SQUID escapes at fixed bias current, that gives

$$\Delta\bar{x} = l\left(W_+ - W_-\right) = l\left(e^{-\Gamma_+ t} - e^{-\Gamma_- t}\right). \tag{H.5}$$

The maximum of this expectation value appears at $t = \frac{\ln\frac{\Gamma_+}{\Gamma_-}}{(\Gamma_+ - \Gamma_-)}$, and then we use it to derive the maximum value of $(W_+ - W_-)$ as a function of Γ_+ and Γ_-:

$$\left(W_+ - W_-\right) = \left(\frac{\Gamma_+}{\Gamma_-}\right)^{\frac{\Gamma_+}{(\Gamma_- - \Gamma_+)}} - \left(\frac{\Gamma_+}{\Gamma_+}\right)^{\frac{\Gamma_+}{(\Gamma_- - \Gamma_+)}}. \tag{H.6}$$

According to this we can find the following diagram for the maximum value of $(W_+ - W_-)$ as a function of

y.

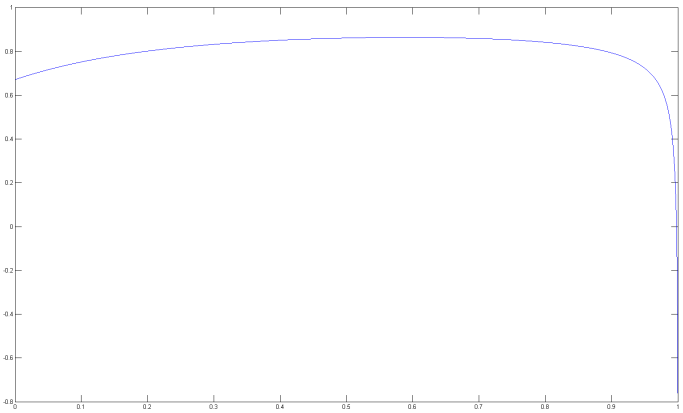

Figure H.1: The maximum value of $(W_+ - W_-)$ at fixed bias current seems not a monotonically decreasing function of y, although it indeed decreases for $y > 0.6$. This result implies that a longer duration of the measurement may not induce a larger entanglement if we assume $\frac{dl}{dt} = 0$.

The result of this special case seems not consistent with our expectation. But actually we need to take the time dependence of l into account. Usually l increases with time, then we may conclude that the displacement in either Eq.(H.5) or Eq.(H.2) should be larger for measurement at lower bias current.

Appendix I

Transition between energy eigenstates during non-adiabatic current ramping

In order to preserve the qubit staying in its initial state until the SQUID escape take place, we need the current ramping rate $r \equiv \frac{dy}{dt}$ faster than the qubit tunnelling rate Δ/h, which is similar to the Landau-Zener problem. According to our numerical analysis with $k/h = 0.7GHz, \omega = 0.9GHz$, and $g\pi = 0.005$, which are almost the same parameters as the Delft group's, this requires $r \geq 10\Delta/h($ for $10^6 Hz < \Delta/h < 10^9 Hz)$ to reach the situation where over 99% population of qubits remain staying in its initial flux state after current ramping to the maximum. To simplify the problem, here we only considered the typical case that the qubit always starts in a flux eigenstate and the net bias energy of the qubit is zero at zero bias current. It can be generalized to other cases. In principle it's not a bad estimation to use Vutha's approximation of the Landau-Zener problem[43] to analytically evaluate the probability of the qubit remaining in the flux eigenstate after the bias current is ramped to the maximum; the derivation is shown as follows.

As we know from the Eq.(2.31), the qubit bias energy has a contribution from the qubit-SQUID coupling energy and therefore changes with the SQUID bias current $I_b(t)$; let's write the net qubit bias energy as

$$\bar{\varepsilon}(y) \approx \varepsilon_{00}^{H} = \varepsilon(f_q) + g\pi k(y)\left(1 - \frac{\omega(y)\hbar}{4k(y)}\right) \tag{I.1}$$

with $k(y) = k_0\sqrt{1-y^2}$ and $\omega(y) = \omega_0\left(1-y^2\right)^{1/4}$, where $\varepsilon(f_q)$ is given by Eq.(2.2) and $y \equiv \frac{I_b(t)}{2I_{C0}\cos\pi f_{SQ}}$ is the current parameter. To understand the behaviour of the qubit state due to a sudden change of the current parameter y from 0 to 1 with the constant rate $r \equiv \frac{dy}{dt}$, we can consider the special situation in which the qubit starts at zero bias current in a flux eigenstate and zero net bias energy($\bar{\varepsilon}(0) = 0$) at zero bias current. Since then $\bar{\varepsilon}(0) = 0$ we can derive

$$\bar{\varepsilon}(y) = \pi g k_0\left(\sqrt{1-y^2} - 1\right) + \frac{\pi g\omega_0\hbar}{4}\left(1 - \left(1-y^2\right)^{1/4}\right) \tag{I.2}$$

Next, let's make our first approximation based on the assumption that most of the transitions of the state happen around the region $y \ll 1$ (or $\bar{\varepsilon}(y) \leq \Delta$), then we can write the approximate form of $\bar{\varepsilon}(y)$ in the small y limit:

$$\bar{\varepsilon}(y) = -\frac{\pi g}{2}\left(k_0 - \frac{\omega_0 \hbar}{8}\right) y^2 \tag{I.3}$$

To estimate the probability of the qubit remaining in its initial flux state during the sudden change of bias current we will use the formula derived by Vutha [43]

$$P(t_f) = \exp\left(-\Omega^2 \int_{t_i}^{t_f} \frac{\gamma}{W^2 + \gamma^2/4} dt\right) \tag{I.4}$$

, where the Landau-Zener problem is simplified by dephasing Rabi oscillations with the virtual detuning

$$W(y) = -2\bar{\varepsilon}(y)/\hbar = \frac{\pi g}{\hbar}\left(k_0 - \frac{\omega_0 \hbar}{8}\right) y^2 \tag{I.5}$$

, the Rabi frequency $\Omega = \Delta/\hbar$, and the decay rate of the Rabi oscillations is obtained from the inverse dephasing time:

$$\gamma(t) \approx \sqrt{\frac{\dot{W}(t)}{4\pi}} = \sqrt{\frac{\frac{d\bar{\varepsilon}(y)}{dy}\frac{dy}{dt}}{-2\pi\hbar}} = \sqrt{\frac{\pi g r}{2\pi\hbar}\left(k_0 - \frac{\omega_0 \hbar}{8}\right) y}. \tag{I.6}$$

Here we always have $y = rt$.

To evaluate $P(t_f)$ in Eq.(I.4), we need to make another approximation to the integral in the exponent and therefore divide the integral into two parts. The first part is the integral from t_i to t_e, where $W^2(t_e) = \gamma(t_e)^2 \Big/ 4$ and $W^2(t) \leq \gamma(t)^2 \Big/ 4$ for all $t_i \leq t \leq t_e$; we make an approximation to this part by assuming $W^2(t) \ll \gamma(t)^2 \Big/ 4$.

$$\begin{aligned} &\int_{t_i}^{t_e} \frac{\gamma}{W^2 + \gamma^2/4} dt \simeq 4 \int_{t_i}^{t_e} \frac{1}{\gamma} dt \\ &= \frac{4}{\sqrt{\frac{\pi g r}{2\pi\hbar}\left(k_0 - \frac{\omega_0 \hbar}{8}\right)}} \int_{t_i}^{t_e} \frac{1}{\sqrt{rt}} dt \\ &= \frac{8\sqrt{t_e}}{r\sqrt{\frac{\pi g}{2\pi\hbar}\left(k_0 - \frac{\omega_0 \hbar}{8}\right)}} \end{aligned} \tag{I.7}$$

Here we have assumed $t_i = 0$ and since $t_e \ll 1$ for most relevant experimental parameters this integral is neglectable.

The second part of integral is within the range $t_e \leq t \leq t_f$ and to approximate it we assume $\sigma^2(t) \gg$

$\gamma(t)^2 \Big/ 4$.

Then we have

$$\begin{aligned}
&\int_{t_e}^{t_f} \frac{\gamma}{W^2+\gamma^2/4}dt \simeq \int_{t_e}^{t_f} \frac{\gamma}{W^2}dt = \int_{t_e}^{t_f} \frac{\sqrt{\frac{\pi g r}{2\pi\hbar}\left(k_0-\frac{\omega_0\hbar}{8}\right)y}}{\left(\frac{\pi g}{\hbar}\left(k_0-\frac{\omega_0\hbar}{8}\right)y^2\right)^2}\frac{dt}{dy}dy \\
&= \left(\frac{\pi g}{\hbar}\left(k_0-\frac{\omega_0\hbar}{8}\right)\right)^{-3/2}\sqrt{\frac{1}{2\pi r}}\int_{y_e}^{y_f} y^{-7/2}dy \\
&= \left(\frac{\pi g}{\hbar}\left(k_0-\frac{\omega_0\hbar}{8}\right)\right)^{-3/2}\sqrt{\frac{1}{2\pi r}}\frac{2}{5}\, y^{-5/2}\Big|_{y_f}^{y_e}
\end{aligned} \tag{I.8}$$

Here we will let $y_f = 1$ (which is a good approximation because most of transition appears at values of y such that $\bar{\varepsilon}(y)$ is of the same order as Δ), neglect the corresponding term, and keep only the term with ${y_e}^{-5/2}$ because we usually have ${y_e}^{-5/2} \gg 1$. Then we get

$$\int_{t_i}^{t_f} \frac{\gamma}{W^2+\gamma^2/4}dt \simeq \left(\frac{\pi g}{\hbar}\left(k_0-\frac{\omega_0\hbar}{8}\right)\right)^{-3/2}\sqrt{\frac{1}{2\pi r}}\frac{2}{5}{y_e}^{-5/2}$$

On the other hand we can derive y_e by the relation $W(y_e)^2 = \gamma^2(y_e)/4$, which gives $y_e = \left(r\hbar/\left(8\pi^2 g\left(k_0-\frac{\omega_0\hbar}{8}\right)\right)\right)^{1/3}$. Finally we can put this value of y_e into the formula and get

$$P = \exp\left[-\frac{8}{5}\pi^{1/3}\left(\frac{\Delta}{\hbar}\right)^2 r^{-4/3}\left(\frac{\pi g}{\hbar}\left(k_0-\frac{\omega_0\hbar}{8}\right)\right)^{-2/3}\right] \tag{I.9}$$

This is our approximate formula for the probability of the qubit remaining in its initial flux state after the change of current parameter from 0 to 1. At least it works well for the current ramping rate $r \geq \Delta/h$ for $10^6 Hz < \Delta/h < 10^9 Hz$, and is more accurate for lower Δ. Here we are more interested in the limit with sudden change($r \geq \Delta/h$ approximately) of bias energy to preserve the qubit state.

Appendix J

The maximum resonance pumping probability under the relaxation to the ground state

To find the maximum value of $\rho_{11}(t)$(the probability of staying in excited state) after resonance pumping, the first step is to find the time $t_{\max}$ at which $\dot{\rho}_{11}(t_{\max})=0$, that is

$$\dot{\rho}_{11}(t_{\max})=e^{-\Gamma t}\frac{\Omega_0^2}{|\Omega|^2}\left|\sin\left(\frac{\Omega t}{2}\right)\right|\times\left(-\Gamma\sin\left(\frac{\Omega t}{2}\right)+\Omega\cos\left(\frac{\Omega t}{2}\right)\right)=0$$

This implies

$$\tan\left(\frac{\Omega t_{\max}}{2}\right)=\frac{\Omega}{\Gamma}\Rightarrow t_{\max}=\frac{2}{\Omega|_{\overline{\Delta}=0}}\tan^{-1}\frac{\Omega|_{\overline{\Delta}=0}}{\Gamma}$$

Put this formula into $\rho_{11}(t)$:

$$\rho_{11}(t_{\max})=e^{-\frac{2\Gamma}{\Omega}\tan^{-1}\frac{\Omega}{\Gamma}}\left|\sin\left(\tan^{-1}\frac{\Omega}{\Gamma}\right)\right|^2\frac{\Omega_0^2}{|\Omega|^2}$$

Because the system is on resonance, we have $\overline{\Delta}=0\Rightarrow\Omega^2\equiv\Omega_0^2-\Gamma^2$, so the equation can be rewritten as

$$\rho_{11}(t_{\max})=e^{-\frac{2\Gamma}{\sqrt{\Omega_0^2-\Gamma^2}}\tan^{-1}\frac{\sqrt{\Omega_0^2-\Gamma^2}}{\Gamma}}\left|\sin\left(\tan^{-1}\frac{\sqrt{\Omega_0^2-\Gamma^2}}{\Gamma}\right)\right|^2\frac{\Omega_0^2}{\Omega_0^2-\Gamma^2}$$

.

In the limit $\frac{\Gamma}{\Omega_0}\ll 1$, we will have:

$$\begin{aligned}
&\rho_{11}(t_{\max})\\
&=\left(1-\frac{2\Gamma}{\sqrt{\Omega_0^2-\Gamma^2}}\tan^{-1}\frac{\sqrt{\Omega_0^2-\Gamma^2}}{\Gamma}\right)\left|\sin\left(\tan^{-1}\frac{\sqrt{\Omega_0^2-\Gamma^2}}{\Gamma}\right)\right|^2\frac{\Omega_0^2}{\Omega_0^2-\Gamma^2}\\
&\approx\left(1-\frac{\pi\Gamma}{\sqrt{\Omega_0^2-\Gamma^2}}\right)\left|\sin\left(\frac{\pi}{2}\right)\right|^2\left(1+\frac{\Gamma^2}{\Omega_0^2}\right)\\
&\approx\left(1-\frac{\pi\Gamma}{\Omega_0}\left(1+\frac{\Gamma^2}{2\Omega_0^2}\right)\right)\left(1+\frac{\Gamma^2}{\Omega_0^2}\right)\\
&\approx 1-\frac{\pi\Gamma}{\Omega_0}\approx 1-\frac{\pi\Gamma_1}{2\Omega_0}\equiv 1-\varepsilon_0
\end{aligned}$$

Here we have assume $\Gamma\approx\frac{1}{2}\Gamma_1$ in the limit of $\Gamma_1>\gamma_{10}(\equiv\Gamma_d)>\gamma_\varphi>\Gamma_0$.

Appendix K

The off resonance pumping of dcSQUID for the qubit in the negative state

We are going to analyze the pumping of the dcSQUID with negative (qubit) state, which is off resonance [47].

We have the relation

$$\begin{aligned}\Omega^2 &= \Omega_0^2 - \left(\Gamma - i\bar{\Delta}\right)^2 = \left(\Omega_0^2 + \bar{\Delta}^2 - \Gamma^2\right) + i2\bar{\Delta}\Gamma \\ &= \sqrt{\left(\Omega_0^2 + \bar{\Delta}^2 - \Gamma^2\right)^2 + \left(2\bar{\Delta}\Gamma\right)^2} e^{i\theta}\end{aligned}$$

Here we have defined

$$\cos\theta = \frac{\left(\Omega_0^2 + \bar{\Delta}^2 - \Gamma^2\right)}{\sqrt{\left(\Omega_0^2 + \bar{\Delta}^2 - \Gamma^2\right)^2 + \left(2\bar{\Delta}\Gamma\right)^2}},$$

$$\sin\theta = \frac{2\bar{\Delta}\Gamma}{\sqrt{\left(\Omega_0^2 + \bar{\Delta}^2 - \Gamma^2\right)^2 + \left(2\bar{\Delta}\Gamma\right)^2}}.$$

Basically, we can rewrite Ω into the following form:

$$\Omega = \left(\left(\Omega_0^2 + \overline{\Delta}^2 - \Gamma^2\right)^2 + \left(2\bar{\Delta}\Gamma\right)^2\right)^{1/4} e^{i\theta/2} = |\Omega|\, e^{i\theta/2}.$$

Inserting this into the formula for $\rho_{11}(t)$:

$$\begin{aligned}\rho_{11}(t) &= e^{-\Gamma t}\frac{\Omega_0^2}{|\Omega|^2}\left|\sin\left(\frac{\Omega t}{2}\right)\right|^2 = e^{-\Gamma t}\frac{\Omega_0^2}{|\Omega|^2}\left|\sin\left(\frac{t\,|\Omega|\, e^{i\theta/2}}{2}\right)\right|^2 \\ &= e^{-\Gamma t}\frac{\Omega_0^2}{|\Omega|^2}\left|\sin\left(\frac{t\,|\Omega|\left(\cos\frac{\theta}{2} + i\sin\frac{\theta}{2}\right)}{2}\right)\right|^2 \\ &= e^{-\Gamma t}\frac{\Omega_0^2}{|\Omega|^2}\left|\sin\left(\frac{t\,|\Omega|\cos\frac{\theta}{2}}{2}\right)\cos\left(\frac{t\,|\Omega|\, i\sin\frac{\theta}{2}}{2}\right) + \cos\left(\frac{t\,|\Omega|\cos\frac{\theta}{2}}{2}\right)\sin\left(\frac{i\,|\Omega|\, t\sin\frac{\theta}{2}}{2}\right)\right|^2 \\ &= e^{-\Gamma t}\frac{\Omega_0^2}{|\Omega|^2}\left|\sin\left(\frac{t\,|\Omega|\cos\frac{\theta}{2}}{2}\right)\cosh\left(\frac{t\,|\Omega|\sin\frac{\theta}{2}}{2}\right) + i\cos\left(\frac{t\,|\Omega|\cos\frac{\theta}{2}}{2}\right)\sinh\left(\frac{|\Omega|\, t\sin\frac{\theta}{2}}{2}\right)\right|^2\end{aligned}$$

$$
\begin{aligned}
&= e^{-\Gamma t}\frac{\Omega_0^2}{|\Omega|^2}\left(\sin^2\left(\frac{t\,|\Omega|\cos\frac{\theta}{2}}{2}\right)\cosh^2\left(\frac{t\,|\Omega|\sin\frac{\theta}{2}}{2}\right)+\cos^2\left(\frac{t\,|\Omega|\cos\frac{\theta}{2}}{2}\right)\sinh^2\left(\frac{|\Omega|\,t\sin\frac{\theta}{2}}{2}\right)\right)\\
&= e^{-\Gamma t}\frac{\Omega_0^2}{|\Omega|^2}\left(\sin^2\left(\frac{t\,|\Omega|\cos\frac{\theta}{2}}{2}\right)\left(1+\sinh^2\left(\frac{t\,|\Omega|\sin\frac{\theta}{2}}{2}\right)\right)+\cos^2\left(\frac{t\,|\Omega|\cos\frac{\theta}{2}}{2}\right)\sinh^2\left(\frac{|\Omega|\,t\sin\frac{\theta}{2}}{2}\right)\right)\\
&= e^{-\Gamma t}\frac{\Omega_0^2}{|\Omega|^2}\left(\sin^2\left(\frac{t\,|\Omega|\cos\frac{\theta}{2}}{2}\right)+\sinh^2\left(\frac{t\,|\Omega|\sin\frac{\theta}{2}}{2}\right)\right)\\
&\approx e^{-\Gamma t}\frac{\Omega_0^2}{\bar{\Delta}^2}\left(\sin^2\left(\frac{t\bar{\Delta}}{2}\right)+\sinh^2\left(\frac{t\Gamma}{2}\right)\right)
\end{aligned}
\tag{K.1}
$$

In the last equation, we have used the approximations $|\Omega|^2 \approx \bar{\Delta}^2$, $|\Omega|\cos\frac{\theta}{2} \approx \bar{\Delta}$, and $|\Omega|\sin\frac{\theta}{2} \approx \Gamma$ in the limit $\bar{\Delta}^2 \gg \Omega_0^2 \text{and} \Gamma^2$. If we denote $t = t_{\max} = \frac{2}{\Omega|_{\bar{\Delta}=0}}\tan^{-1}\frac{\Omega|_{\bar{\Delta}=0}}{\Gamma} \approx \frac{2}{\Omega_0}\tan^{-1}\frac{\Omega_0}{\Gamma_1}$ as the pumping time for the state on resonance, and assume $\frac{\Gamma}{\Omega_0} \approx \frac{\Gamma_1}{\Omega_0}$ as in appendix J, the off resonance upper dcSQUID states (corresponding to the negative qubit state) can still have a nonzero probability of being excited, namely

$$
\begin{aligned}
&\rho_{11}\left(t_{\max}\right)\\
&= \quad e^{-\frac{2\Gamma}{\Omega|_{\bar{\Delta}=0}}\tan^{-1}\frac{\Omega|_{\bar{\Delta}=0}}{\Gamma}}\frac{\Omega_0^2}{\bar{\Delta}^2}\left(\sin^2\left(\frac{\bar{\Delta}}{\Omega|_{\bar{\Delta}=0}}\tan^{-1}\frac{\Omega|_{\bar{\Delta}=0}}{\Gamma}\right)+\sinh^2\left(\frac{\Gamma}{\Omega|_{\bar{\Delta}=0}}\tan^{-1}\frac{\Omega|_{\bar{\Delta}=0}}{\Gamma}\right)\right)\\
&\approx \quad \frac{\Omega_0^2}{\bar{\Delta}^2}e^{-\frac{\pi\Gamma}{\Omega|_{\bar{\Delta}=0}}}\left(\sin^2\left(\frac{\pi\bar{\Delta}}{2\Omega|_{\bar{\Delta}=0}}\right)+\sinh^2\left(\frac{\pi\Gamma}{2\Omega|_{\bar{\Delta}=0}}\right)\right)
\end{aligned}
\tag{K.2}
$$

Basically, we have $\rho_{11} \approx \zeta_2 \equiv \frac{\Omega_0^2}{\bar{\Delta}^2}$ as the largest term of approximation.

References

[1] A. J. Leggett and Anupam Garg. Phys. Rev. Lett. 54, 857 (1985)

[2] We do not address in this paper the debated question of the precise definition of "macroscopic" or "macroscopically distinct ", an issue which will not affect the arguments below.

[3] A.Mizel and A.Wilde, Found. Phys. 42, 256-265(2012).

[4] G. C.Knee et al., Nature Comm. 3, 606 (2012).

[5] A. Palacios-Laloy et al., Nature Phys. 6, 442(2010).

[6] A. Fedrizzi et al., Phys. Rev. Lett. 106, 200402 (2011).

[7] G. Waldherr et al., Phys. Rev. Lett. 107, 090401 (2011).

[8] Emary, C., Lambert, N. & Nori, F. Leggett-Garg inequalities. Reports on Progress in Physics 77, 016001 (2014).

[9] A. J. Leggett, Foundations of Physics 18, pp 939-952 (1988)

[10] Clarke and Wilhelm, Nature 453, 1031-1042 (2008). M. H. Devoret and R. J. Schoelkopf, Science 339, 1169-1174(2013).

[11] J. R. Friedman et al., Nature 406, 43 (2000)

[12] J. E. Mooij et al., Science 285, 1036 (1999)

[13] T. P. Orlando et al., Phys. Rev. B 60, 15398(1999).

[14] A.J.Leggett, chapter in "Chance and Matter", ed. J.Souletie et al, North-Holland, Amsterdam 1987 (Proceedings of the 1985 Les Houches summer school)

[15] Physics and Applications of the Josephson Effect, Barone and Paterno

[16] Yakir Aharonov, David Z. Albert, and Lev Vaidman. PRL 60, 1351 (1998)

[17] C. H. van der Wal, A. C. J. ter Haar, F. K. Wilhelm, R. N. Schouten, C. J. P. M. Harmans, T. P. Orlando, S. Lloyd, and J. E. Mooij,Science **290**, 773 (2000).

[18] I. Chiorescu, Y. Nakamura, C. J. P. M. Harmans, and J. E. Mooij ,Science**299** , 1869 (2003).

[19] Martinis, J. M., Nam, S., Aumentado, J. Urbina, C. Rabi oscillations in a large Josephson-junction qubit. Physical Review Letters 89, 117901 (2002).

[20] Alec Maassen van den Brink: Resonance eigenstates of the SQUID-qubit system, arXiv:cond-mat/0606381v1.

[21] Nakano, H., Tanaka, H., Saito, S., Semba, K., Takayanagi, H., Ueda, M.: A theoretical analysis of flux-qubit measurements with a dcSQUID, cond-mat/0406622.

[22] Nakano, H. and Takayanagi, H., J. Phys. Soc. Jpn. 72(Supplement A), 1-2 (2003).

[23] T.P. Orlando, Lin Tian, D.S. Crankshaw, S. Lloyd, C.H. van der Wal,J.E. Mooij, F. Wilhelm, Physica C 368, 294299 (2002)

[24] Tanaka H., Sekine Y., Saito S., and Takayanagi H., Physica C 368, 300 (2002); H. Takayanagi, H. Tanaka, S. Saito, and H. Nakano, Physica Scripta T102, 95-102 (2002); H. Tanaka, S. Saito and H. Takayanagi, p. 366 in Toward the Controllable Quantum States, edited by H.Takayanagi and J. Nitta (World Scientific Pub., Singapore, 2003).

[25] Hideaki Takayanagi,Hirotaka Tanaka, Shiro Saito ,and Hayato Nakano, Superlattices and Microstructures 32, 221 (2003)

[26] Quantitatively, the trailing plateau is of this order of magnitude, but its actual value depends on the details of the SQUID circuit.

[27] H. A. Kramers, Physica (Utrecht) 7, 284 (1940). M. B*ü*ttiker, E. P. Harris, and R. Landauer, Phys. Rev. B 28, 1268 (1983).

[28] We consider the qubit designed with three Josephson junctions, which is discussed in most of papers [17, 18]. The qubit maximum persistent current is given by $I_p \approx 2\alpha\pi E_J/\Phi_0$, where α is the area ratio between the (smaller) middle junction and the other outer ones and E_J is the Josephson coupling energy of the outer ones.

[29] This formula is true for the bias current approaching its critical value. A more general expression for the turning point is given by $R_c^2 = 27\left(1 - \left(\frac{\pi}{2} - x_0\right)\tan\left[x_0\right]\right)$. Qualitatively, there would not be a big difference between these two formulas for the turning point if we consider the switching current behavior near the critical value.

[30] The traditional WKB formula for tunneling can be found in A. Schmid, Ann. Phys.**170** , 333 (1986); the dissipative correction and the corresponding experimental test can be respectively found in A.O. Caldeira and A. J. Leggett, Ann. Phys. (N.Y.) 149, 374 (1983) and John M. Martinis et al., Phys. Rev. B 35, 4682 (1987).

[31] The other variable of the dcSQUID, which corresponds to the phase difference between the two junctions, is uncontrollable and unmeasurable but can be integrated out by the path integral method, see ref [21]. Its effect is independent of σ_z and much smaller than the coupling term between the qubit and dc SQUID.

[32] Here we assume the currrent increase linearly. But the escape rate does not increase linearly with the current. Instead, it rather increases exponentially. Therefore we expect the required escape rate should be much larger than the inverse of current ramping time; this is not hard to be justified numerically.

[33] Here the elimination of the off diagonal elements of the time evolution operator seems a stronger condition for realizing a flux-basis projective measurement.

[34] M-C.Yeh and A.J.Leggett, in preparation. This paper considers a generalization of the experimental technique of Knee et al. [4] to the macroscopic level(flux qubit).

[35] The approximation in Eq.(B.16) is more appropriate for the NTT data where $g\omega\hbar$ can be much smaller than $\sqrt{\varepsilon_{00}^2 + \Delta^2}$.

[36] The strong decoherence can make the qubit state into a statistical mixture of flux states [21]; the qubit is trapped in either side of its double potential probabilistically due to the strong decoherence which prohibits the tunnelling between the wells. This effect is not included in our dynamical analysis of qubit-SQUID composite system.

[37] A. N. Korotkov, Phys. Rev. B 60, 5737 (1999)

[38] The decoherence during the measurement could reduce the off diagonal density matrix element so that we will have instead $|\sigma_{+-}(t+\tau)| < \sqrt{\sigma_{++}(t+\tau)\,\sigma_{--}(t+\tau)}$.

[39] Also see Eq.(2.35), which gives us a more general condition to achieve a flux-basis measurement. Because it equally includes both the conditions $|\Gamma_{0L} - \Gamma_{0R}| \gg \Delta/\hbar$ and $\varepsilon' \gg \Delta$, it indeed supports that the escape rate difference plays similar role as the effective bias energy to rotate the basis. Here ε' is the effective qubit bias energy, which is defined by Eq.(2.39).

[40] In general our system may not have definite spin basis for the bias current being not in the lower and higher escape rate limits because the spin angle of eigenbasis of composite system can be SQUID phase dependent. But basically, we believe that the idea of decomposition of wave function into two channels is true for all range of bias current.

[41] The purpose for minimization is to make the perturbation correction as small as possible. Therefore, roughly speaking, although the motivations are different, the minimization criterion in Appendix B can be Eq.(B.14), and the corresponding one in the harmonic approximation is the requirement that the energy correction to H_d(in Eq.(2.21) due to the perturbation V^H should be smaller than the energy scale of the escape rate near the current corresponding to the maximum switching probability.

[42] As we know, the dissipation effect from a net resistance R_s can effectively enlarge the bounce action by the factor $\left(1+\frac{0.87}{Q}\right)$ and thus reduce the escape rate at the same bias current. Consequently the peak of switching probability distribution will move to higher bias current due to the decrease of the escape rate in the presence of dissipation. Also, the width of the switching current distribution is narrower. Therefore, reducing the resistance R_s is another way to make two switching distributions of the qubit states to be distinguishable from one another. Besides, according to our numerical simulation, the escape rate at the maximum switching probability will be larger for the larger dissipation which corresponds to smaller resistance R_s. This can be understood as follows. If we take the y derivative of the switching probability formula (as shown in Eq.(2.29)) and set it equal to zero then we will have a equation $\Gamma^{-2}\frac{d\Gamma}{dy} = -\frac{1}{\frac{dy}{dt}}$ for the maximum switching probability. On the other hand, from Eq.(2.15) we can approximately have $\frac{d\Gamma}{dy} \approx \Gamma\frac{d}{dy}\left(\frac{B}{\hbar}\left(1+\frac{0.87}{Q}\right)\right) = \Gamma\left(\frac{d}{dy}\frac{B}{\hbar} + \frac{d}{dy}\left(\frac{0.87B}{Q\hbar}\right)\right)$, and we can see that there are two terms contributing to the $\frac{d\Gamma}{dy}$. The first term $\Gamma\frac{d}{dy}\frac{B}{\hbar}$ comes from the bounce action itself, and this is always negative. The second term $\Gamma\frac{d}{dy}\left(\frac{0.87B}{Q\hbar}\right)$, which comes from the dissipation correction, is proportional to the $\Gamma\frac{dR_c^2}{dy}$ which is always negative. As a consequence, larger dissipation makes $\left|\frac{d\Gamma}{dy}\right|$ larger and hence we will have larger escape rate at maximum switching probability according to the formula $\left(\frac{d}{dy}\frac{B}{\hbar} + \frac{d}{dy}\left(\frac{0.87B}{Q\hbar}\right)\right) \approx -\frac{\Gamma}{\frac{dy}{dt}}$. Besides, according to this formula we can qualitatively see that larger current ramping rate can give larger escape rate at maximum switching probability.

[43] Amar C Vutha, A simple approach to the Landau-Zener formula, Eur. J. Phys. 31, 389 (2010)

[44] According to Eq.(2.9), the shift of the minimum x_0 due to the qubit-SQUID coupling is $\Delta x_0 = \pi\tan x_0 \tan[\pi f_{SQ}]\,\sigma_z$, which increases from zero with bias current by the factor $\tan x_0 = \frac{y}{\sqrt{1-y^2}}$. In particular, we can evaluate the inner product between the two harmonic ground state wave functions of the channels and get $|\langle\psi_+ \mid \psi_-\rangle| \approx \left(1+\frac{\pi^2 g^2\tan^2[\pi f_{SQ}]}{8}\right)^{-\frac{1}{2}} e^{-\left(\frac{\pi^2 g^2\tan^2 x_0\tan^2\left[\pi f_{SQ}\right]}{a_0^2}\right)}$, where $a_0 = \sqrt{\frac{\hbar}{m\omega}}$. Please note that the exponential factor is due to the shift of the potential minimum and the rest comes from the change of curvature of the potential. Since we know that $\pi g \approx 10^{-2}$ to 10^{-3}, then we have $|\langle\psi_+ \mid \psi_-\rangle| \approx 1 - 10^{-5}$ at zero bias current($y = 0$) and

$|\langle\psi_+ \mid \psi_-\rangle| \approx 1 - 10^{-2}$ at $y = 0.9$. The result implies that the mutual orthogonality between ground state wave functions of two channels is negligible.

[45] Yuriy Makhlin, Gerd Schon,and Alexander Shnirman, Review of Modern Physics **73** , 357 (2001).

[46] Lucas Clemente and Johannes Kofler, Phys. Rev. A 91, 062103 (2015)

[47] Yu et al.,Science 296 889-892(2002).

[48] Han et al.,Science 293,1457(2001)

[49] Its well known that $\frac{1}{T_2} = \frac{1}{T_\varphi} + \frac{1}{2T_1}$ (or $\frac{1}{T_2} = \gamma_\varphi + \frac{1}{2}\gamma_{10}$ in our representation), therefore we have the relation $T_2 \leq 2T_1$. But this doesn't mean that we must have $T_1 \leq T_2$, because we do not have any constraint or relation between $\gamma_\varphi$andγ_{10} (or T_1 and T_φ). In the Yang-Yu paper in 2002, they claimed that the situation $(\Gamma_1 >) \gamma_{10} > \gamma_\varphi (> \Gamma_0)$ is a situation likely to be applicable to their experiment.

[50] George C. Knee, Kosuke Kakuyanagi, Mao-Chuang Yeh, Yuichiro Matsuzaki, Hiraku Toida, Hiroshi Yamaguchi, Shiro Saito, Anthony J. Leggett, William J. Munro, A strict experimental test of macroscopic realism in a superconducting flux qubit, arXiv:1601.03728v2 [quant-ph]

[51] Markus Jerger, Yarema Reshitnyk, Markus Oppliger, Anton Potonik, Mintu Mondal, Andreas Wallraff, Kenneth Goodenough, Stephanie Wehner, Kristinn Juliusson, Nathan K. Langford, Arkady Fedorov, Contextuality without nonlocality in a superconducting quantum system, arXiv:1602.00440v1 [quant-ph]

[52] Anthony J. Leggett, Note on the "size" of Schroedinger cats, arXiv:1603.03992 [quant-ph]